TVA-TR79-01

VERIFICATION OF TVA STEADY-STATE BWR PHYSICS METHODS

Topical Report

Tennessee Valley Authority

January 31, 1979

TABLE OF CONTENTS

LIST OF FIGURES

LIST OF FIGURES (Cont.)

LIST OF FIGURES (Cont.)

LIST OF FIGURES (Cont.)

LIST OF TABLES

LIST OF TABLES (Cont.)

ABSTRACT

The Tennessee Valley Authority has developed the LATTICE program for the detailed physics analyses of fuel bundles and the CORE code for the simulation of light water reactor cores. This report documents comparisons made to measured data and to results from more theoretically exact codes in order to verify the suitability of the models used in the CORE/LATTICE system for steady-state boiling water reactor analyses.

1. INTRODUCTION

This topical report is being submitted for NRC review concurrently with two other topical reports:

TVA-TR78-02 METHODS FOR THE LATTICE PHYSICS ANALYSIS OF LWR's

TVA-TR78-03 THREE-DIMENSIONAL LWR CORE SIMULATION METHODS

The purpose of this report is to demonstrate that the methods described in TVA-TR78-02 and TVA-TR78-03 reflect the state of the art of boiling water reactor steady-state analysis methods. Because the lattice physics analysis method and the core simulation analysis method will be used as a system, a single verification report is being submitted. The verification data is presented in two main divisions, one for lattice physics and one for core simulation. For the lattice physics analysis method (the computer code LATTICE), comparisons to measured data are presented for the calculation of reactivity, local power distributions, and isotopics. Additional comparisons are presented against results from a Monte Carlo code for reactivity, local power distributions and reaction rates, and against results from a two-dimensional collision probability code for local power distributions. For the core simulation method (the computer code CORE), comparisons are presented to measured data from eight cycles of four different BWR's, including the gamma scan measurements made at Quad Cities unit 1. These results together demonstrate that TVA core analysis methods reflect the current state of the art for BWR analyses.

2. UNIT CELL PHYSICS

In order to demonstrate the validity of the basic components of the physics methods used in LATTICE, a set of 25 critical experiments was selected and analyzed. These experiments cover a wide range of hydrogen-to-heavy metal (H/M) atom ratios, fuel compositions, and lattice pitches. For 15 of the criticals, calculations were performed using a general Monte Carlo reactor analysis code, including detailed comparisons of absorption and nu-fission reaction rate distributions in space and energy. To verify the correctness of the calculation of the buildup or depletion of uranium and plutonium isotopes, comparisons to the Yankee Rowe isotopic measurements are included.

2.1 REACTIVITY COMPARISONS

The effective multiplication factor was calculated for each of 25 critical H_2O moderated lattices of slightly enriched fuel rods using LATTICE unit cell physics parameters. The results show that LATTICE adequately predicts few group absorption, fission, and removal cross sections, and the corresponding diffusion coefficients over a range of experimental configurations.

Table 2.1-1 describes the criticals that were analyz ⁴. The first 15 critical configurations were taken from the LEOPARD verification report (Reference 2-1). The lattices contained stainless steel clad UO_2 rods with enrichments that ranged from 2.70 to 4.02 weight percent U-235. The H/M atom ratios varied from 3.08 to 14.65. The critical k-effectives were estimated by correcting the LATTICE cell infinite multiplication factors for

TABLE 2.1-1

LATTICE Results for Critical Experiments

Critical No.	Reference	Lattice Type*	H/M	Enrichment Wt. %	PPM Boron	Clad	Lattice Pitch Inches	Critical Buckling cm^{-2}	K-eff
1	2-1 (case 9)	S	3.08	2.70	0.0	SS	.405	0.004075	0.9978
2	2-1 (case 10)	S	4.13	2.70	0.0	SS	.435	0.005323	0.9931
3	2-1 (case 11)	S	5.45	2.70	0.0	SS	0.470	0.006326	0.9866
4	2-1 (case 12)	S	9.92	2.70	0.0	SS	0.573	0.006564	0.9898
5	2-1 (case 13)	S	11.99	2.70	0.0	SS	0.615	0.006007	0.9934
6	2-1 (case 14)	S	14.65	2.70	0.0	SS	0.665	0.005292	0.9909
7	2-1 (case 15)	S	3.53	2.70	0.0	SS	0.418	0.004750	0.9927
8	2-1 (case 17)	S	3.53	3.70	0.0	SS	0.418	0.006880	0.9856
9	2-1 (case 18)	S	6.37	3.70	0.0	SS	0.493	0.009510	0.9705
10	2-1 (case 20)	S	6.37	3.70	461	SS	0.493	0.007464	0.9770
11	2-1 (case 21)	S	6.37	3.70	717	SS	0.493	0.006366	0.9810
12	2-1 (case 22)	S	6.37	3.70	1274	SS	0.493	0.004099	0.9895
13	2-1 (case 23)	S	6.37	3.70	1346	SS	0.493	0.003839	0.9899
14	2-1 (case 24)	S	6.37	3.70	1489	SS	0.493	0.003338	0.9904
15	2-1 (case 26)	S	3.60	4.02	3428	SS	0.595	0.001720	1.0022
16	2-2 (UO_2)	S	5.27	2.459	2041	Al	0.640	0.0	0.9964
17	2-2 (PuO_2)	S	5.03	1.50**	2256	Zr	0.747	0.0	1.0065
18	2-3 (8BMB)	S	13.07	1.98**	1213	Zr	1.0	0.0	1.0026
19	2-3 (8SC)	S	12.87	2.08**	1286	Zr	1.0	0.0	1.0042
20	2-3 (8BME)	S	13.22	2.10**	1274	Zr	1.0	0.0	1.0030
21	2-4 (core 3)	S	4.12	3.04	0.0	Al	0.531	0.009182	1.0055
22	2-4 (core 8)	S	2.84	3.04	0.0	SS	0.488	0.004747	1.0059
23	2-4 (core 10)	S	2.89	3.04	0.0	Al	0.488	0.007076	1.0063
24	2-4 (core 11)	T	2.27	3.04	0.0	Al	0.50	0.005538	1.0076
25	2-4 (core 13)	T	1.32	3.04	0.0	Al	0.459	0.002436	1.0159
								Average	0.9954
								Standard Deviation	0.0107

*S: square lattice; T: triangular lattice

**PuO_2 in PuO_2 + natural UO_2

fast and thermal leakage using the age-diffusion equation

$$k_{eff} = k_{\infty} \frac{e^{-\tau B^2}}{1 + L^2 B^2} \qquad (2\text{-}1)$$

where τ is the LATTICE value of neutron age to thermal, L^2 is the LATTICE value of the thermal diffusion area, and B^2 is the measured buckling. The k-effectives calculated using this method are listed in Table 2.1-1 for the appropriate criticals. The average value is 0.9887 with a standard deviation of 0.0079.

The criticals numbered 16 through 20 in Table 2.1-1 (References 2-2, 2-3, and 2-12) were small lattices surrounded by a driver lattice and poisoned with soluble boron to a zero leakage configuration. Experiment 16 was aluminum clad UO_2 with a U-235 enrichment of 2.46 weight percent. Criticals 17 through 20 were Zircaloy clad mixed-oxide pins with 1.5 to 2.1 weight percent PuO_2. The H/M atom ratios varied from 5.27 to 13.22. Since there was zero leakage, the LATTICE k_{∞} was used as the calculated k-effective for each critical. For these five experiments, the average k-effective is 1.0025 with a standard deviation of 0.0038.

The remaining five experiments (Reference 2-4) were constructed in a near cylindrical configuration surrounded by an effectively infinite water reflector. The criticals had H/M atom ratios varying from 1.32 to 4.12. All were aluminum clad UO_2 rods with 3.04 weight percent enrichment, except for number 22, which was clad in stainless steel. For these five cases, LATTICE two group unit cell diffusion theory parameters were used in a one-dimensional diffusion theory code (Reference 2-5) with the experimental critical cylindrical radius and the measured axial buckling to calculate the

k-effective entered in Table 2.1-1. Group properties for the reflector region were also calculated using LATTICE. The average k-effective for these cases is 1.0082 with a standard deviation of 0.0044.

For all 25 critical experiments, the average calculated k-effective is 0.9954 with a standard deviation of 0.0107. However, if the criticals calculated using the less exact age-diffusion leakage correction are omitted, the average reactivity is 1.0054 and the standard deviation is reduced to 0.0049. This division of results into two groups is justified since the age-diffusion correction is inaccurate for small, high-leakage lattices and because of the uncertainty in measured total bucklings. Note, however, that cases 1 through 15 which were calculated using the age-diffusion equation have an acceptable standard deviation. Thus, the results from the 25 criticals analyzed indicate that LATTICE correctly calculates physics parameters for unit cells.

2.2 REACTION RATE COMPARISONS

Fifteen of the criticals selected for analysis with the lattice physics design method were also analyzed with the ESP Monte Carlo code (Reference 2-6). ESP is a full energy range reactor analysis code capable of using versions I through III of the ENDF/B neutron cross section data. For the present calculations, ENDF/B-III data was used except for natural zirconium, stainless steel, and hydrogen. ENDF/B-I neutron cross section data was used for natural zirconium and the components of stainless steel. For hydrogen, a modification of ENDF/B-I material 1001 was made

by setting the scattering cross section below 1.0 eV as a function of energy to the value obtained when the water scattering law data was processed with the FLANGE-II (Reference 2-7) computer code. Over 6000 neutron energy groups were used in ESP to represent the cross section data of the fuel media. All of the criticals were represented as single cells.

Comparisons of fractional reaction rates are summarized in Table 2.2-1. A thermal cutoff of 1.855 eV was used. The particular parameters presented are k_∞, the neutron source due to thermal neutrons ($\nu\Sigma_{f2}\phi_2$), the fraction of fast neutrons absorbed in the fuel ($\Sigma_{a1}\phi_1^{fuel}$), the fraction of thermal neutrons absorbed in the fuel ($\Sigma_{a2}\phi_2^{fuel}$), and the fraction of thermal neutrons absorbed in the entire cell ($\Sigma_{a2}\phi_2^{cell}$). Following is a summary of biases of LATTICE relative to ESP and standard deviations:

Quantity	Bias	Standard Deviation
k_∞	0.00228	0.0108
$\nu\Sigma_{f2}\phi_2$	0.000369	0.0130
$\Sigma_{a1}\phi_1^{fuel}$	-0.0239	0.0222
$\Sigma_{a2}\phi_2^{fuel}$	0.00452	0.0143
$\Sigma_{a2}\phi_2^{cell}$	0.00415	0.00734

The bias was calculated as $[(\Sigma\ X_{LAT}/X_{ESP})/N] - 1.0$, where X is the quantity of interest. The standard deviation is that of the ratio X_{LAT}/X_{ESP} for the 15 cases. The largest bias is in the absorption in the fuel of neutrons with energies above 1.855 eV. Because these systems are thermal, there is relatively little

TABLE 2.2-1

REACTION RATE COMPARISONS

Critical No.	Code	k_∞	$\nu\Sigma_{f2}\phi_2$	fuel $\Sigma_{a1}\phi_1$	fuel $\Sigma_{a2}\phi_2$	cell $\Sigma_{a2}\phi_2$
1	ESP	1.1782±.0034	0.9420	0.3527	0.5288	0.6359
	LAT	1.1710	0.9218	0.3595	0.5203	0.6264
2	ESP	1.2012±.0027	0.9983	0.3098	0.5593	0.6782
	LAT	1.2063	1.0022	0.2976	0.5638	0.6899
3	ESP	1.2323±.0033	1.0674	0.2482	0.5969	0.7413
	LAT	1.2273	1.0608	0.2450	0.5951	0.7439
4	ESP	1.2289±.0023	1.1234	0.1585	0.6264	0.8320
	LAT	1.2187	1.1158	0.1534	0.6234	0.8375
5	ESP	1.2108±.0029	1.1204	0.1342	0.6244	0.8571
	LAT	1.1979	1.1105	0.1306	0.6200	0.8607
6	ESP	1.1821±.0025	1.1035	0.1147	0.6144	0.8765
	LAT	1.1661	1.0928	0.1097	0.6096	0.8820
9	ESP	1.3413±.0033	1.1653	0.2361	0.6281	0.7550
	LAT	1.3322	1.1552	0.2339	0.6243	0.7557
15	ESP	1.0488±.0031	0.7718	0.3462	0.4154	0.6280
	LAT	1.0686	0.7833	0.3448	0.4234	0.6289
16	ESP	0.9933±.0036	0.8273	0.2403	0.4700	0.7448
	LAT	0.9964	0.8329	0.2355	0.4748	0.7467
17	ESP	0.9842±.0039	0.8085	0.2553	0.5127	0.7225
	LAT	1.0065	0.8358	0.2446	0.5341	0.7336
18	ESP	1.0008±.0035	0.9070	0.1221	0.5208	0.8624
	LAT	1.0026	0.9162	0.1143	0.5298	0.8704
19	ESP	1.0022±.0036	0.9066	0.1217	0.5196	0.8626
	LAT	1.0042	0.9148	0.1165	0.5283	0.8678
21	ESP	1.3637±.0033	1.1426	0.3127	0.6305	0.6831
	LAT	1.3766	1.1425	0.3096	0.6325	0.6844
22	ESP	1.1856±.0025	0.9103	0.3929	0.5045	0.5942
	LAT	1.1970	0.9052	0.3884	0.5038	0.5968
23	ESP	1.3076±.0028	1.0302	0.3915	0.5701	0.6051
	LAT	1.3253	1.0268	0.3896	0.5705	0.6042

absorption of fast neutrons and therefore greater statistical uncertainty in the Monte Carlo calculation. There is no apparent trend in cases 1 through 6, for which only the H/M ratio was varied. For k_∞ and the thermal neutron reaction rates, the small biases and standard deviations demonstrate the acceptability of the basic physics methods utilized in the LATTICE code.

2.3 ISOTOPIC COMPARISON

LATTICE results were compared to isotopic measurements made at the end of the first cycle of the Yankee-Rowe PWR (Reference 2-8). The isotopics were calculated for a single pin in an asymptotic spectrum; input data was generated using design information in Reference 2-9. The calculated concentrations and the experimental data were converted to isotopic ratios for the comparison. The results are plotted in Figures 2.3-1 through 2.3-6.

Agreement is excellent except that the Pu-242/Pu-241 ratio is underpredicted. This result has been reported by others (References 2-10 and 2-11) and is probably caused by an error in the ENDF Pu-242 cross section. Since Pu-242 is unimportant relative to the other fuel nuclides, the uncertainty in its cross section has insignificant effect on LATTICE calculations of physics parameters.

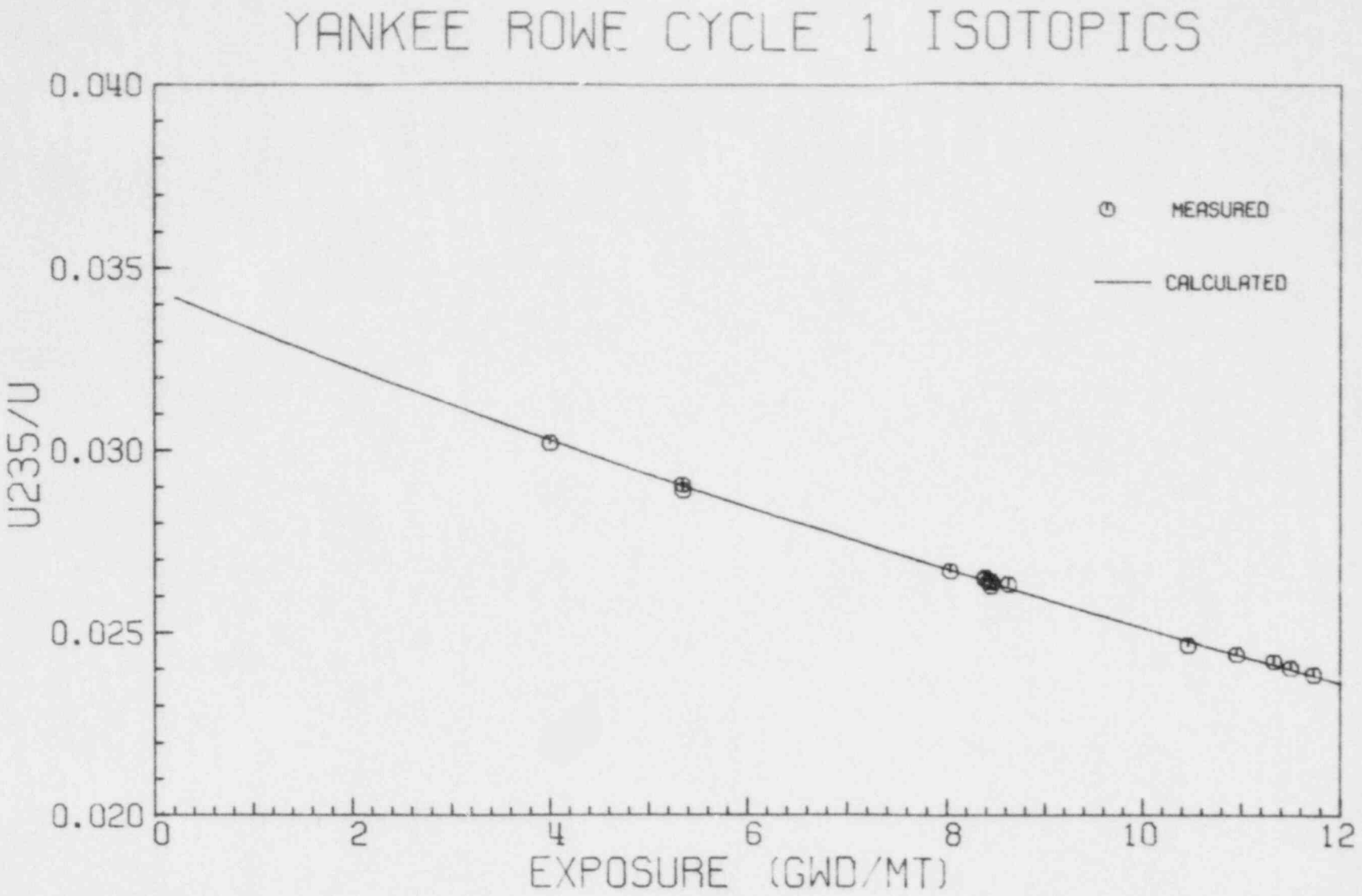
YANKEE ROWE CYCLE 1 ISOTOPICS
0.040
0.035
0.030
0.025
0.020
U235/U
0
2
4
6
8
10
12
EXPOSURE (GWD/MT)
MEASURED
CALCULATED

Figure 2.3-1

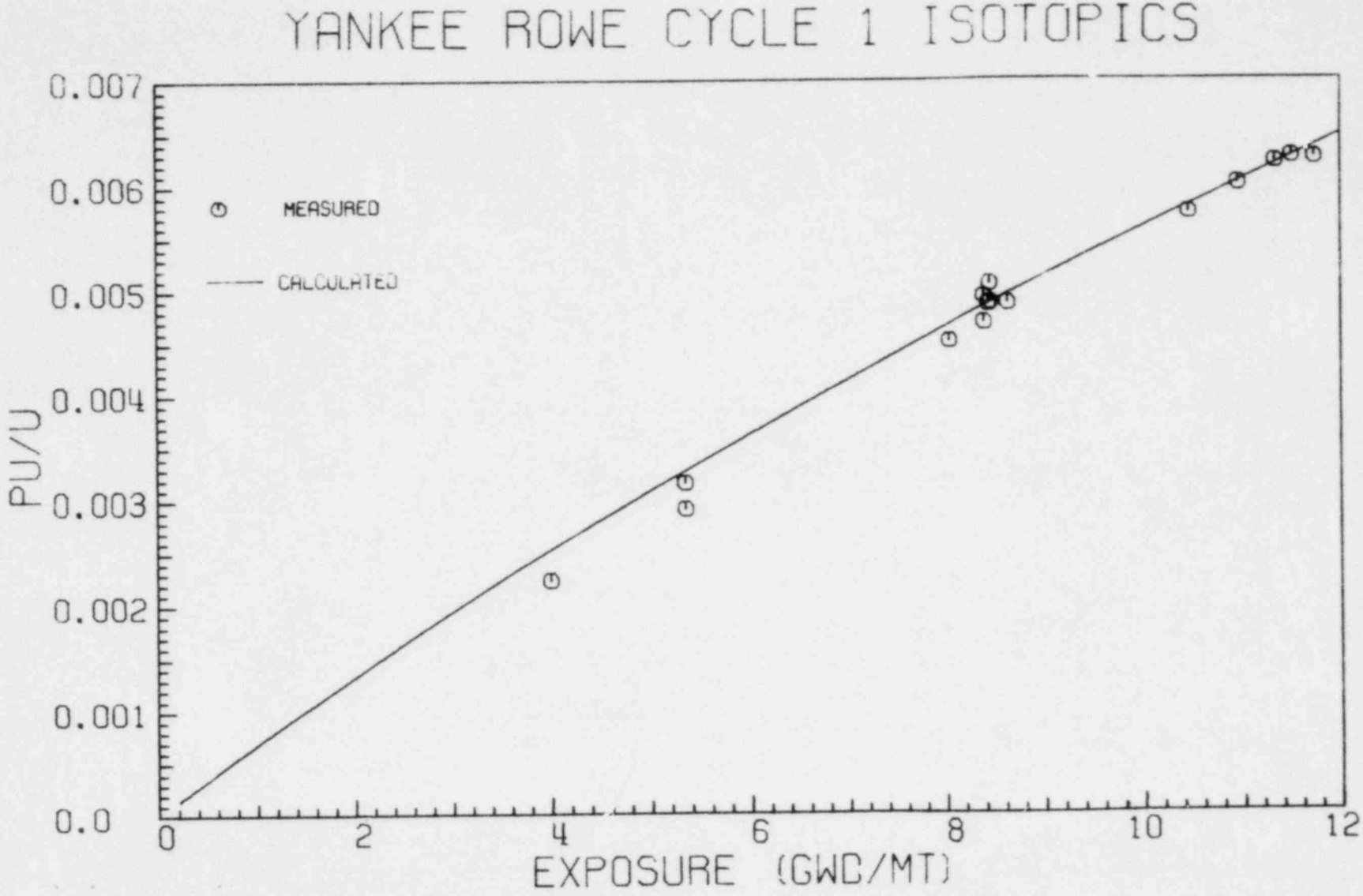
YANKEE ROWE CYCLE 1 ISOTOPICS
MEASURED
CALCULATED
PU/U
0.0
0.001
0.002
0.003
0.004
0.005
0.006
0.007
0
2
4
6
8
10
12
EXPOSURE (GWD/MT)

Figure 2.3-2

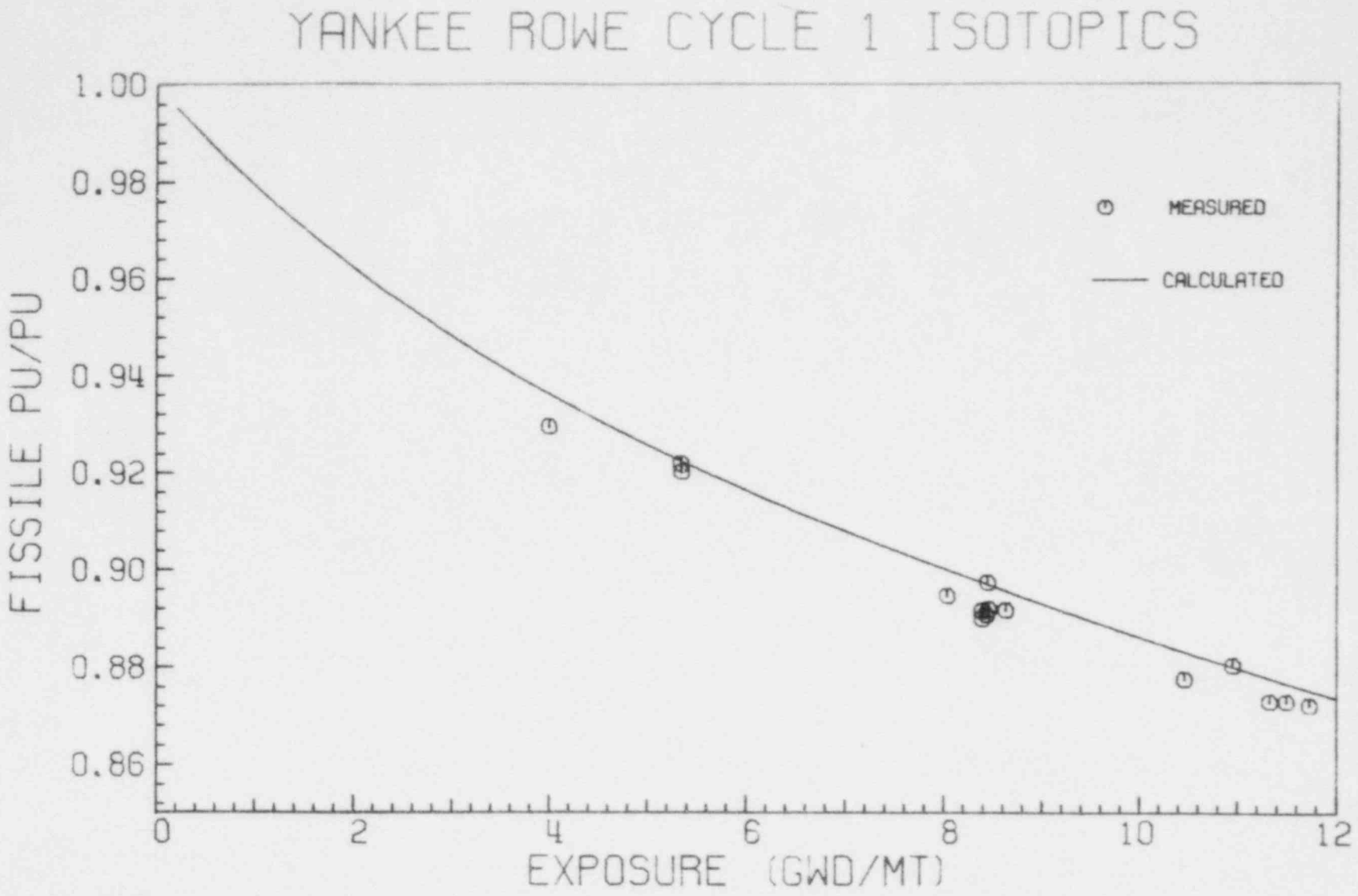
YANKEE ROWE CYCLE 1 ISOTOPICS
FISSILE PU/PU
1.00
0.98
0.96
0.94
0.92
0.90
0.88
0.86
0
2
4
6
8
10
12
EXPOSURE (GWD/MT)
MEASURED
CALCULATED

Figure 2.3-3

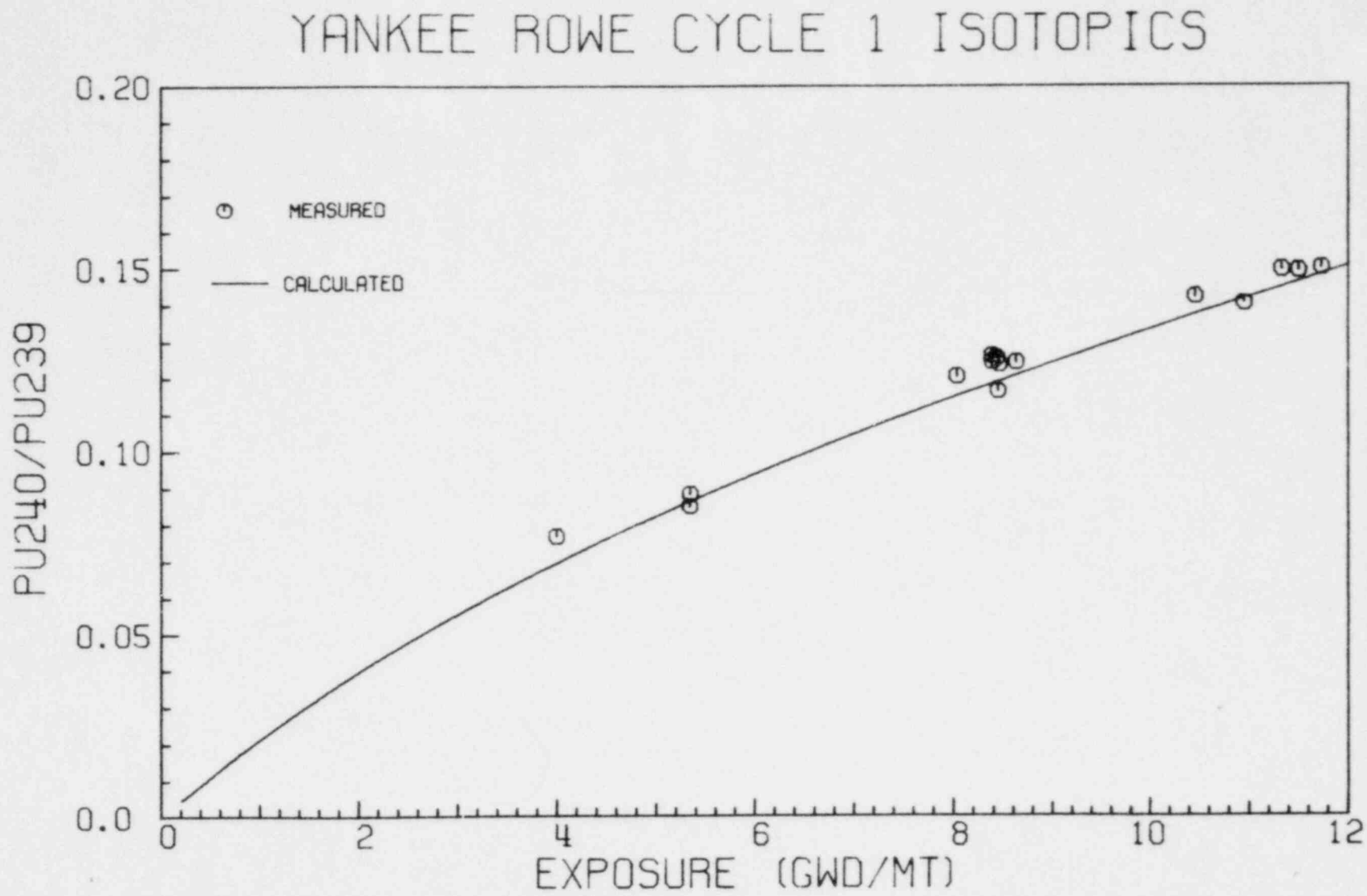
YANKEE ROWE CYCLE 1 ISOTOPICS
MEASURED
CALCULATED
PU240/PU239
0.20
0.15
0.10
0.05
0.0
0
2
4
6
8
10
12
EXPOSURE (GWD/MT)

Figure 2.3-4

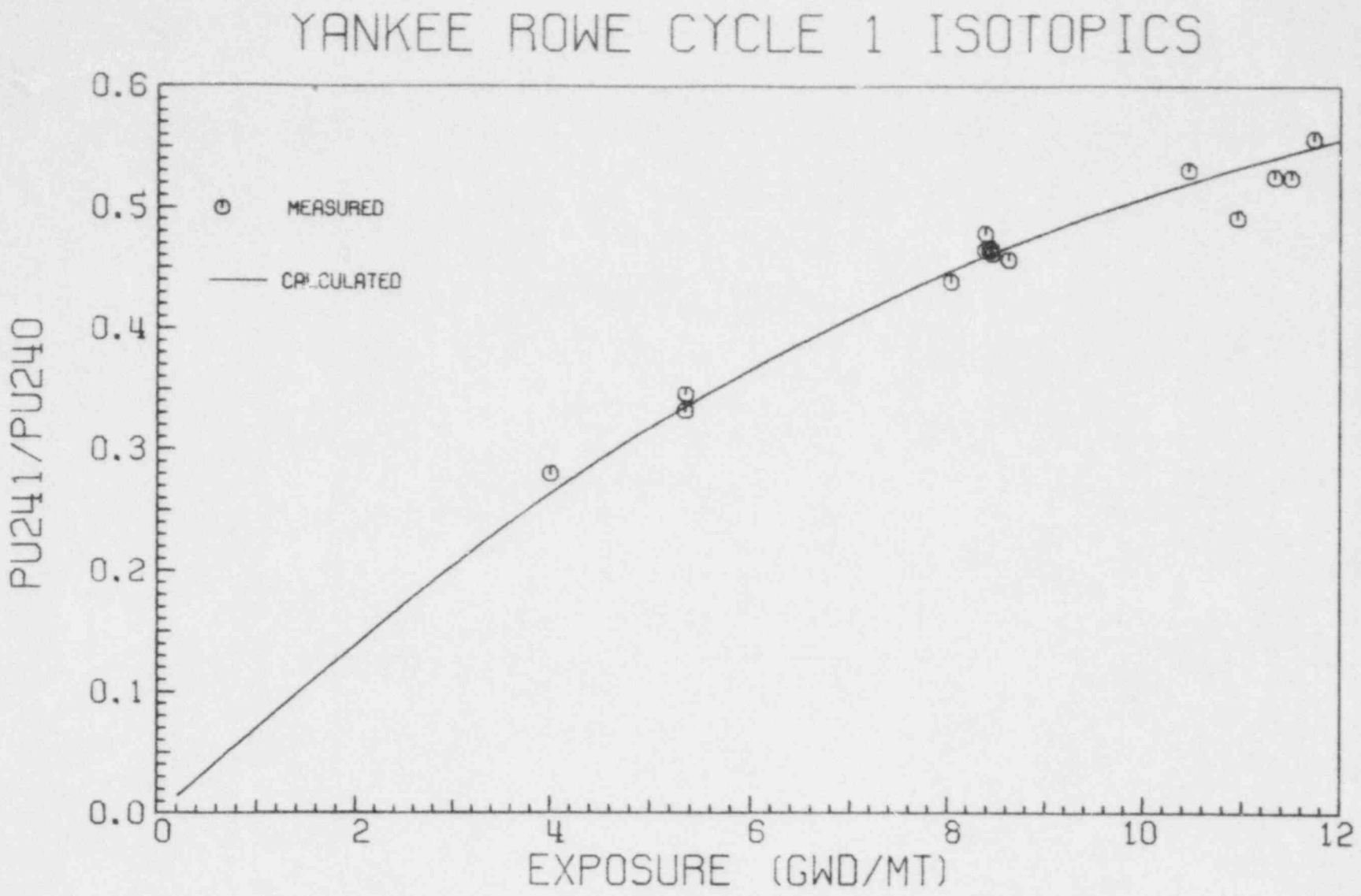
YANKEE ROWE CYCLE 1 ISOTOPICS
MEASURED
CALCULATED
PU241/PU240
EXPOSURE (GWD/MT)
0.0
0.1
0.2
0.3
0.4
0.5
0.6
0
2
4
6
8
10
12

Figure 2.3-5

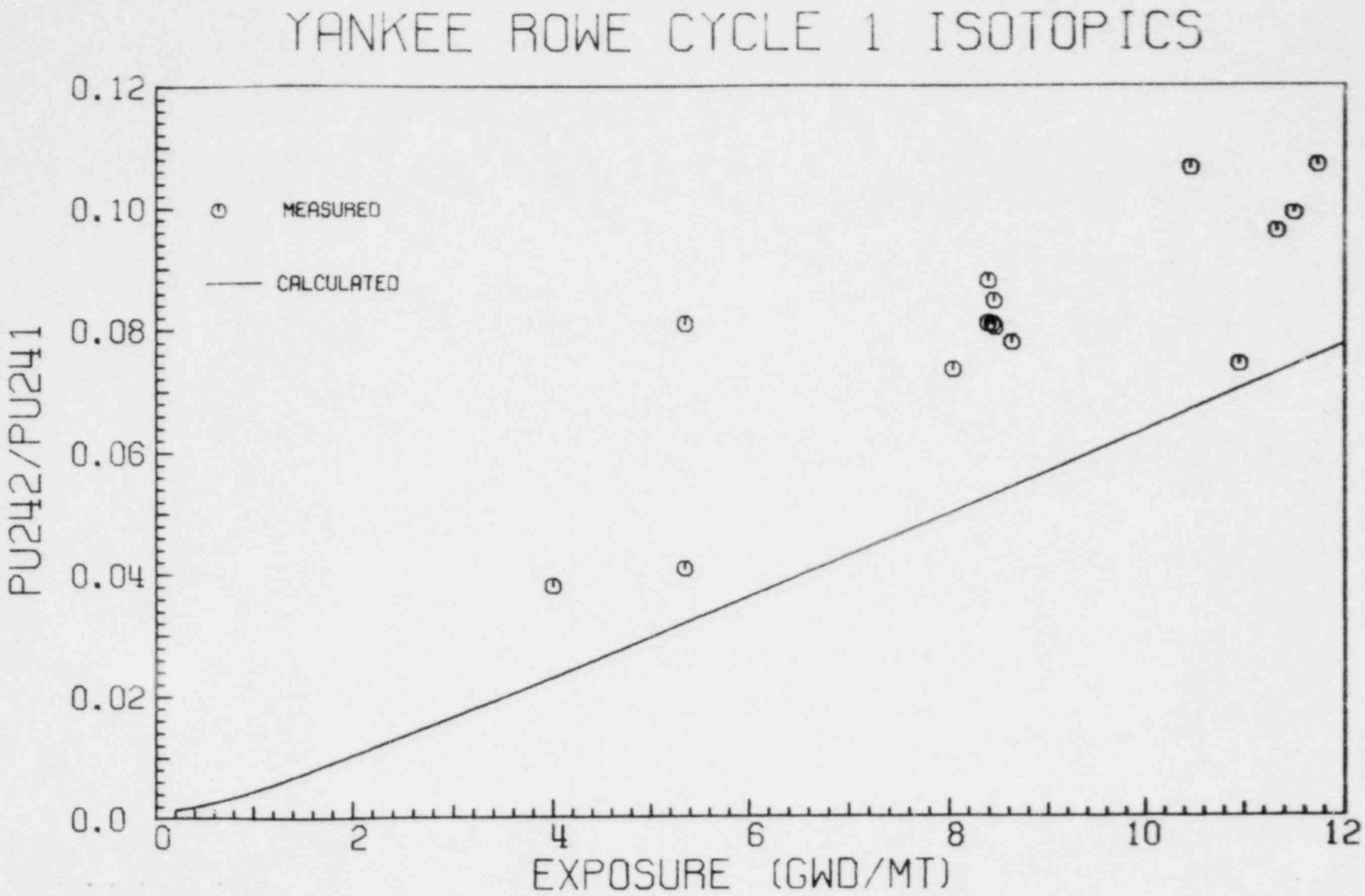
YANKEE ROWE CYCLE 1 ISOTOPICS
MEASURED
CALCULATED
PU242/PU241
0.0
0.02
0.04
0.06
0.08
0.10
0.12
0
2
4
6
8
10
12
EXPOSURE (GWD/MT)

Figure 2.3-6

CHAPTER 2 REFERENCES

1. L. E. Strawbridge and R. F. Barry, "Criticality Calculations for Uniform Water-Moderated Lattices," Nucl. Sci. Eng., Vol. 23, pp. 58-73, 1965.

2. D. F. Newman, "Measurement of k_∞ and Relative Reaction Rates in an H_2O-Moderated UO_2-PuO_2 Particulate Fueled Lattice," Nuc. Tech., Vol. 15, pp. 192-208, 1972.

3. M. N. Baldwin, et. al., "Physics Verification Program, Part III, Tasks 2 and 3, Final Report," BAW-3647-16, 1970.

4. A. R. Boynton, et. al., "High Conversion Critical Experiments," ANL-7203, 1967.

5. D. C. Baller, "The FAIM Code, A Multigroup, One-Dimensional Diffusion Equation Code," AMTD-118, 1962.

6. S. N. Cramer, et. al., "ESP: A General Monte Carlo Reactor Analysis Code," ORNL-TM-3164, 1972.

7. H. C. Honeck and D. R. Finch, "FLANGE II (Version 71-1): A Code to Process Thermal Neutron Data from an ENDF/B Tape," DP-1278, 1971.

8. J. Jedruch and R. J. Nodvik, "Experimentally Determined Burnup and Spent Fuel Composition of Yankee Core I," WCAP-6071, 1965.

9. H. W. Graves, Jr., R. F. Janz, and C. G. Poncelet, "The Nuclear Design of the Yankee Core," YAEC-136, 1961.

10. W. J. Eich and M. L. Kennedy, "EPRI-CELL Isotopics Benchmarking," ARMP System Documentation, Part I, Chapter 3, Electric Power Research Institute, 1976.

11. C. L. Martin, "Lattice Physics Methods Verification," NEDO-20939, 1976.

12. M. N. Baldwin and G. T. Fairburn, "Physics Verification Program Part III, Tasks 5 and 6, Quarterly Technical Report, January-March 1971," BAW-3647-21, 1971.

3. BUNDLE PHYSICS

For the verification of the lattice physics analysis method (computer code LATTICE) applied to typical BWR bundles, comparisons were made both to measured data and to results calculated by other computer codes which employ more exact physics models, geometric models, and cross section representations. Because of a lack of critical experiments in the public domain, reliance for verification of bundle reactivity is placed on comparisons to the ESP Monte Carlo reactor analysis code (Reference 3-1). Of course, the best evidence that LATTICE calculates bundle physics acceptably is the results obtained from the CORE simulator, which are discussed in Chapter 4. For local power distributions, comparisons are presented for one 8 x 8 bundle and three 7 x 7 bundles at a total of seven axial positions to the gamma scan measurements made at end-of-cycle 2 at Quad Cities unit 1 (Reference 3-2). The LATTICE calculation of the local power distribution for unexposed fuel is verified by comparison to results from the ESP Monte Carlo code and the CPM collision probability method code (Reference 3-3). Comparisons are given for eight 7 x 7 bundles and two 8 x 8 bundles. Results are presented only at 40 percent in-channel steam voids for most cases, but results are included at 0 and 80 percent in-channel steam voids for one of the 7 x 7 assemblies. Following is a description of the bundles for which comparisons are made against calculated data.

Type	Description
A	7 x 7 with an average enrichment of 2.5 weight percent. The first cut from the bottom of the bundle labelled Type 3 on page 6 of Reference 3-4.
B	7 x 7 with an average enrichment of 2.5 weight percent. The second cut from the bottom of the bundle labelled Type 3 on page 6 of Reference 3-4.
C	7 x 7 with an average enrichment of 2.5 weight percent. The third cut from the bottom of the bundle labelled Type 3 on page 6 of Reference 3-4.
D	7 x 7 with an average enrichment of 1.1 weight percent. The bundle labelled Type 1 on page 6 of Reference 3-4.
E	Typical of 8 x 8 designs with one water rod. Has an average enrichment of 2.2 weight percent.
F	Typical of 8 x 8 designs with two water rods. Has an average enrichment of 3.0 weight percent.
G	7 x 7 with an average enrichment of 2.3 weight percent. See page A-2 of Reference 3-5.
H	7 x 7 with an average enrichment of 2.5 weight percent. The first cut from the bottom of the bundle labelled Type 2 on page 6 of Reference 3-4.
I	7 x 7 with an average enrichment of 2.5 weight percent. The second cut from the bottom of the bundle labelled Type 2 on page 6 of Reference 3-4.
J	7 x 7 mixed oxide bundle, labelled Assembly Type 5 on page A-6 of Reference 3-5.

3.1 REACTIVITY COMPARISONS

Monte Carlo calculations of beginning-of-life reactivity have been made for five 7 x 7 bundles and two 8 x 8 bundles at a total of 23 different conditions, using the ESP reactor analysis code. Reactivity differences were calculated as the logarithm of the ratio of k_∞ values. As can be seen from Table 3.1-1, the agreement is good. The average bias of LATTICE relative to ESP

TABLE 3.1-1

Comparisons of k_∞ at BOL as Calculated by LATTICE and ESP

Fuel Type	In-channel Voids	k_∞ (LAT)	k_∞ (ESP)	Reactivity Difference
A	cold	1.1463	1.1469±.0046	-.0005
	cold*	0.9555	0.9541±.0055	.0015
	0	1.1487	1.1375±.0017	.0098
	40	1.1315	1.1268±.0016	.0042
	80	1.0855	1.0854±.0016	.0001
B	40	1.0700	1.0619±.0039	.0076
C	0	1.0435	1.0216±.0049	.0212
	40	1.0229	1.0105±.0050	.0122
	80	0.9885	0.9662±.0058	.0228
D	0	1.0416	1.0385±.0038	.0030
	20	1.0463	1.0445±.0043	.0017
	40	1.0496	1.0518±.0035	-.0021
	60	1.0472	1.0475±.0055	-.0003
	80	1.0351	1.0338±.0066	.0013
E	0	1.0824	1.0640±.0039	.0171
	40	1.0688	1.0626±.0017	.0058
	70	1.0430	1.0451±.0036	-.0020
F	0	1.0771	1.0597±.0033	.0163
	40	1.0596	1.0521±.0017	.0071
	80	1.0222	1.0228±.0038	-.0006
I	0	1.1028	1.0829±.0051	.0182
	40	1.0857	1.0741±.0033	.0107
	80	1.0477	1.0327±.0045	.0144
			Bias =	.0074
			Standard Deviation =	.0079

*controlled

is 0.0074 with a standard deviation of 0.0079. The reactivity differences for the 7 x 7 bundles show no apparent trend with in-channel water density. For the 8 x 8 bundles (Types E and F), the Monte Carlo code shows a slower variation with water density than does the LATTICE design method. Results for the Type J 7 x 7 mixed oxide bundle at 40 percent in-channel steam voids have been obtained for a vendor's Monte Carlo code (1.0763±0.0014, Reference 3-6) and lattice physics design method (1.0884, Reference 3-6), and the CASMO code (1.077, References 3-7 and 3-8). These results compare to 1.0857±0.0012 and 1.0875 from ESP and LATTICE, respectively. This is excellent agreement for a mixed oxide bundle heavily loaded with gadolinia.

Comparisons of the reactivity worth of the burnable poison calculated by LATTICE and ESP were made for bundle Type E at cold conditions, and at 0, 40, and 70 percent in-channel voids. The following results, expressed in percent, were obtained:

	COLD	0	40	70
ESP	14.5	18.2	18.3	18.4
LAT	15.4	18.8	18.8	18.5

These results for bundle reactivity and for the worth of burnable poison demonstrate the adequacy of the LATTICE calculation of reactivity for clean bundles; results discussed in Section 2.3 and Chapter 4 demonstrate the adequacy of LATTICE depletion methods.

3.2 LOCAL POWER DISTRIBUTION COMPARISONS

Comparisons to demonstrate the adequacy of the LATTICE calculation of the local power distribution have been made against gamma scan measurements taken at end-of-cycle 2 of Quad Cities unit 1. Comparisons are presented in Subsection 3.2.2 for four bundles at a total of seven axial positions, at average in-channel voids ranging from 10 to 70 percent. Bundles were selected for benchmarking which did not exhibit large gradients across the bundle to facilitate direct comparison to single bundle, infinite lattice calculations. Additional evidence in the form of comparisons to results from more sophisticated codes are presented in Subsection 3.2.1. These numerical comparisons are for unexposed fuel. The LATTICE results were generated utilizing a standard BWR representation including four neutron energy groups in the two-dimensional diffusion theory calculation of the local power distribution, with transport-corrected cross sections for the explicitly represented fuel pins and associated moderator regions.

3.2.1 Unexposed Bundles

Beginning-of-life local power distributions calculated by LATTICE have been compared to distributions obtained from the ESP Monte Carlo reactor analysis code (Reference 3-1) and the CPM collision probability method code (Reference 3-3) which is distributed by the Electric Power Research Institute. ESP, which is essentially a continuous energy code, is capable of utilizing version I, II or III of the ENDF/B neutron cross section data. For these comparisons, over 6,000 neutron energy groups for the fuel media were used, with basic cross sections coming from ENDF/B-III for all materials except

natural zirconium and hydrogen bound in water. For natural zirconium, ENDF/B-I data was used. For hydrogen bound in water, a modification to the ENDF/B-I data for free hydrogen was used. This modification was made by processing the ENDF/B-II scattering law data for water using FLANGE-II (Reference 3-9), and setting the scattering cross section below 1.0 eV for free hydrogen to the FLANGE-II values. This was done at temperatures of 300 and 558°K. From 90,000 to 100,000 neutron histories were processed for each case for which local power distributions are given. CPM used 69 neutron energy groups in spectrum calculations and 20 groups (9 thermal) in the two-dimensional collision probability calculation of the local power distribution. Cross section libraries based on ENDF/B-III and distributed by EPRI were utilized. Comparisons are presented for eight 7 x 7 fuel designs at 40 percent in-channel voids and for two 8 x 8 fuel designs at 40 percent in-channel voids. For the 7 x 7 Type A bundle, additional comparisons are given for 0 and 80 percent in-channel voids.

For the Quad Cities mixed oxide bundle (Type J in this report), comparisons are made not only for LATTICE, ESP, and CPM, which were run by TVA, but also to results from a vendor's Monte Carlo code and lattice physics design code (Reference 3-6), and to CASMO (Reference 3-7). The peak pin powers calculated by the various codes for this bundle are as follows:

CASMO	1.203
CPM	1.243
ESP	1.201
Vendor Design Method	1.21
Vendor Monte Carlo	1.26
LATTICE	1.216

The pin-by-pin distributions for this bundle are presented in Figure 3.2-1. Even though this bundle is very different from conventional designs, the power distributions follow the same general trends. This comparison serves to strengthen the case for the use of CPM and ESP as benchmarks. The root-mean-square (RMS) differences of CPM relative to the other codes are 2.5, 3.1, 3.0, and 4.6 percent respectively. The RMS differences of ESP relative to the other codes are 2.4, 3.1, 3.6, and 4.8 percent respectively. The agreement of LATTICE with the other codes is good (3.3, 4.4, 4.2, 4.2, and 4.3 percent respectively) but this is fortuitous since LATTICE is primarily intended for analyses of standard design UO_2 bundles, and a judicious choice of input was necessary to obtain these results. This bundle, an island design with black burnable poison UO_2 pins located between black mixed oxide pins and gray UO_2 pins, has five different UO_2 enrichments and four different plutonium concentrations, and is therefore a difficult bundle to analyze accurately. Figure 3.2-1 is presented mainly to demonstrate the suitability of ESP and CPM as benchmark codes for calculating local power distributions at beginning of life. Reference 3-10 presents information supporting the CPM calculation of local power distribution. Data presented in the remainder of this subsection confirms that LATTICE calculates the local power distribution with acceptable accuracy for bundle designs typical of those commercially available.

Figures 3.2-2, 3.2-3, and 3.2-4 are comparisons of LATTICE local power maps to those calculated by ESP and CPM at 0, 40, and 80 percent in-channel steam voids for bundle Type A. The

W-W

1.165	CASMO
1.138	CPM
1.171	ESP
1.19	Vendor Design Method
1.25	Vendor Monte Carlo
1.172	LATTICE

1.203	1.039					
1.207	1.018					
1.199	1.005					
1.21	1.05					
1.26	1.06					
1.215	1.061					
1.063	1.047	0.282				
1.070	1.055	0.294				
1.060	1.046	0.246				
1.07	1.08	0.30				
1.08	1.08	0.30				
1.061	1.085	0.223				
1.114	1.172	1.053	0.544	1.050		
1.119	1.175	1.055	0.535	1.091		
1.110	1.153	1.100	0.569	1.048		
1.12	1.19	1.07	0.55	1.00		
1.12	1.19	1.05	0.56	0.99		
1.110	1.216	0.986	0.598	1.010		
1.104	1.158	1.032	1.050	0.239		
1.106	1.155	1.037	1.091	0.241		
1.085	1.129	1.067	1.087	0.204		
1.10	1.17	1.05	1.05	0.25		
1.12	1.17	1.03	1.04	0.25		
1.100	1.201	0.983	1.072	0.201		
1.164	1.012	0.278	1.174	1.178	0.268	
1.159	0.994	0.282	1.229	1.243	0.268	
1.146	0.986	0.242	1.201	1.201	0.232	
1.16	1.03	0.30	1.17	1.17	0.28	
1.17	1.03	0.29	1.13	1.12	0.28	
1.161	1.050	0.220	1.157	1.179	0.215	
1.162	1.005	0.983	1.064	1.035	1.115	1.133
1.126	0.979	0.977	1.045	1.013	1.097	1.080
1.171	0.984	1.012	1.079	1.037	1.137	1.151
1.17	0.97	0.98	1.04	1.00	1.06	1.09
1.19	1.00	0.99	1.03	1.00	1.08	1.04
1.149	1.004	1.004	1.089	1.054	1.140	1.111

Figure 3.2-1

Local Power Distribution for the Quad Cities 1 Cycle 2, Central Mixed Oxide Bundle at 40% In-channel Steam Voids

W-W

Figure 3.2-2

1.079	CPM					
1.114	ESP					
1.073	LATTICE					
1.153	1.022					
1.113	0.976					
1.139	1.035					
1.042	1.256	1.024				
1.046	1.203	1.039				
1.029	1.232	1.035				
1.104	1.149	0.892	0.242			
1.106	1.128	0.885	0.211			
1.078	1.138	0.926	0.216			
1.082	1.097	0.838	0.790	0.872		
1.111	1.060	0.859	0.823	0.897		
1.062	1.105	0.883	0.838	0.895		
1.116	1.109	0.263	0.878	0.997	1.122	
1.115	1.093	0.239	0.869	0.983	1.103	
1.097	1.133	0.247	0.909	1.004	1.112	
1.080	0.965	1.138	1.134	1.225	0.965	1.096
1.127	1.005	1.157	1.149	1.224	0.958	1.160
1.096	0.976	1.135	1.119	1.179	0.944	1.096

Local Power Distribution for a Type A Bundle at 0% In-channel Steam Voids

RMS(ESP-CPM) = 2.8%
RMS(ESP-LAT) = 3.1%
RMS(CPM-LAT) = 2.4%

W-W

Figure 3.2-3

1.115 CPM
1.148 ESP
1.107 LATTICE

Local Power Distribution for a Type A Bundle
at 40% In-channel Steam Voids

RMS(ESP-CPM) = 3.1%
RMS(ESP-LAT) = 3.9%
RMS(CPM-LAT) = 2.5%

1.182	1.040					
1.170	1.039					
1.166	1.061					
1.059	1.271	1.030				
1.054	1.210	1.002				
1.042	1.253	1.049				
1.115	1.158	0.900	0.287			
1.095	1.114	0.893	0.256			
1.080	1.149	0.936	0.258			
1.092	1.108	0.844	0.780	0.840		
1.103	1.077	0.861	0.789	0.845		
1.061	1.114	0.886	0.829	0.870		
1.129	1.123	0.317	0.863	0.955	1.066	
1.133	1.112	0.290	0.848	0.924	1.039	
1.098	1.146	0.297	0.896	0.976	1.076	
1.088	0.966	1.136	1.107	1.175	0.920	1.044
1.148	0.996	1.198	1.145	1.191	0.932	1.105
1.100	0.972	1.123	1.088	1.137	0.911	1.063

W-W

Figure 3.2-4

1.128	CPM					
1.214	ESP					
1.085	LATTICE					
1.191	1.055					
1.216	1.041					
1.150	1.077					
1.065	1.297	1.063				
1.078	1.247	1.008				
1.031	1.279	1.098				
1.116	1.184	0.941	0.368			
1.112	1.108	0.909	0.321			
1.062	1.175	0.993	0.345			
1.092	1.133	0.878	0.795	0.822		
1.082	1.107	0.854	0.762	0.805		
1.038	1.137	0.928	0.863	0.875		
1.123	1.140	0.410	0.860	0.913	0.992	
1.144	1.137	0.369	0.824	0.895	0.996	
1.067	1.163	0.383	0.909	0.964	1.033	
1.071	0.954	1.125	1.069	1.104	0.848	0.953
1.164	1.004	1.173	1.093	1.127	0.883	1.037
1.056	0.955	1.114	1.060	1.079	0.853	0.977

Local Power Distribution for a Type A Bundle
at 80% In-channel Steam Voids

RMS(ESP-CPM) = 4.1%
RMS(ESP-LAT) = 6.3%
RMS(CPM-LAT) = 3.7%

agreement lessens as the void fraction increases, as shown by the following table of RMS differences.

	0% stm	40% stm	80% stm
LAT-CPM	2.4	2.5	3.7
LAT-ESP	3.1	3.9	6.3
CPM-ESP	2.8	3.1	4.1

Figure 3.2-5 is a comparison of the local power map produced by LATTICE to that calculated by CPM for the Type B bundle design at 40 percent in-channel voids. The RMS difference is 3.3 percent. The slightly worse agreement is because Type B has one more gadolinia rod than Type A, and is therefore slightly more nonuniform. Since LATTICE somewhat underpredicts the power in the burnable poison rods, increasing the number of such rods increases the RMS difference. LATTICE evidently does not significantly underpredict absorption in the burnable poison rods, since good agreement with Monte Carlo results is obtained (see Table 3.1-1) and since the core simulator well predicts core reactivity versus core average burnup (see Figures 5.2-1 and 5.2-2). Comparisons of the worth of the burnable poison rods in the Type E bundle are presented in Section 3.1.

Figure 3.2-6 is a comparison of the local power map calculated with LATTICE to CPM results for the Type C bundle design at 40 percent in-channel void fraction. The RMS difference is 3.7 percent. Again, Type C is slightly worse than Type B because of the addition of another gadolinia rod.

A comparison of the local power map from LATTICE to ESP results for the Type D bundle design at 40 percent in-channel voids is given in Figure 3.2-7. The Type D bundle, average

W-W

Figure 3.2-5

1.019 CPM
1.029 LATTICE

Local Power Distribution for a Type B Bundle at 40% In-channel Steam Voids

1.031 0.247
1.051 0.258

RMS(CPM-LAT) = 3.6%

0.977	1.078	0.932				
0.982	1.134	0.993				
1.097	1.119	0.887	0.297			
1.069	1.131	0.935	0.269			
1.121	1.128	0.869	0.823	0.899		
1.083	1.138	0.914	0.866	0.917		
1.187	1.173	0.341	0.920	1.027	1.151	
1.142	1.194	0.313	0.946	1.036	1.146	
1.157	1.029	1.218	1.195	1.277	1.003	1.141
1.153	1.022	1.185	1.153	1.209	0.972	1.136

W-W

Figure 3.2-6

1.097	CPM					
1.088	LATTICE					
1.109	0.264					
1.110	0.274					
1.047	1.146	0.985				
1.036	1.193	1.041				
1.171	1.182	0.929	0.308			
1.124	1.187	0.977	0.277			
1.191	1.186	0.898	0.816	0.833		
1.136	1.191	0.948	0.874	0.876		
1.257	1.227	0.354	0.894	0.894	0.336	
1.195	1.247	0.321	0.938	0.940	0.321	
1.221	1.077	1.248	1.174	1.175	0.87/	1.034
1.206	1.063	1.214	1.141	1.132	0.866	1.039

Local Power Distribution for a Type C Bundle at 40% In-channel Steam Voids

RMS(CPM-LAT) = 3.7%

W-W

Figure 3.2-7

0.996	ESP					
0.916	LATTICE					
1.428	1.227					
1.383	1.208					
1.333	1.149	0.608				
1.292	1.140	0.644				
1.274	0.663	0.621	0.605			
1.257	0.658	0.634	0.569			
1.234	1.049	0.599	0.590	0.642		
1.251	1.107	0.631	0.622	0.619		
1.255	1.087	0.610	0.603	0.612	0.994	
1.280	1.128	0.638	0.627	0.624	1.065	
1.404	1.204	1.150	1.171	1.097	1.160	1.333
1.361	1.216	1.150	1.122	1.119	1.143	1.218

Local Power Distribution for a Type D Bundle at 40% In-channel Steam Voids

RMS(ESP-LAT) = 3.7%

enrichment 1.1 weight percent, was represented in the ESP run as one assembly in a 4-assembly module; the other three bundles were Type A bundles which have an average enrichment of 2.5 weight percent. The resulting RMS difference is 3.7 percent, demonstrating that the effect of having neighboring bundles of different composition was insignificant.

Figure 3.2-8 is a comparison of the local power distribution calculated by LATTICE to one from ESP for the Type E bundle design at 40 percent in-channel void fraction. The RMS difference is 4.5 percent.

Figure 3.2-9 is a comparison of the LATTICE and ESP local power distributions for the Type F bundle at an average in-channel void fraction of 40 percent. The RMS difference between the distributions is 6.5 percent.

Figure 3.2-10 compares the LATTICE local power distribution to CPM results (Reference 3-8) for the Type G bundle at an average in-channel void fraction of 40 percent. The RMS difference between the maps is 3.0 percent.

LATTICE and CPM local power distributions are compared in Figure 3.2-11 for the Type H bundle at 40 percent in-channel voids. The resulting RMS difference is 2.7 percent.

Figure 3.2-12 is a comparison of LATTICE and CPM local power distributions for the Type I bundle at an in-channel void fraction of 40 percent. A RMS difference of 3.6 percent was obtained.

W-W

Figure 3.2-8

1.152 ESP
1.107 LATTICE

Local Power Distribution for Type E Bundle at 40% In-Channel Steam Voids

RMS(ESP-LAT) = 4.5%

1.177	1.168						
1.173	1.200						
1.046	0.995	1.052					
1.055	1.048	1.094					
1.210	1.158	0.901	0.246				
1.183	1.174	0.941	0.276				
1.189	1.061	0.836	0.797	0.0			
1.141	1.111	0.891	0.831	0.0			
1.202	1.061	0.251	0.818	0.805	0.249		
1.153	1.106	0.283	0.852	0.849	0.279		
1.047	1.192	0.980	0.945	0.918	0.922	1.019	
1.012	1.221	1.009	0.953	0.934	0.943	1.072	
1.184	1.162	1.046	1.222	1.190	1.184	1.056	1.001
1.111	1.133	0.997	1.143	1.117	1.147	1.007	0.936

W-W

Figure 3.2-9

Local Power Distribution for a Type F Bundle at 40% In-channel Steam Voids

RMS(ESP-LAT) = 6.5%

1.084	ESP						
1.057	LATTICE						
1.129	1.127						
1.133	1.238						
1.160	0.948	0.342					
1.164	1.016	0.327					
1.072	1.086	0.953	1.157				
1.067	1.140	1.026	1.168				
1.189	1.062	1.071	0.0	1.053			
1.148	1.116	1.133	0.0	1.095			
1.131	0.339	0.918	1.008	0.962	0.857		
1.113	0.322	1.061	1.041	0.998	0.938		
1.237	1.089	0.264	0.997	0.986	0.256	1.018	
1.180	1.124	0.281	1.035	1.011	0.272	1.063	
1.233	1.128	1.202	1.169	1.139	1.141	1.196	1.238
1.145	1.067	1.163	1.091	1.061	1.061	1.070	1.040

W-W

Figure 3.2-10

1.179	CPM		Local Power Distribution for a Type G Bundle			
1.149	LATTICE		at 40% In-channel Steam Voids			
1.163	1.072		RMS(CPM-LAT) = 3.0%			
1.140	1.080					
1.040	1.123	0.321				
1.025	1.137	0.286				
1.167	1.076	0.839	0.793			
1.133	1.092	0.893	0.767			
1.166	1.101	0.882	0.761	0.778		
1.133	1.107	0.913	0.828	0.832		
1.225	1.176	0.927	0.310	0.836	0.967	
1.186	1.173	0.953	0.279	0.880	0.993	
1.148	1.088	1.147	1.018	1.055	1.163	1.067
1.118	1.075	1.134	1.029	1.054	1.142	1.048

W-W

Figure 3.2-11

1.096 CPM
1.090 LATTICE

Local Power Distribution for a Type H Bundle
at 40% In-channel Steam Voids

1.155 0.989
1.142 1.021

RMS(CPM-LAT) = 2.7%

1.034	1.171	0.326				
1.020	1.179	0.298				
1.099	1.114	0.870	0.771			
1.066	1.120	0.928	0.810			
1.091	1.106	0.863	0.848	0.892		
1.059	1.115	0.907	0.881	0.909		
1.138	1.134	0.324	0.897	0.993	1.100	
1.104	1.158	0.299	0.922	1.004	1.101	
1.101	0.980	1.160	1.138	1.212	0.948	1.075
1.109	0.984	1.142	1.110	1.161	0.930	1.084

W-W

Figure 3.2-12

1.150	CPM					
1.131	LATTICE					
1.210	1.033					
1.184	1.056					
1.080	1.219	0.340				
1.056	1.2 6	0.307				
1.145	1.151	0.869	0.733			
1.101	1.151	0.940	0.796			
1.135	1.139	0.853	0.768	0.322		
1.091	1.142	0.911	0.839	0.291		
1.182	1.168	0.330	0.862	0.915	1.058	
1.136	1.185	0.306	0.902	0.955	1.075	
1.143	1.012	1.183	1.138	1.199	0.942	1.076
1.142	1.008	1.160	1.113	1.154	0.928	1.088

Local Power Distribution for a Type I Bundle at 40% In-channel Steam Voids

RMS(CPM-LAT) = 3.6%

Table 3.2-1 compares peaking factors of the three codes LATTICE, ESP, and CPM. The bias of LATTICE relative to ESP is 0.1 percent, and the standard deviation is 2.2 percent. For LATTICE compared to CPM, the bias and standard deviation are -2.1 percent and 1.6 percent. Since 40 percent in-channel steam voids is most typical of core regions at peak power, the bias and standard deviation relative to both codes were calculated, with resulting values of -1.3 percent and 2.5 percent, respectively. All 7 x 7 cases were considered separately, yielding a bias of -1.1 percent and a standard deviation of 2.6 percent. For 8 x 8 bundles, values of -1.0 percent and 0.9 percent were obtained for the bias and standard deviation.

These RMS differences for local power maps and biases and standard deviations for peaking factors demonstrate that the LATTICE code adequately predicts local power distributions for typical BWR bundles at beginning of life. Comparisons to gamma scan measurements are presented in Subsection 3.2.2 to demonstrate that the LATTICE calculation of the local power is acceptable for exposed fuel.

TABLE 3.2-1

COMPARISON OF LOCAL PEAKING FACTORS

Type	Void Fraction	LATTICE	ESP	CPM
A	0	1.232	1.224	1.256
A	40	1.258	1.210	1.271
A	80	1.277	1.247	1.297
B	40	1.209	-	1.277
C	40	1.247	-	1.257
D	40	1.383	1.428	-
E	40	1.221	1.222	-
E	70	1.219	1.238	-
F	0	1.221	1.236	-
F	40	1.238	1.238	-
F	80	1.236	1.263	-
G	40	1.186	-	1.225
H	40	1.179	-	1.212
I	40	1.216	-	1.219

.2.2 Exposed Bundles

Local power maps generated by LATTICE have also been compared to rod-by-rod results from the 1976 Quad Cities unit 1 gamma scan (Reference 3-2). Table 3.2-2 lists the assemblies chosen for the analysis, covering a wide range of exposure and void fraction for several fuel designs. The exposures and exposure averaged void fractions were obtained from nodal edits of the Quad Cities end-of-cycle 2 CORE simulator case discussed in Subsection 4.1.4. Figures 3.2-13 through 3.2-19 compare the calculated and measured local power distributions. The measured powers were averaged for diagonally symmetric rods in order to further reduce experimental uncertainty. Root-mean-square (RMS) power differences and the bias in local peaking factors (maximum relative rod powers) are also listed in Table 3.2-2. General agreement is good except for the mixed oxide bundle which has a 4.9 percent RMS power difference. The local peaking factor in this assembly is overpredicted by 5.3 percent. LATTICE underestimates the local peaking factor in the UO_2 bundles by an average of 1.2 ± 1.5 percent relative to the gamma scan. The average RMS power difference is 2.4 percent for the UO_2 assemblies, which is comparable to the 3 percent uncertainty in the measured data (Reference 3-2). The power in gadolina bearing rods was also accurately predicted with a bias of -2.9 ± 2.6 percent.

TABLE 3.2-2

LOCAL POWER DISTRIBUTION COMPARISONS FOR EXPOSED BUNDLES

Bundle Label	Core Location	Fuel Design	Inches From Bottom	Exposure (GWD/MT)	Percent In-channel Voids	LPF Bias	Percent RMS Power Difference
CX-214	33-34	7 x 7 Initial 2.12 enr	57	20.606	37.8	-0.0056	2.7
			129	13.106	63.3	-0.0341	3.5
CX-672	15-36	7 x 7 Initial 2.12 enr	51	20.680	31.9	-0.0167	2.3
GEB-159	31-32	7 x 7 Reload MO_2	51	10.457	41.7	0.0532	4.9
GEH-002	13-36	8 x 8 Reload 2.50 enr	15	10.823	7.3	0.0091	1.6
			51	10.307	42.9	-0.0063	2.0
			129	6.199	69.8	-0.0168	2.5
					Average*	-0.0117	2.4
					Standard Deviation	0.0145	

*for UO_2 bundles only

W-W

Figure 3.2-13

1.064	Gamma Scan		EOC 2 Local Power Distribution for			
1.017	LATTICE		QC Bundle CX-214 at 57 Inches from Bottom of Core			
1.000	0.997					
0.963	0.999		RMS(SCAN-LAT) = 2.7%			
	0.940	1.019				
	0.959	0.992				
1.022	1.062	0.987				
0.979	1.054	0.987				
	1.041	0.972	0.968	0.936		
	1.058	0.990	0.962	0.962		
1.017	1.043	1.002	1.002	0.959	0.998	
0.997	1.039	1.034	0.953	1.006	1.034	
0.988	0.949		1.021		1.052	0.925
0.973	0.972		1.029		1.048	0.978

W-W

1.114
1.074

1.031
0.996

1.079
1.012

1.053
1.036

1.029
0.988

Gamma Scan
LATTICE

1.034
1.039

0.965 1.005
0.967 0.972

1.059 0.939
1.076 0.969

1.050 0.942 0.898 0.891
1.073 0.965 0.921 0.915

1.054 0.963 0.962 0.925 0.969
1.066 1.021 0.901 0.969 1.005

1.000 1.056 1.018 0.946
0.987 1.020 1.047 0.969

Figure 3.2-14

EOC 2 Local Power Distribution for QC Bundle CX-214 at 129 Inches from Bottom of Core

RMS(SCAN-LAT) = 3.5%

W-W

0.994 Gamma Scan
1.008 LATTICE

0.935 0.944
0.955 0.992

0.919 1.039
0.953 1.012

0.981 1.072 0.989
0.973 1.053 0.988

1.075 0.985 0.982
1.057 0.993 0.967

0.984 1.049 1.033 1.019 0.990 1.010
0.992 1.039 1.037 0.961 1.012 1.039

0.963 0.947 1.028 1.043 1.020
0.966 0.969 1.032 1.050 0.976

Figure 3.2-15

EOC 2 Local Power Distribution for QC Bundle CX-672 at 51 Inches from Bottom of Core

RMS(SCAN-LAT) = 2.3%

Figure 3.2-16

EOC 2 Local Power Distribution for QC Bundle GEB-159 at 51 Inches from Bottom of Core

RMS(SCAN-LAT) = 4.9%

W-W	Gamma Scan LATTICE					
1.040						
1.007						
1.055						
1.020						
	1.023	0.878				
	1.028	0.801				
1.022	1.108	0.948				
0.987	1.167	0.924				
	1.064	0.931	0.992	0.506		
	1.087	0.949	1.092	0.581		
1.035	0.999	0.863	1.069	1.074	0.769	
1.015	1.011	0.762	1.085	1.151	0.708	
1.054	0.990		1.070		1.080	1.048
1.010	0.951		1.067		1.115	1.055

W-W

Figure 3.2-17

1.008 Gamma Scan
0.981 LATTICE

EOC 2 Local Power Distribution for QC Bundle GEH-002 at 15 Inches from Bottom of Core

1.034 0.990
1.023 0.988

RMS(SCAN-LAT) = 1.6%

	1.084	0.985					
	1.076	0.957					
1.033	1.042	0.950	0.921				
1.010	1.034	0.953	0.923				
1.034	1.022	0.933	0.932	0.0			
1.002	1.023	0.943	0.932	0.0			
	1.032	0.957	0.924	0.930	0.926		
	1.039	0.959	0.929	0.938	0.935		
1.042	1.090	1.006	0.959	0.940	0.945	1.000	
1.044	1.086	0.972	0.968	0.957	0.973	0.982	
1.042	0.995		1.052	1.036		1.096	0.964
1.031	1.005		1.059	1.047		1.106	1.014

W-W

Figure 3.2-18

1.055 Gamma Scan
1.046 LATTICE

EOC 2 Local Power Distribution for QC Bundle GEH-002 at 51 Inches from Bottom of Core

1.057 1.009
1.075 1.027

RMS(SCAN-LAT) = 2.0%

	1.105	1.015					
	1.098	0.951					
1.044	1.036	0.953	0.922				
1.039	1.046	0.952	0.904				
1.034	1.021	0.926	0.940	0.0			
1.027	1.030	0.935	0.901	0.0			
	1.044	0.946	0.917	0.929	0.899		
	1.045	0.951	0.904	0.901	0.903		
1.060	1.078	0.989	0.943	0.921	0.931	0.960	
1.073	1.095	0.948	0.950	0.933	0.948	0.943	
1.072	0.990		1.035	1.031		1.082	0.974
1.069	1.024		1.043	1.025		1.089	1.015

W-W

Figure 3.2-19

1.107	Gamma Scan		EOC 2 Local Power Distribution for				
1.070	LATTICE		QC Bundle GEH-002 at 129 Inches from				
			Bottom of Core				
1.133	1.043						
1.106	1.039		RMS(SCAN-LAT) = 2.5%				
	1.126	0.994					
	1.114	0.940					
1.086	1.062	0.942	0.898				
1.054	1.053	0.945	0.892				
1.058	1.033	0.912	0.895	0.0			
1.037	1.032	0.925	0.888	0.0			
	1.047	0.922	0.880	0.884	0.858		
	1.049	0.942	0.890	0.886	0.887		
1.121	1.111	0.973	0.924	0.884	0.885	0.918	
1.093	1.105	0.932	0.940	0.920	0.934	0.922	
1.115	1.028		1.044	1.006		1.039	0.965
1.091	1.029		1.042	1.021		1.091	1.010

CHAPTER 3 REFERENCES

1. S. N. Cramer, et. al., "ESP: A General Monte Carlo Reactor Analysis Code," ORNL-TM-3164, 1972.

2. M. B. Cutrone and G. F. Valby, "Gamma Scan Measurements at Quad Cities Nuclear Power Station Unit 1 Following Cycle 2," EPRI NP-214, 1976.

3. A. Ahlin and M. Edenius, "The Collision Probability Module EPRI-CPM," ARMP System Documentation, Part II, Chapter 6, Electric Power Research Institute, 1975.

4. N. H. Larsen, "Core Design and Operating Data for Cycles 1 and 2 of Peach Bottom 2," EPRI NP-563, 1978.

5. N. H. Larsen, G. R. Parkos, and O. Raza, "Core Design and Operating Data for Cycles 1 and 2 of Quad Cities 1," EPRI NP-240, 1976.

6. R. L. Crowther, et. al., "GE/EPRI Quad Cities 1 Plutonium Recycle Nuclear and Fuel Performance Measurements," Trans. Am. Nucl. Soc., Vol. 27, pp. 472-474, 1977.

7. A. Ahlin and M. Edenius, "CASMO - A Fast Transport Assembly Depletion Code for LWR Analysis," Trans. Am. Nucl. Soc., Vol. 26, pp. 604-605, 1977.

8. Letter, B. A. Zolotar (EPRI) to G. W. Perry (TVA), December 21, 1978.

9. H. C. Honeck and D. R. Finch, "FLANGE II (Version 71-1): A Code to Process Thermal Neutron Data from an ENDF/B Tape," DP-1278, 1971.

10. M. Edenius, "EPRI-CPM Benchmarking," ARMP System Documentation, Part I, Chapter 5, Electric Power Research Institute, 1975.

4. CORE SIMULATION

The primary method of determining the accuracy of the CORE code (Reference 4-1) in BWR analyses is by comparison of its predictions to observed data from operating reactors. The operating reactors used for CORE comparisons have similar core design characteristics to those on which CORE will be used for reload analyses. Comparison of calculated and measured reactor data provides a check not only on the core simulator program but also provides additional insight into the adequacy of the overall BWR analysis (including lattice physics methods and analysis procedures).

CORE code calculations will be compared to data recorded for the following reactor cores:

1. Quad Cities unit 1, cycles 1 and 2
2. Browns Ferry units 1 and 2, cycles 1 and 2
3. Browns Ferry unit 3, cycle 1 and beginning of cycle 2

The Quad Cities 1 reactor has a slightly smaller core than the Browns Ferry units (724 versus 764 fuel bundles), its flow rate at rated conditions is approximately 2 percent less, and the rated power is approximately 24 percent lower. The Browns Ferry units 1 and 2 and Quad Cities unit 1 initial cores were composed of 7 x 7 fuel bundles while the Browns Ferry unit 3 initial core and all reload cores contained 8 x 8 fuel bundles. The average initial fissile enrichment of the bundles ranged from 1.10 to 2.74 weight percent. Each of the cores analyzed contained gadolinia in at least a portion of the fuel bundles.

4.1 QUAD CITIES COMPARISONS

Comparison of CORE calculations to observed critical configurations in Quad Cities unit 1 for both cold and operating conditions were performed to assess CORE's capability to calculate reactivity. Comparisons to end-of-cycle gamma scan data were used to determine the accuracy of the calculated power distributions and comparisons to Traversing Incore Probe (TIP) measurements were used to confirm the adequacy of the calculated power distribution during the cycles.

The design information on fuel bundles used in the Quad Cities analyses and the core loading patterns are given in Reference 4-2. The lattice physics data utilized in CORE was generated as a function of control state, exposure, water density, and history effects using the LATTICE program (Reference 4-3). The complete functional dependence of the lattice physics data for CORE is discussed in Reference 4-1. The dependence of individual bundle flows on the bundle power, power shape, core pressure, pressure drop, and inlet enthalpy was developed using the THAS program as described in Reference 4-1 with the input values of the total form loss coefficients (and their two-phase multipliers) adjusted to force agreement with vendor supplied data. The albedo boundary conditions used at the top, bottom, and sides of the reactor core were based on previous studies (analytical and fine mesh diffusion theory calculations) performed for use in analysis of the Browns Ferry cores.

The CORE model for Quad Cities employed a full-core description

with nodes for each 6-inch segment of each fuel bundle (and its associated water gaps). The critical configurations of rod pattern, power, flow, pressure, and inlet subcooling throughout the first two cycles were taken from Reference 4-2 with error corrections and supplemental information obtained directly from EPRI. Reference 4-2 also recommended the depletion steps used in this analysis.

4.1.1 Cold, Xenon-Free Criticals

Reference 4-2 contains some of the cold, xenon-free, in-sequence critical configurations which occurred during cycles 1 and 2 for Quad Cities unit 1. Each of the eight cold criticals in Reference 4-2 were calculated with the CORE code; the results are summarized in Table 4.1-1. Since the CORE code uses lattice physics data represented as a continuous function of water density (and temperature) over the complete range encountered in BWR cores, the calculations were performed at the recorded temperatures and no moderator temperature corrections were required. The calculated k-effectives were corrected for the reactivity equivalent of the measured reactor period, but no other adjustments, corrections, normalizations or biases were employed. The average k-effective calculated by CORE was 0.9963 with a standard deviation of 0.0027.

One important use of the CORE code is shutdown margin calculations. Shutdown margin calculations are performed at the most reactive core state (normally cold) with the highest worth control rod withdrawn. Verification of CORE's capability to accurately calculate cold reactivity is partially provided by comparisons to

TABLE 4.1-1

QUAD CITIES 1, CYCLES 1 AND 2, IN-SEQUENCE COLD CRITICALS

Date	Core Average GWD/MTM	Coolant Temperature (°F)	Reactor Period (Sec)	Corrected* k-eff
4/05/72	0.0	147	230	1.0018
2/08/73	2.866	160	300	0.9983
5/07/73	3.749	120	300	0.9972
8/07/73	4.940	120	45	0.9954
1/06/74	6.912	180	300	0.9948
10/06/74	8.277	185	100	0.9943
12/16/74	9.142	160	45	0.9954
5/04/75	10.604	190	130	0.9935
			Average	0.9963
			Standard Deviation	0.0027

*The corrected k-eff has the reactivity equivalent of the observed period subtracted from the calculated k-eff.

in-sequence criticals such as shown in Table 4.1-1. However, shutdown margin calculations involve a very localized area of high reactivity compared to normal in-sequence rod patterns and thus introduce very large neutron flux gradients. In order to verify the capability of CORE to predict very localized reactivity configurations, it is necessary to examine criticals employing rod patterns similar to the stuck rod configuration. A series of local (two or three adjacent rods withdrawn) criticals were performed during the startup testing of Quad Cities unit 1. Ten of these criticals were calculated using data obtained from the Commonwealth Edison Company; the results are given in Table 4.1-2.

The average k-effective value (corrected for the reactor period) from CORE was 1.0009 with a standard deviation of 0.0006. The k-effective for the beginning-of-cycle 1 in-sequence critical was 1.0018. Thus a bias of less than 0.1 percent reactivity between the localized and distributed criticals was obtained from CORE. This is strong evidence that CORE can accurately perform reactivity calculations for localized reactivity configurations and that comparisons to in-sequence criticals provide an accurate measure of the calculational error for such localized configurations.

4.1.2 Hot Operating Reactivity

Each of the data sets in Reference 4-2 (plus three additional data sets obtained from EPRI) represents a high-power critical reactor configuration which occurred during the first two cycles of operation of Quad Cities unit 1. Each of these hot operating critical configurations was analyzed with CORE. Equilibrium xenon

TABLE 4.1-2

QUAD CITIES 1 LOCAL COLD CRITICALS AT BOC 1

Control Rods Fully Withdrawn	Partially Withdrawn Rod	Partially Withdrawn Notch	Coolant Temperature (°F)	Reactor Period (Sec)	Corrected* k-eff
30-47; 30-43	26-43	06	156	160	1.0011
30-47; 34-47	-	-	158	45	1.0003
34-43; 34-47	30-43	06	158	60	1.0003
26-43; 26-47	30-43	06	157	148	1.0010
18-35; 22-35	18-31	06	159	238	1.0003
18-35; 18-39	22-35	08	158	25	1.0017
14-39; 18-39	-	-	159	260	1.0005
14-35; 18-35	18-31	06	159	350	1.0011
22-23; 26-23	26-27	08	160	30	1.0018
14-35; 14-39	-	-	160	175	1.0013
				Average	1.0009
				Standard Deviation	0.0006

*The corrected k-eff has the reactivity equivalent of the observed period subtracted from the calculated k-eff.

concentration was assumed since Reference 4-2 (page 2) indicates that steady-state operation was held at each configuration for at least 48 hours before the data was recorded. Table 4.1-3 lists the results of the CORE k-effective calculation for each of the 29 data sets. The tabulated k-effectives are the direct code output values without adjustment. The average k-effective value obtained by CORE was 0.9980 with a standard deviation of 0.0044. However, there is an obvious trend of higher predicted k-effective values for higher core average exposures. This trend is consistent with that reported in Reference 4-4 for gadolinia-bearing first cycles. The first cycle of Quad Cities unit 1 was terminated well before full power reactivity depletion; thus the second cycle has characteristics much like the end of a normal first cycle. The average k-effective value from CORE for core average exposures less than 10,000 MWD/MTU was 0.9961 with a standard deviation of 0.0027. The corresponding values for core average exposures above 10,000 MWD/MTU were 1.0041 and 0.0027 respectively.

4.1.3 TIP Comparisons During Cycles 1 and 2

For 27 of the 29 data sets in Reference 4-2, detailed incore detector measurements were available. This data consisted of 24 axial values in each of 41 Traversing Incore Probe (TIP) thimble locations. The data was normalized such that for each detector used, there resulted an average reading of 100 when inserted in the common thimble location (32-33). The simulated TIP readings calculated by CORE for each of the 27 data sets were normalized such that the average of all 24 x 41 segments was the same as the averaged measured value. Since the TIP reading is closely related

TABLE 4.1-3

QUAD CITIES 1, CYCLES 1 AND 2, HOT OPERATING k-eff

Data Set	Date	Core Average GWD/MTM	Rod Notches Inserted	Fraction of Rated: Power	Flow	Calculated k-eff
1	6/29/72	0.273	1936	0.870	0.861	0.9904
2	8/30/72	0.712	2032	0.897	1.016	0.9960
3	9/11/72	0.882	2056	0.892	0.966	0.9942
4	11/01/72	1.471	2192	0.875	0.996	0.9961
5	12/26/72	2.239	2056	0.976	1.000	0.9951
6	3/08/73	3.190	2156	0.961	0.[illegible]	0.9950
7	5/16/73	3.837	2436	0.875	0.968	0.9946
8	6/06/73	4.075	2316	0.924	0.967	0.9961
9	7/17/73	4.738	2290	0.947	0.948	0.9950
10	8/30/73	5.301	2254	0.931	0.928	0.9947
11	11/01/73	6.031	2104	0.802	0.750	0.9940
12	12/11/73	6.558	2064	0.886	0.999	0.9978
13	12/29/73	6.807	1892	0.880	0.961	0.9995
14	2/13/74	7.397	1924	0.903	0.976	0.9975
15	3/05/74	7.660	1840	0.871	0.997	0.9981
16	3/26/74	7.980	1688	0.878	0.979	0.9984
17*	7/26/74	7.303	1788	0.567	0.503	0.9909
18	8/15/74	7.532	1408	0.865	0.855	0.9963
19	9/12/74	7.964	1202	0.859	0.898	1.0021
20	10/23/74	8.424	1332	0.835	0.837	0.9942
21	11/18/74	8.790	1164	0.960	0.994	0.9977
22	12/11/74	9.142	956	0.996	0.987	0.9997
23	4/03/75	10.174	748	0.981	0.992	1.0021
24	6/19/75	11.239	36	0.985	0.980	0.9991
25	8/08/75	11.936	338	0.858	1.002	1.0038
26	10/20/75	12.897	32	0.682	0.960	1.0055
27	11/13/75	13.199	0	0.682	0.960	1.0053
28	12/19/75	13.612	0	0.616	0.977	1.0064
29	12/31/75	13.742	0	0.592	0.968	1.0068
					Average	0.9980
					Standard Deviation	0.0044

*First data set in cycle 2

to the power in the surrounding nodes, comparisons of measured and simulated readings can be utilized to evaluate the ability of the CORE code to calculate operating power distributions. Table 4.1-4 summarizes the results of these comparisons. The percent difference (D_i) between measured (M_i) and calculated (C_i) TIP readings was determined by:

$$D_i = 200*(M_i - C_i)/(M_i + C_i) \qquad (4\text{-}1)$$

and the standard deviation computed by Equation 4-2:

$$\sigma = \sqrt{\frac{\sum_{i=1}^{n} (D_i - \bar{D})^2}{n - 1}} \qquad (4\text{-}2)$$

where $\bar{D}$ is the average D_i value and n is the number of values. Table 4.1-4 presents the standard deviation of the difference between individual 6-inch axial segment (nodal) readings as well as the standard deviation of the difference between axially integrated thimble values. The combined standard deviation for all 27 data sets is 11.17 and 5.40 percent for nodal and integrated values respectively.

The TIP thimbles in the Quad Cities reactor have half-core symmetry about a diagonal line; the core loading patterns are also symmetric about this line. For fifteen of the data sets, the control rod pattern maintained reflective symmetry about the diagonal line of thimble symmetry, allowing comparison of measured TIP values from symmetric locations. From Table 4.1-4, the combined standard deviation of the differences between symmetric measured readings was 11.24 and 7.55 percent for nodal and integrated values respectively. Thus the standard deviation of differences

TABLE 4.1-4

QUAD CITIES 1, CYCLES 1 AND 2, TIP DATA COMPARISONS

Data Set	Date	Core Average GWD/MTM	Measured - Calculated Standard Deviation (%) Nodal	Integrated	Symmetric Measurements Standard Deviation (%) Nodal	Integrated
1	6/29/72	0.273	10.28	5.21	10.73	8.62
2	8/30/72	0.712	8.22	5.49	12.04	8.62
3	9/11/72	0.882	8.50	5.60	12.44	8.99
4	11/01/72	1.471	8.60	5.73	-	-
5	12/26/72	2.239	8.38	5.75	-	-
6	3/08/73	3.190	8.95	6.02	12.50	8.75
7	5/16/73	3.836	9.55	6.04	-	-
8	6/06/73	4.057	10.48	6.25	-	-
9	7/17/73	4.738	9.44	5.82	-	-
10	8/30/73	5.301	10.82	5.85	-	-
11	11/01/73	6.031	12.59	5.21	-	-
12	12/11/73	6.558	10.62	5.62	12.16	8.57
13	12/29/73	6.807	10.70	5.44	13.05	8.50
14	2/13/74	7.397	10.43	5.46	-	-
15	3/05/74	7.660	11.14	5.41	10.89	8.20
16	3/26/74	7.980	-	-	-	-
17*	7/26/74	7.303	13.37	4.38	11.25	5.91
18	8/15/74	7.532	13.49	5.11	12.33	7.49
19	9/12/74	7.964	11.66	4.78	10.88	6.28
20	10/23/74	8.424	11.84	5.21	-	-
21	11/18/74	8.790	11.03	5.04	-	-
22	12/11/74	9.142	10.85	5.22	-	-
23	4/03/75	10.174	11.30	5.76	10.11	6.34
24	6/19/75	11.239	12.78	4.79	-	-
25	8/08/75	11.936	12.17	5.60	-	-
26	10/20/75	12.897	-	-	-	-
27	11/13/75	13.199	11.74	4.76	9.74	6.37
28	12/19/75	13.612	14.12	4.62	9.18	5.74
29	12/31/75	13.742	14.95	5.11	9.23	5.86
		Combined	11.17	5.40	11.24	7.55

*First data set in cycle 2

between measured and calculated TIP readings was approximately the same as that for the symmetric measurements. For many of the data sets, the measured versus calculated standard deviation was less than the symmetric measurements standard deviation. The only non-symmetrical effect in the calculated values was due to a slightly non-symmetric exposure accumulation occurring during depletion with rod patterns with rotational symmetry only. Thus the two symmetric calculated values were always very nearly the same and were often bounded by the two symmetric measured readings.

The maximum values of nodal and integrated TIP readings from the CORE simulation and measured data were also compared. On the average, CORE underpredicted the maximum measured nodal TIP reading for the 27 data sets by 4.04 percent with a standard deviation of 4.26 percent. The maximum integrated thimble readings from CORE averaged 3.55 percent lower than the maximum measured value, with a standard deviation of 4.00 percent.

In Figures 4.1-1 through 4.1-15, the average TIP reading versus axial position is plotted for each of the data sets in cycle 1. Figures 4.1-16 through 4.1-27 present similar plots for each of the data sets in cycle 2. Comparison of calculated and measured average TIP readings versus axial position yields a good indication of CORE's ability to calculate gross axial power distributions. The agreement between the calculated and measured axial TIP distributions is excellent for both cycles. A slight deterioration in agreement occurred near end-of-cycle 1, and was worse in cycle 2.

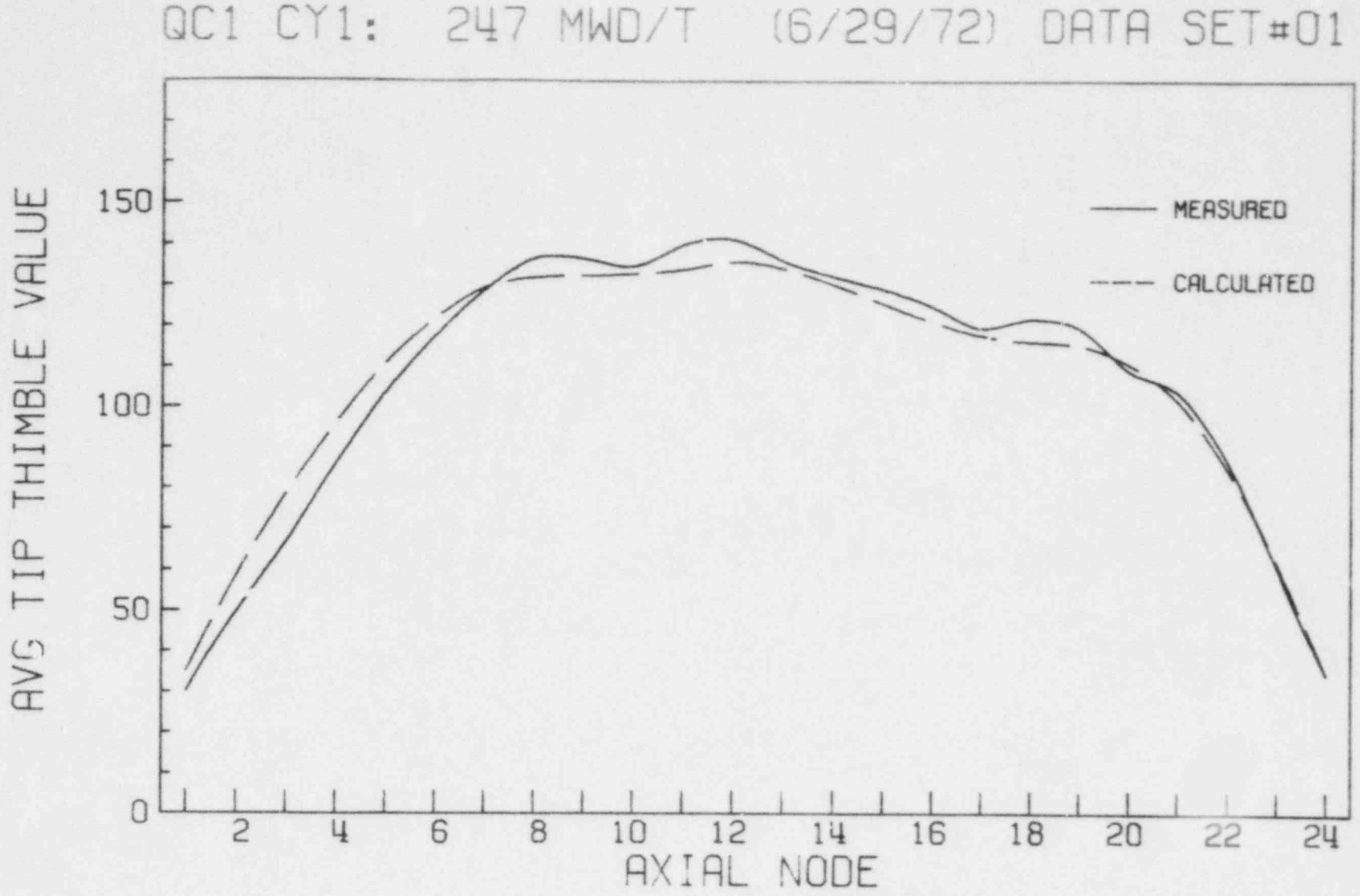
QC1 CY1: 247 MWD/T (6/29/72) DATA SET#01
AVG TIP THIMBLE VALUE
150
100
50
0
2
4
6
8
10
12
14
16
18
20
22
24
AXIAL NODE
MEASURED
CALCULATED

Figure 4.1-1

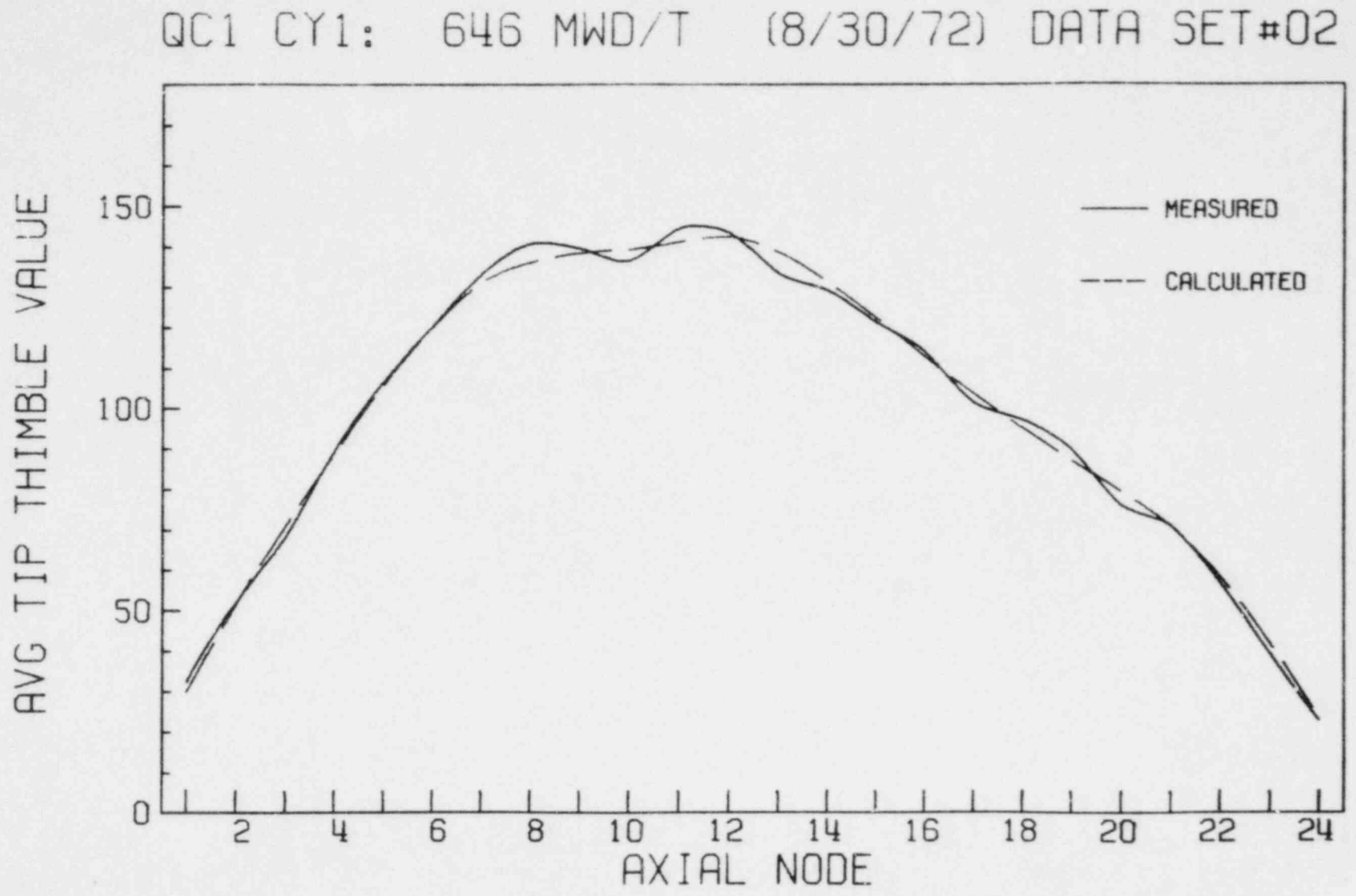
QC1 CY1: 646 MWD/T (8/30/72) DATA SET#02
AVG TIP THIMBLE VALUE
150
100
50
0
2
4
6
8
10
12
14
16
18
20
22
24
AXIAL NODE
MEASURED
CALCULATED

Figure 4.1-2

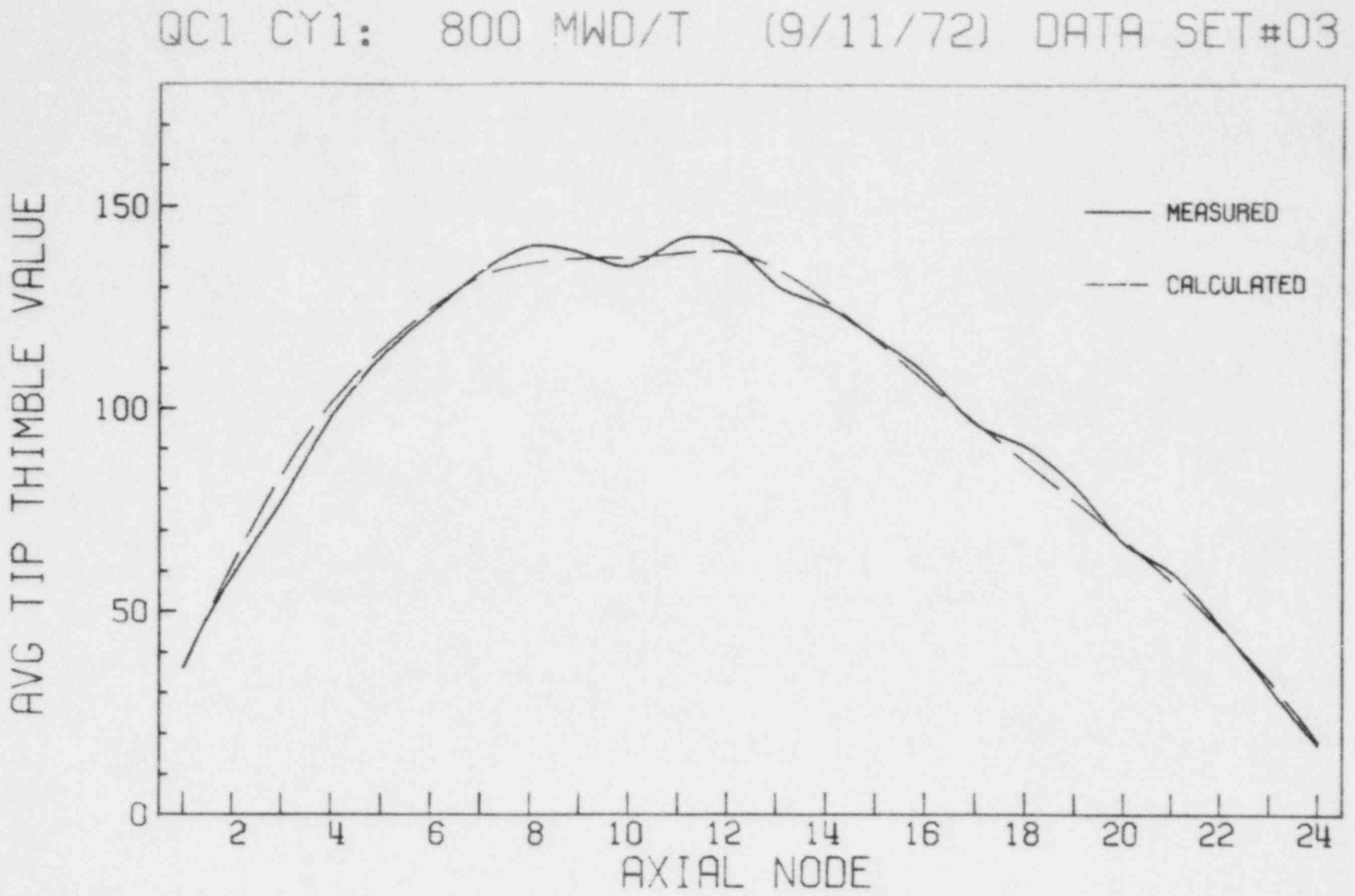
QC1 CY1: 800 MWD/T (9/11/72) DATA SET#03
AVG TIP THIMBLE VALUE
150
100
50
0
2
4
6
8
10
12
14
16
18
20
22
24
AXIAL NODE
MEASURED
CALCULATED

Figure 4.1-3

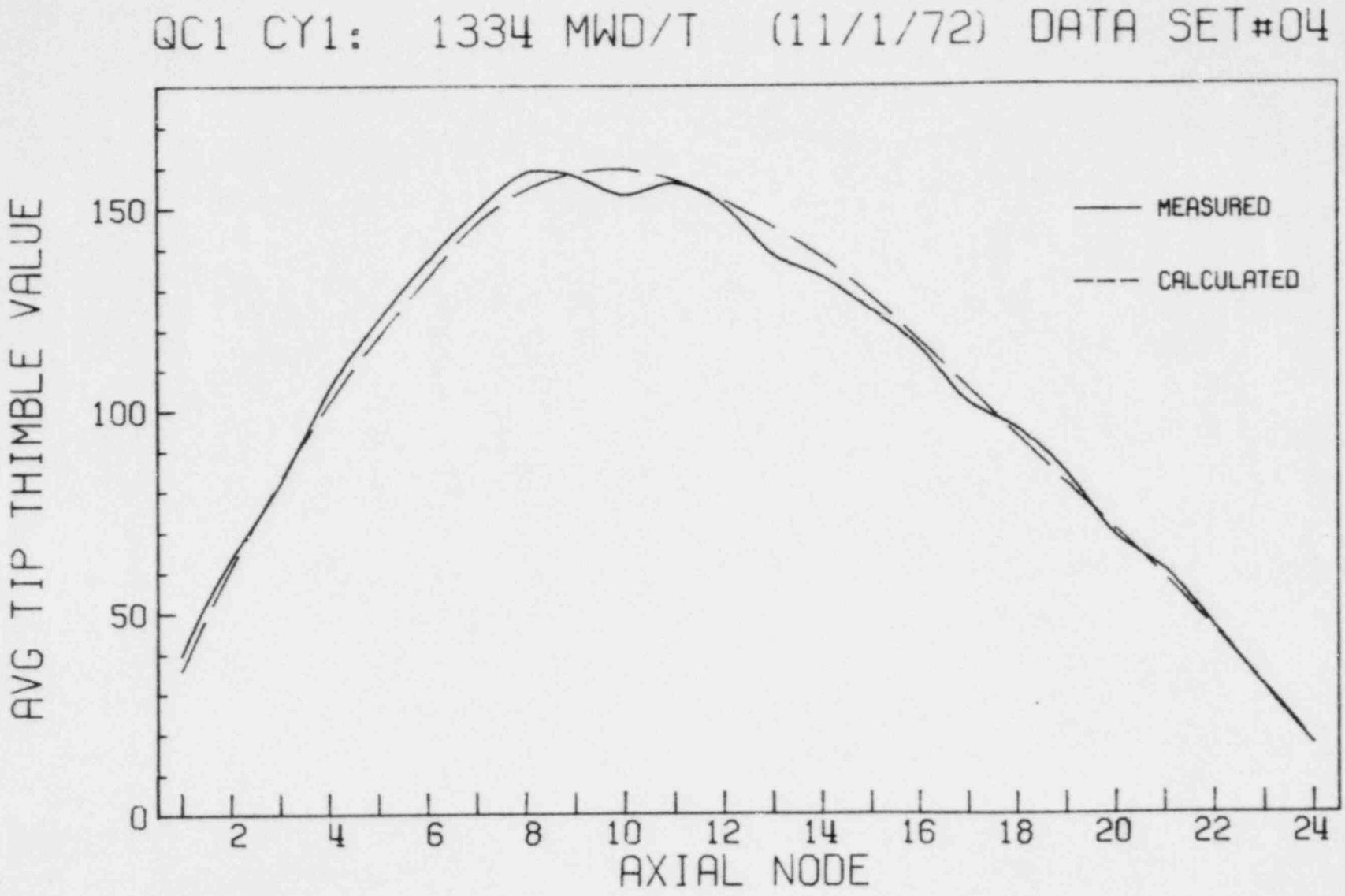
QC1 CY1: 1334 MWD/T (11/1/72) DATA SET#04
AVG TIP THIMBLE VALUE
150
100
50
0
2
4
6
8
10
12
14
16
18
20
22
24
AXIAL NODE
MEASURED
CALCULATED

Figure 4.1-4

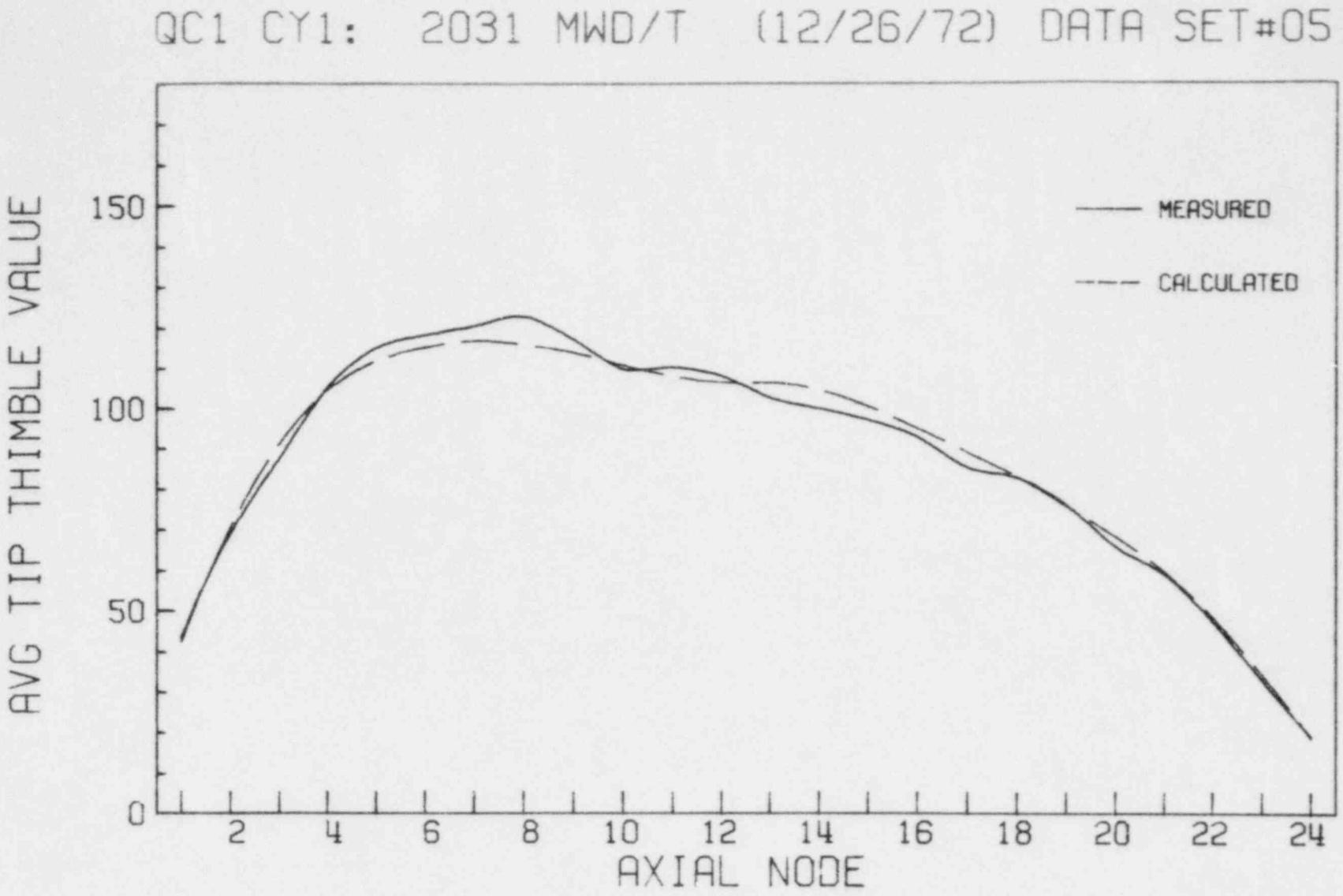
QC1 CY1: 2031 MWD/T (12/26/72) DATA SET#05
AVG TIP THIMBLE VALUE
150
100
50
0
2
4
6
8
10
12
14
16
18
20
22
24
AXIAL NODE
MEASURED
CALCULATED

Figure 4.1-5

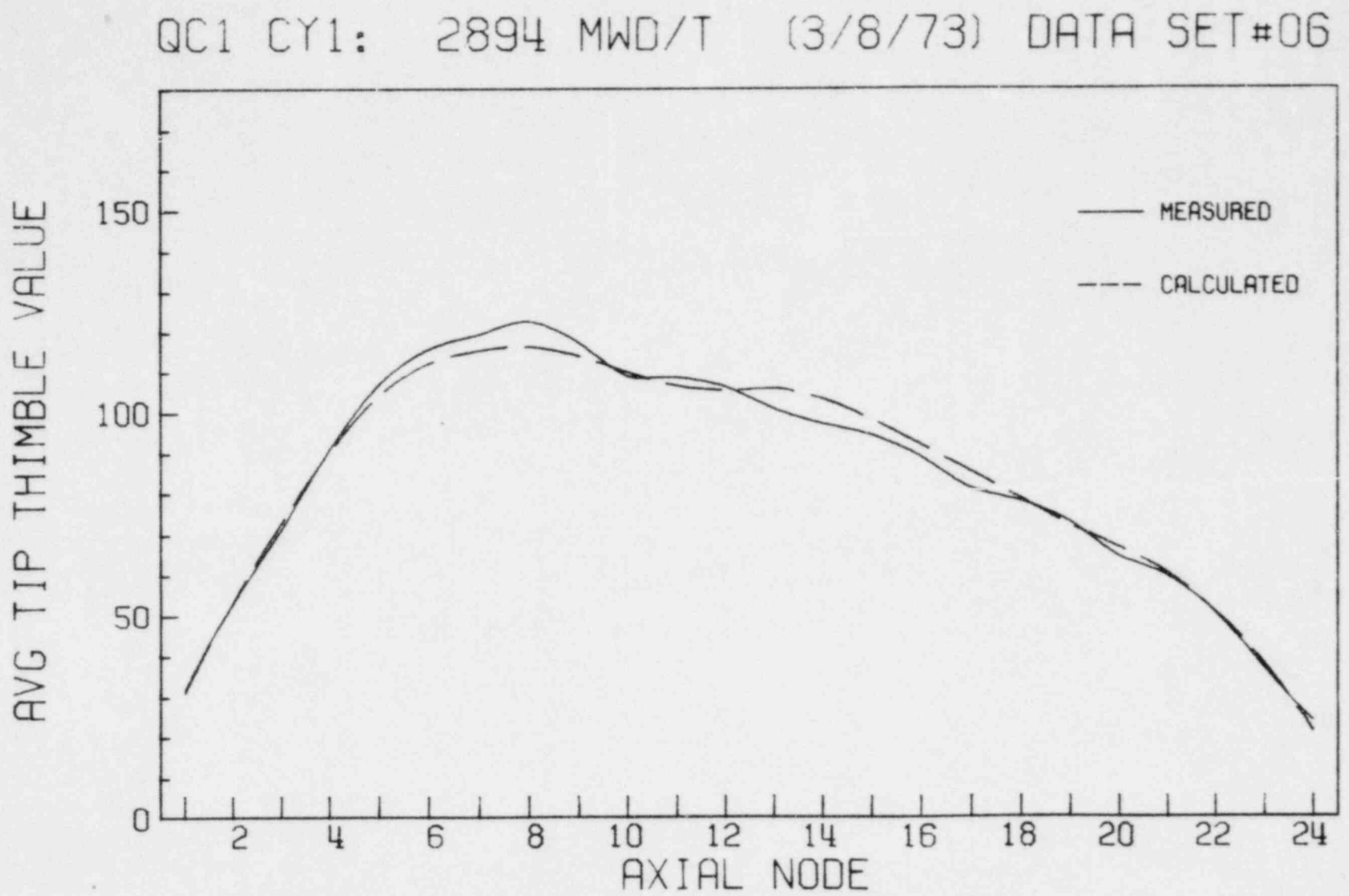
QC1 CY1: 2894 MWD/T (3/8/73) DATA SET#06
AVG TIP THIMBLE VALUE
0
50
100
150
2
4
6
8
10
12
14
16
18
20
22
24
AXIAL NODE
MEASURED
CALCULATED

Figure 4.1-6

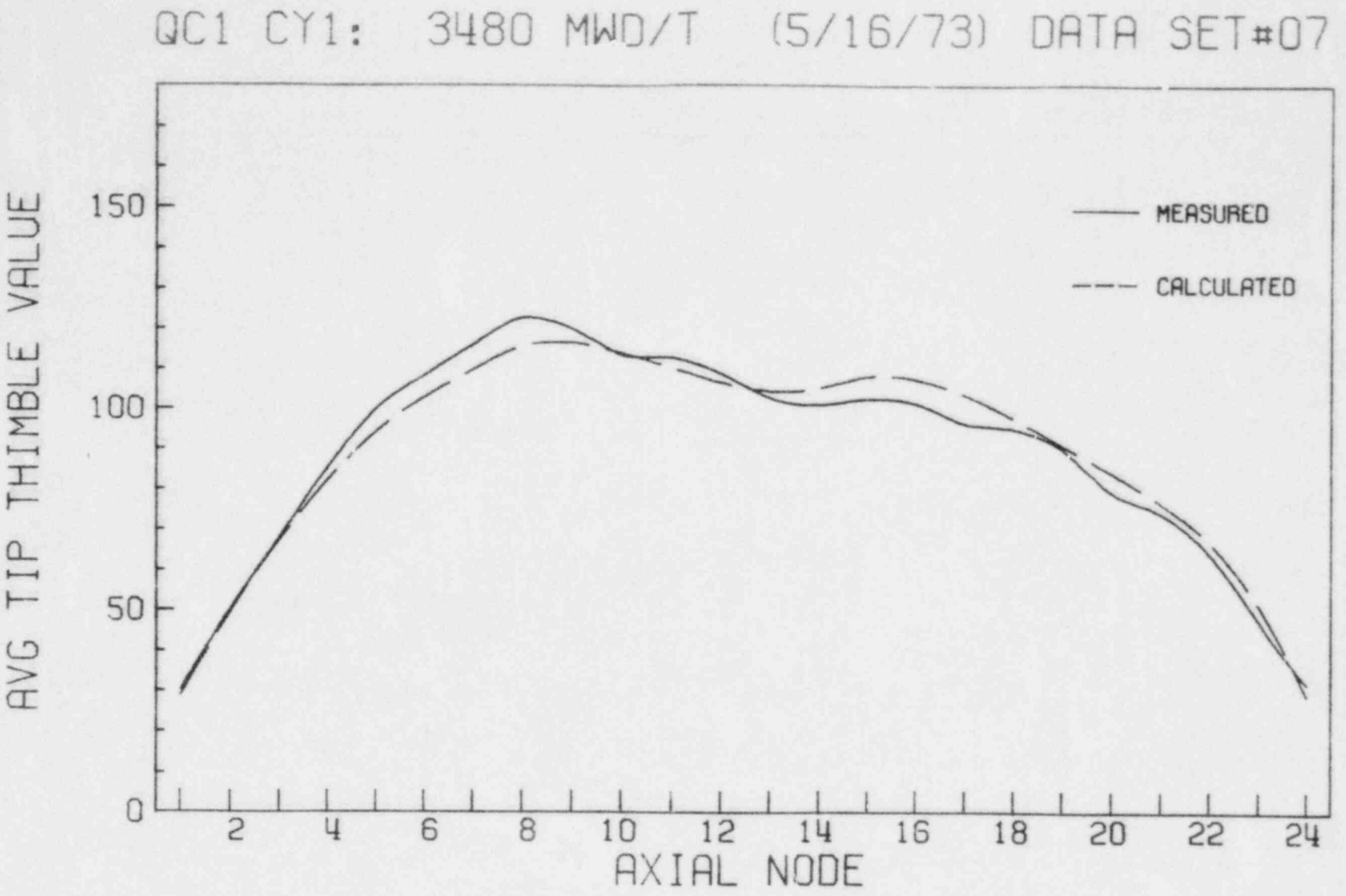
QC1 CY1: 3480 MWD/T (5/16/73) DATA SET#07
AVG TIP THIMBLE VALUE
150
100
50
0
2
4
6
8
10
12
14
16
18
20
22
24
AXIAL NODE
MEASURED
CALCULATED

Figure 4.1-7

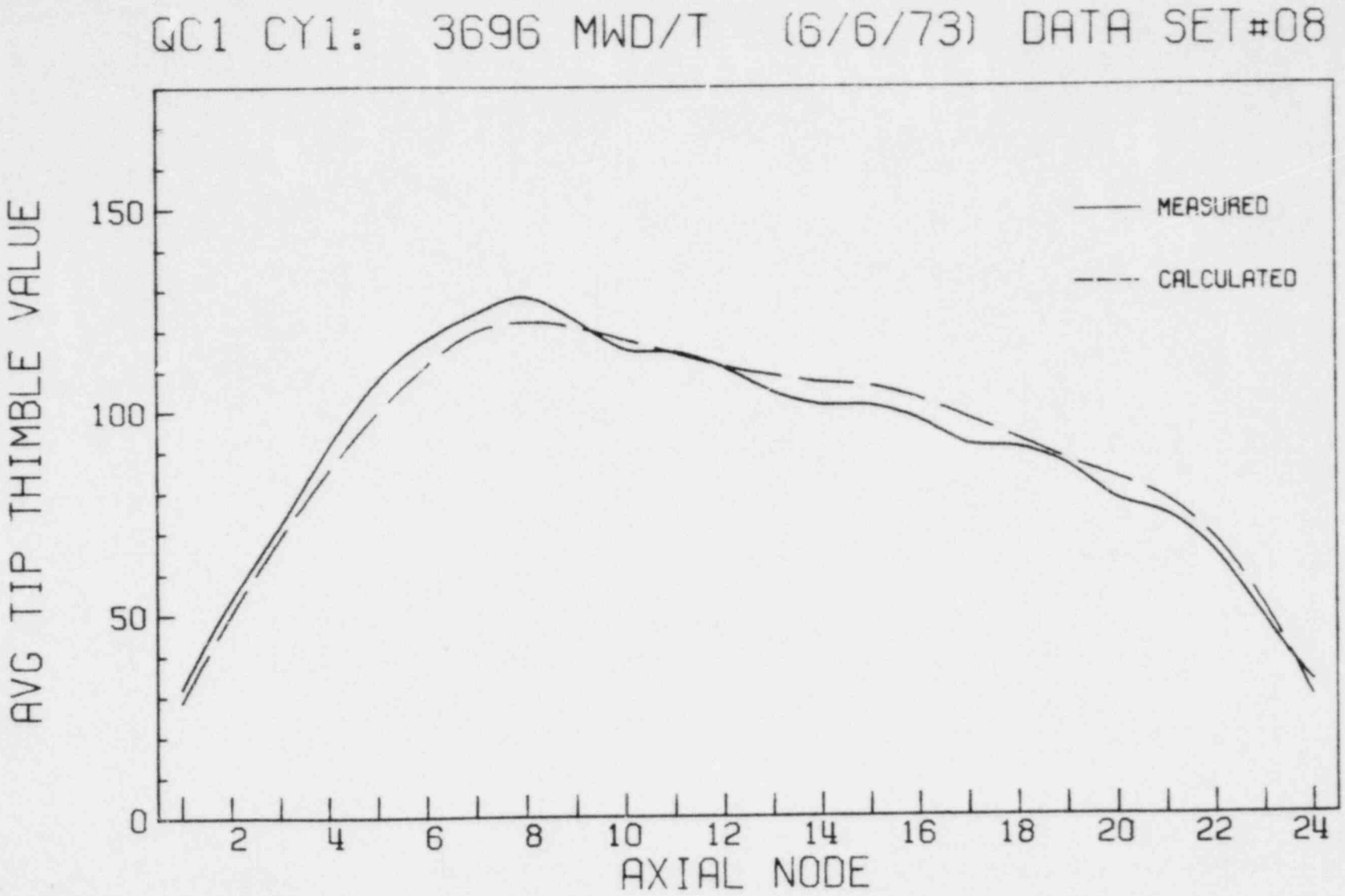
GC1 CY1: 3696 MWD/T (6/6/73) DATA SET#08
AVG TIP THIMBLE VALUE
150
100
50
0
2
4
6
8
10
12
14
16
18
20
22
24
AXIAL NODE
MEASURED
CALCULATED

Figure 4.1-8

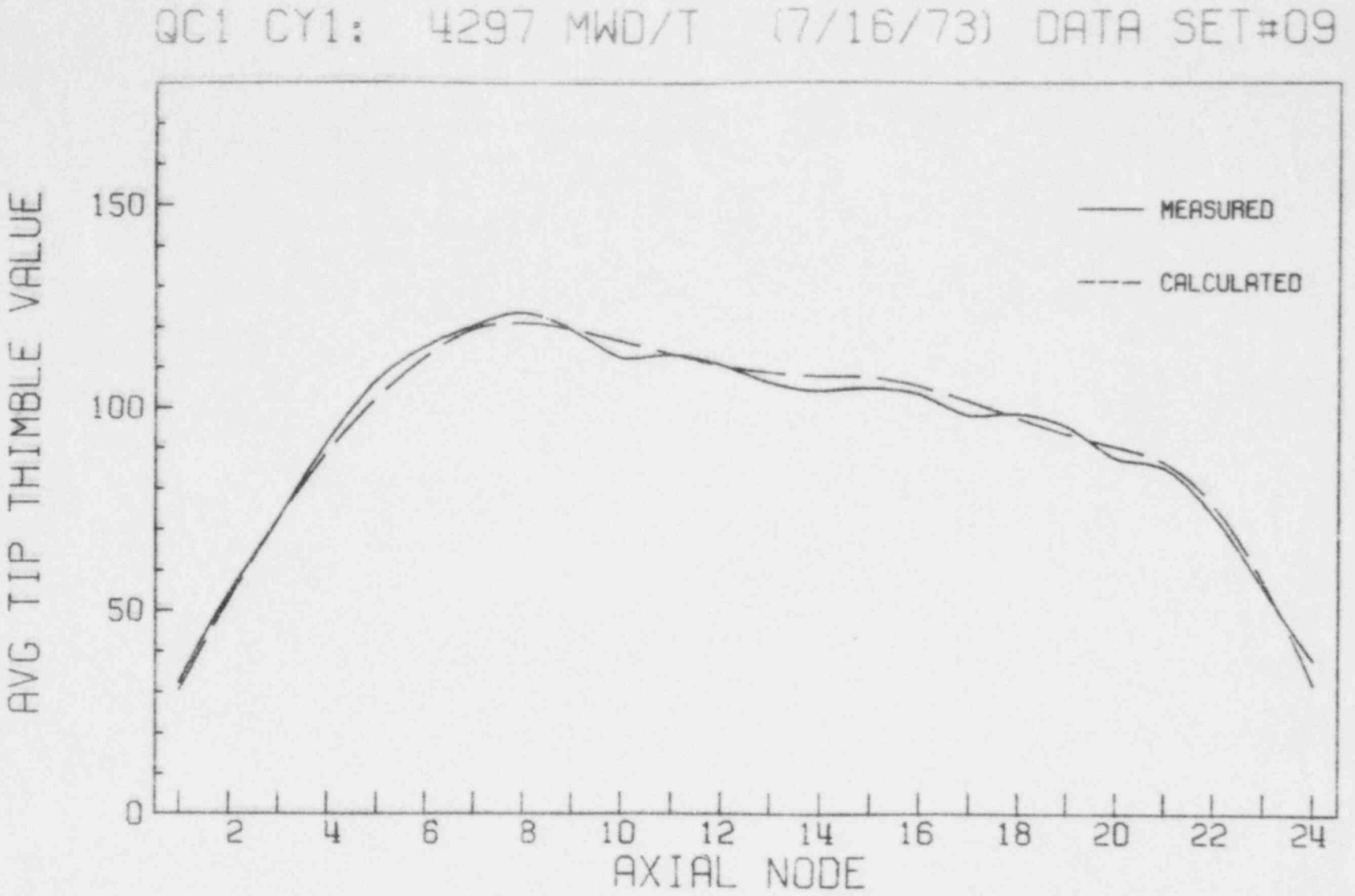
QC1 CY1: 4297 MWD/T (7/16/73) DATA SET#09
AVG TIP THIMBLE VALUE
150
100
50
0
2
4
6
8
10
12
14
16
18
20
22
24
AXIAL NODE
MEASURED
CALCULATED

Figure 4.1-9

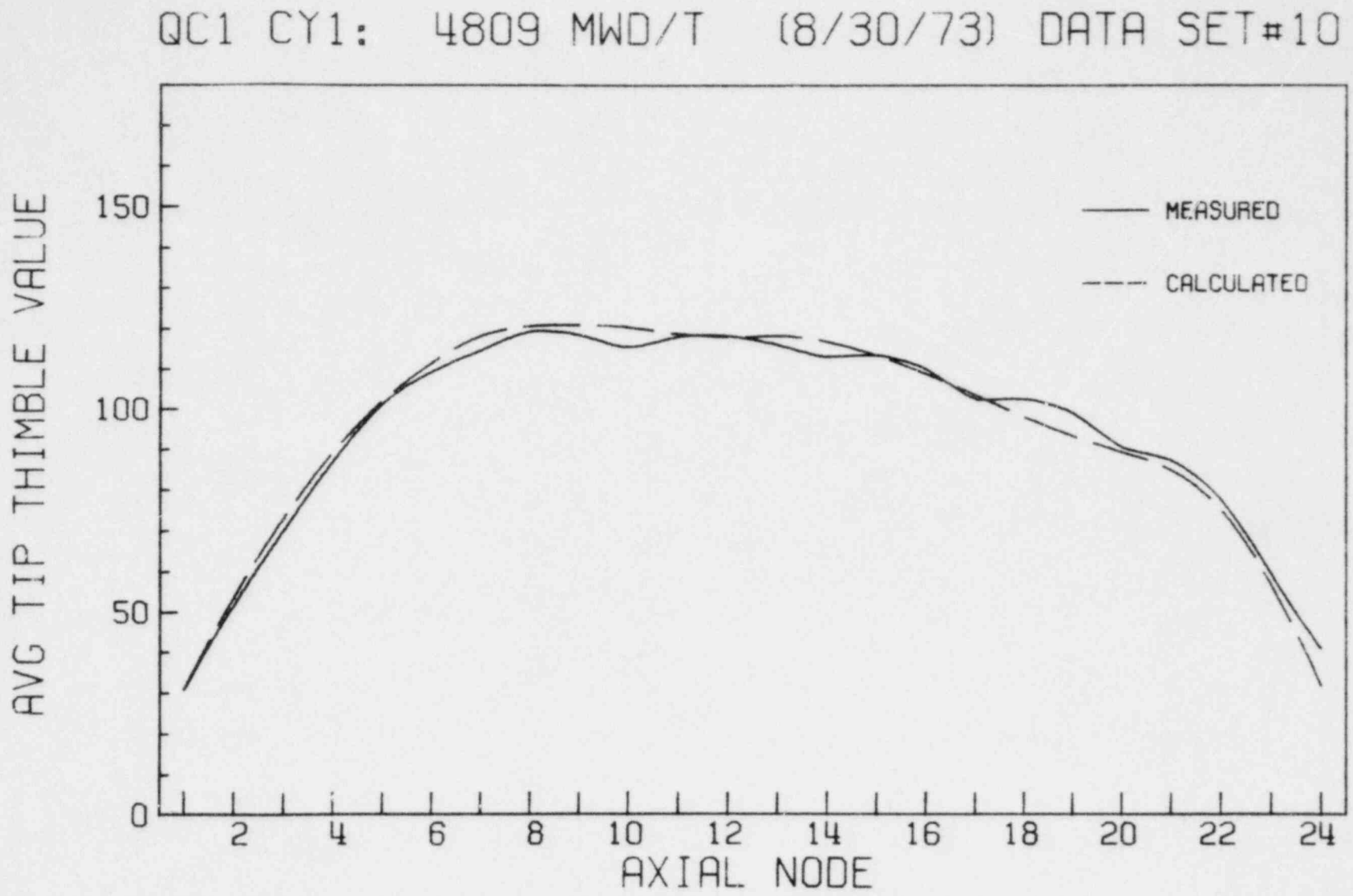
QC1 CY1: 4809 MWD/T (8/30/73) DATA SET#10
AVG TIP THIMBLE VALUE
150
100
50
0
2
4
6
8
10
12
14
16
18
20
22
24
AXIAL NODE
MEASURED
CALCULATED

Figure 4.1-10

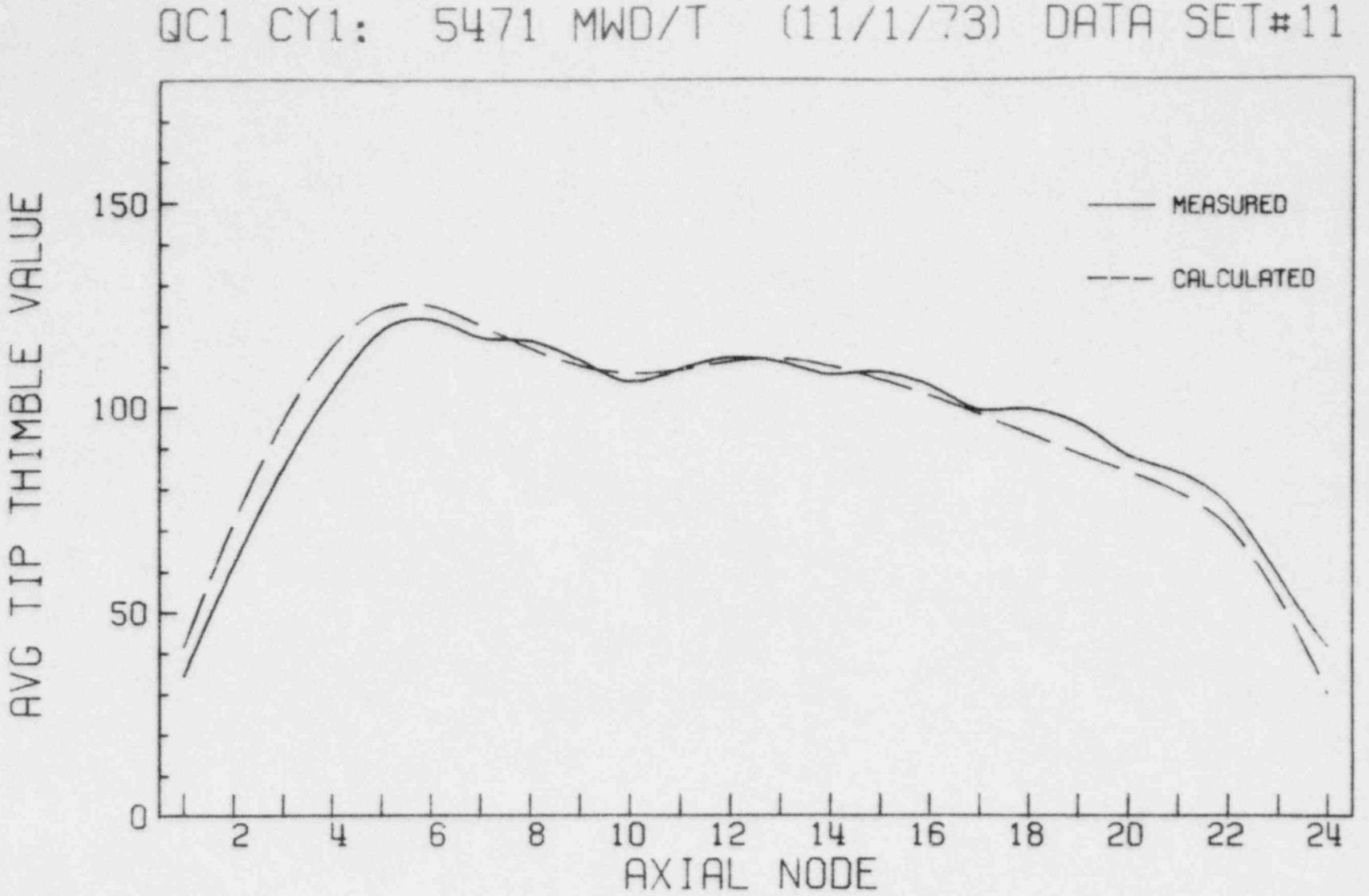
QC1 CY1: 5471 MWD/T (11/1/73) DATA SET#11
AVG TIP THIMBLE VALUE
150
100
50
0
2
4
6
8
10
12
14
16
18
20
22
24
AXIAL NODE
MEASURED
CALCULATED

Figure 4.1-11

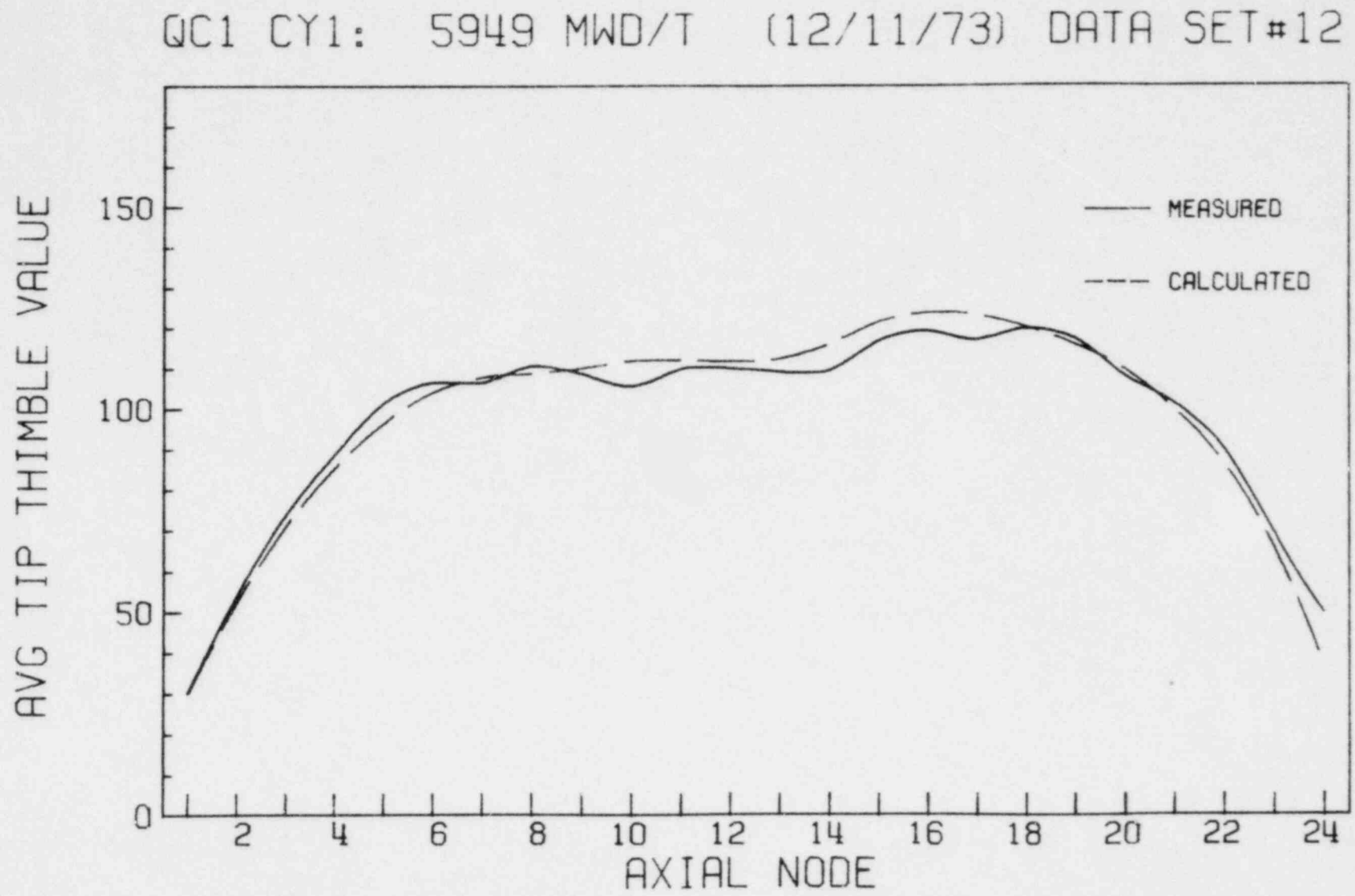
QC1 CY1: 5949 MWD/T (12/11/73) DATA SET#12
AVG TIP THIMBLE VALUE
150
100
50
0
2
4
6
8
10
12
14
16
18
20
22
24
AXIAL NODE
MEASURED
CALCULATED

Figure 4.1-12

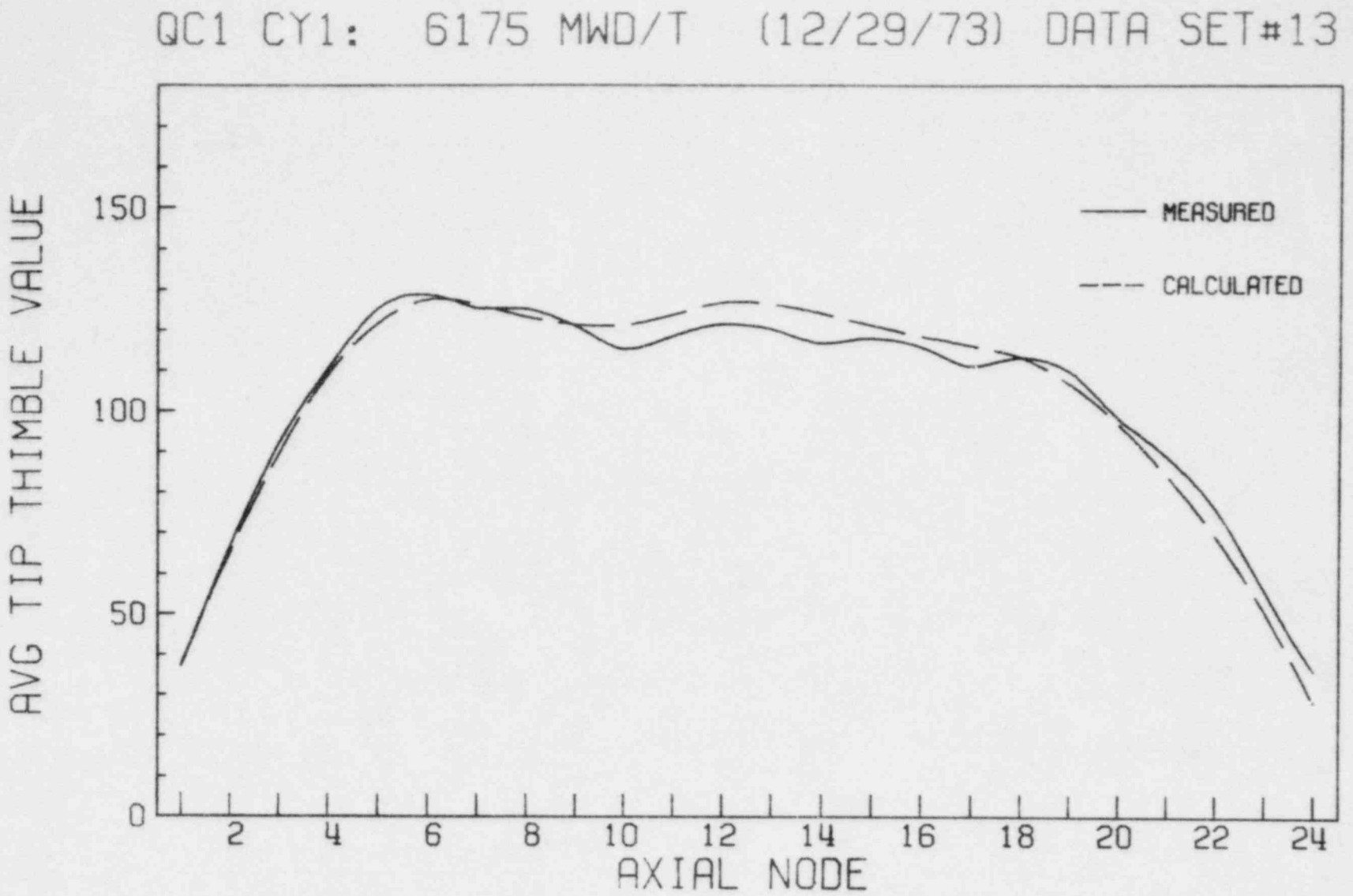
QC1 CY1: 6175 MWD/T (12/29/73) DATA SET#13
AVG TIP THIMBLE VALUE
150
100
50
0
2
4
6
8
10
12
14
16
18
20
22
24
AXIAL NODE
MEASURED
CALCULATED

Figure 4.1-13

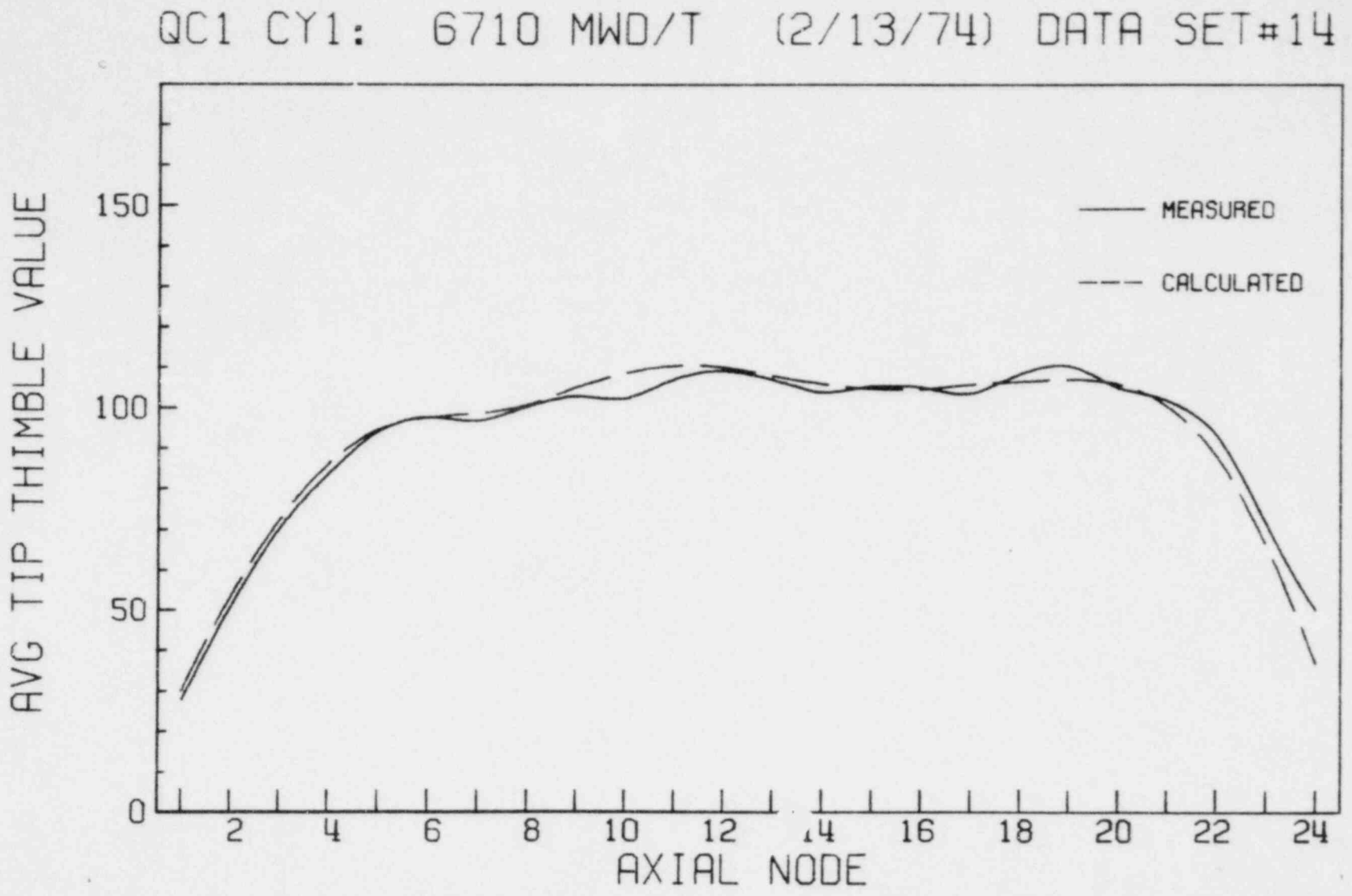
QC1 CY1: 6710 MWD/T (2/13/74) DATA SET#14
AVG TIP THIMBLE VALUE
150
100
50
0
2
4
6
8
10
12
14
16
18
20
22
24
AXIAL NODE
MEASURED
CALCULATED

Figure 4.1-14

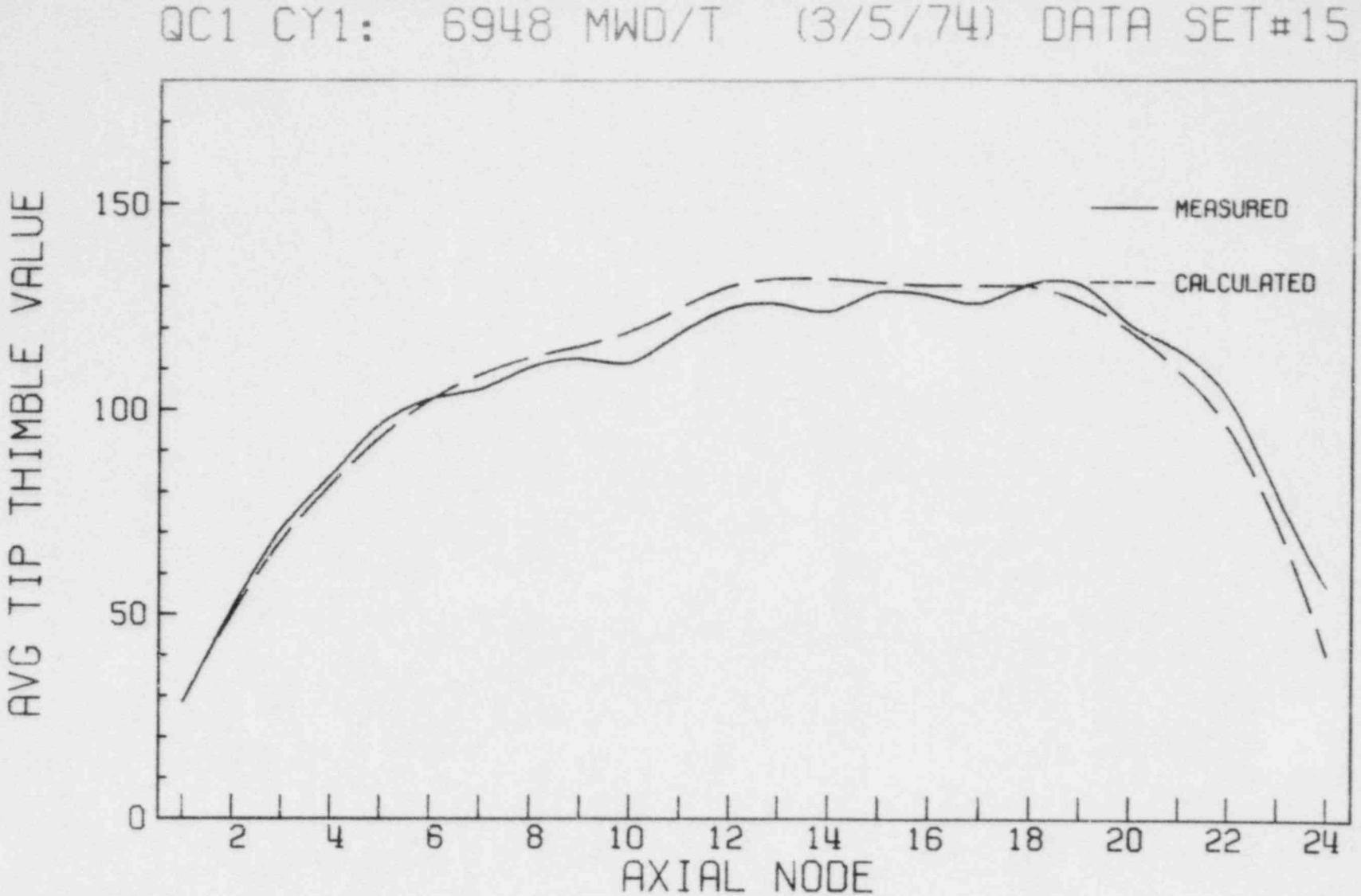
QC1 CY1: 6948 MWD/T (3/5/74) DATA SET#15
AVG TIP THIMBLE VALUE
150
100
50
0
2
4
6
8
10
12
14
16
18
20
22
24
AXIAL NODE
MEASURED
CALCULATED

Figure 4.1-15

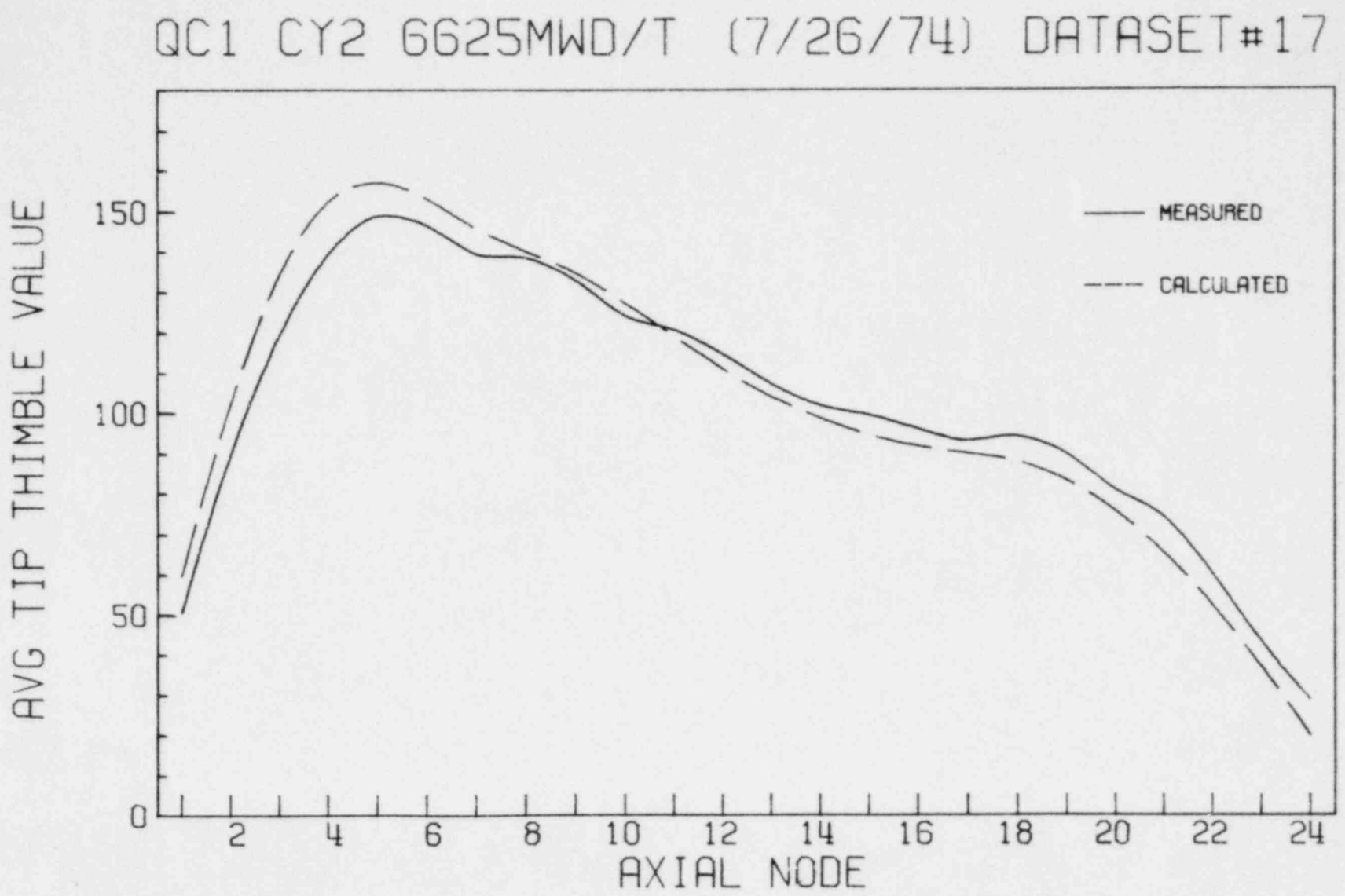
QC1 CY2 6625MWD/T (7/26/74) DATASET#17
AVG TIP THIMBLE VALUE
150
100
50
0
2
4
6
8
10
12
14
16
18
20
22
24
AXIAL NODE
MEASURED
CALCULATED

Figure 4.1-16

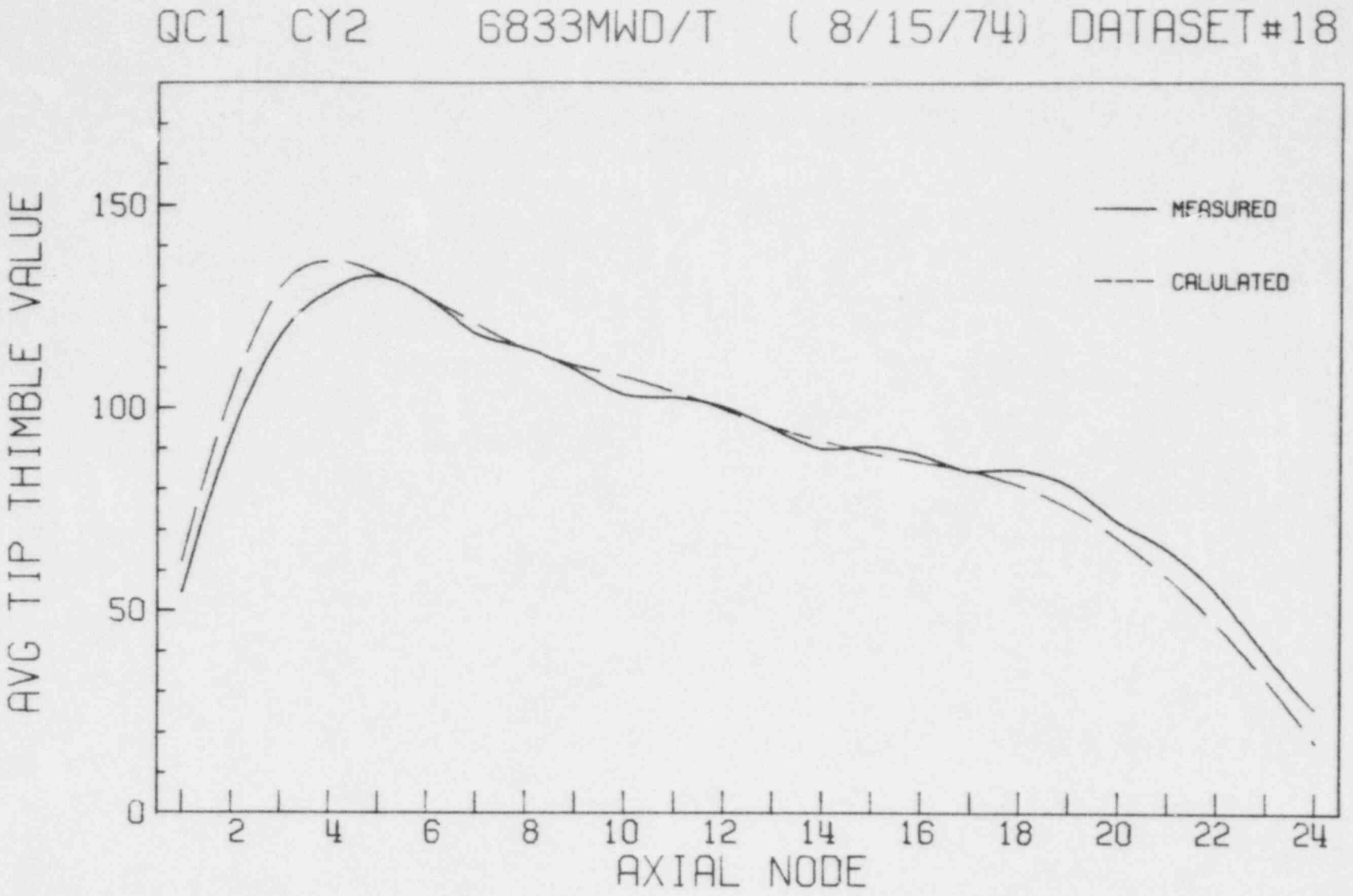
QC1 CY2 6833MWD/T (8/15/74) DATASET#18
AVG TIP THIMBLE VALUE
150
100
50
0
2
4
6
8
10
12
14
16
18
20
22
24
AXIAL NODE
MEASURED
CALULATED

Figure 4.1-17

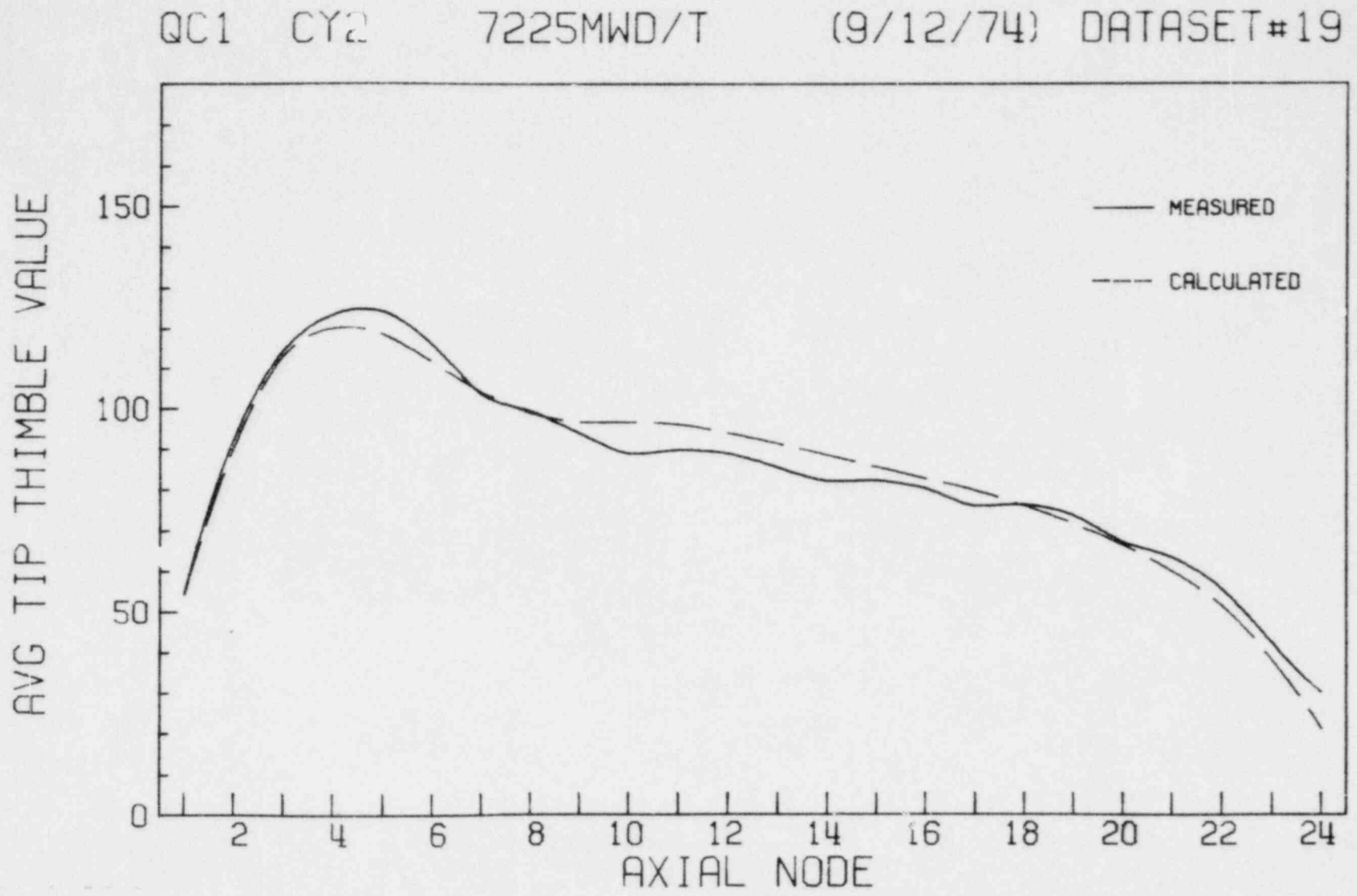
QC1 CY2 7225MWD/T (9/12/74) DATASET#19
AVG TIP THIMBLE VALUE
150
100
50
0
2
4
6
8
10
12
14
16
18
20
22
24
AXIAL NODE
MEASURED
CALCULATED

Figure 4.1-18

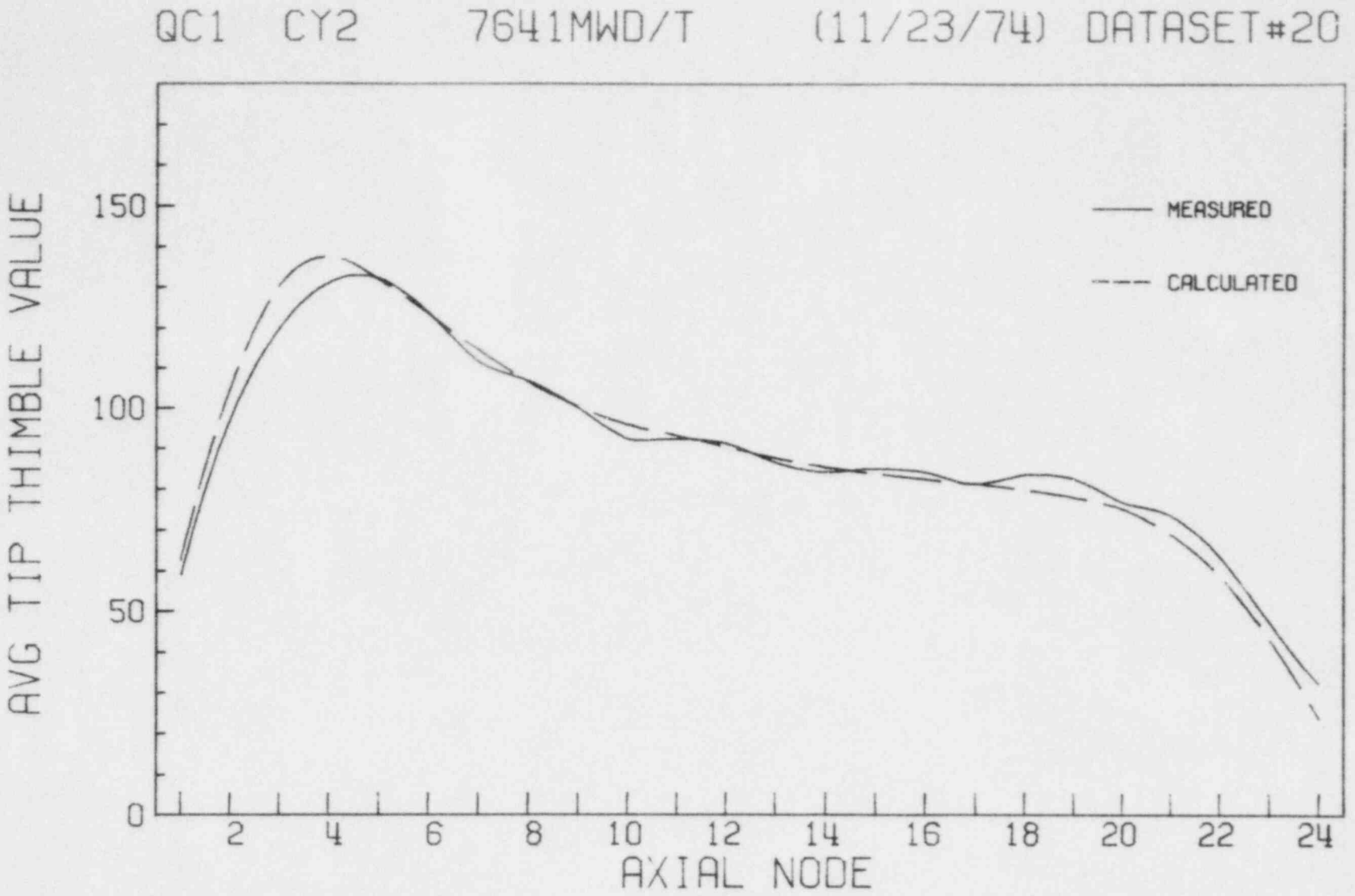
QC1 CY2 7641MWD/T (11/23/74) DATASET#20
AVG TIP THIMBLE VALUE
150
100
50
0
2
4
6
8
10
12
14
16
18
20
22
24
AXIAL NODE
MEASURED
CALCULATED

Figure 4.1-19

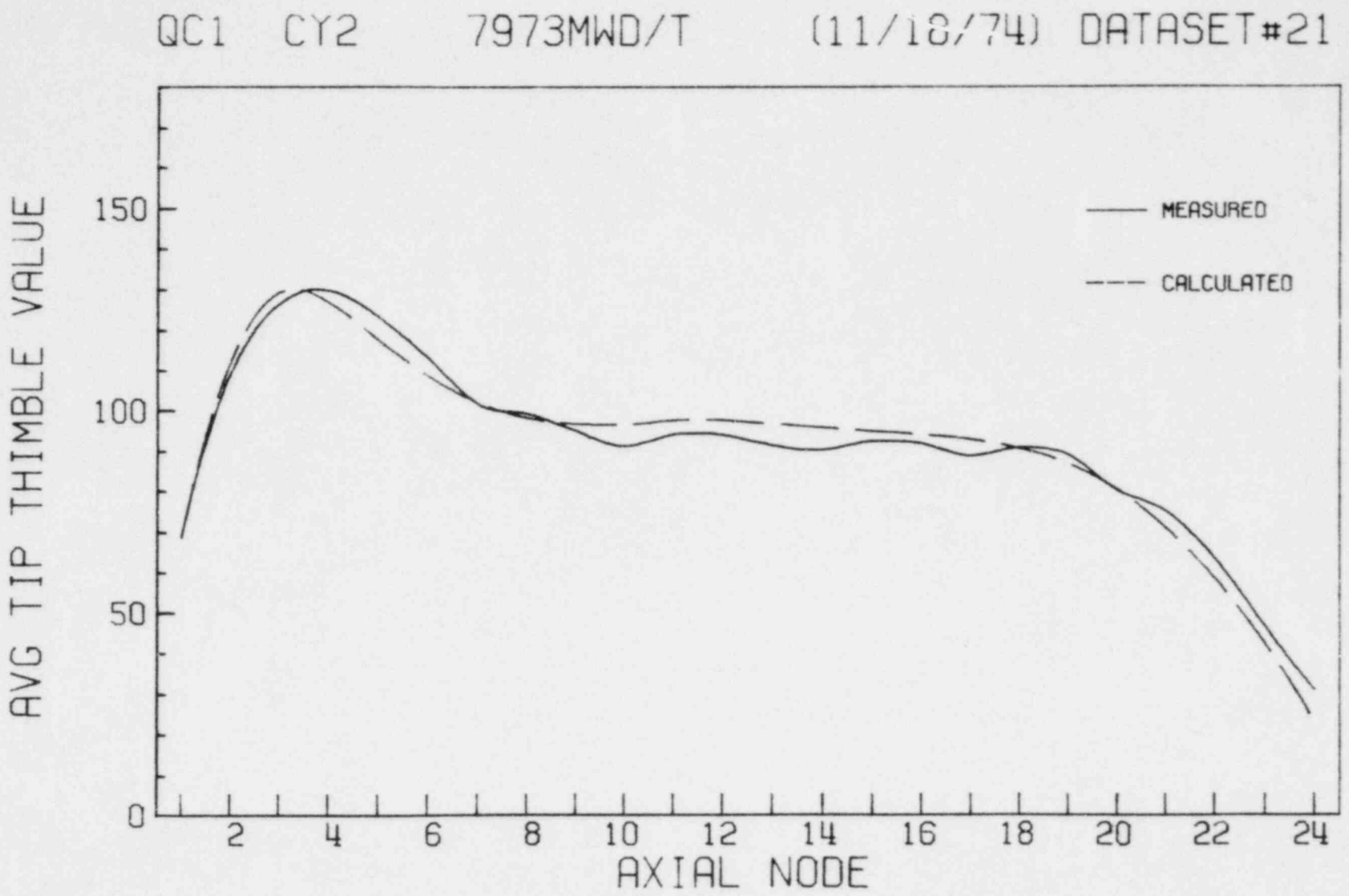
QC1 CY2 7973MWD/T (11/18/74) DATASET#21
AVG TIP THIMBLE VALUE
150
100
50
0
2
4
6
8
10
12
14
16
18
20
22
24
AXIAL NODE
MEASURED
CALCULATED

Figure 4.1-20

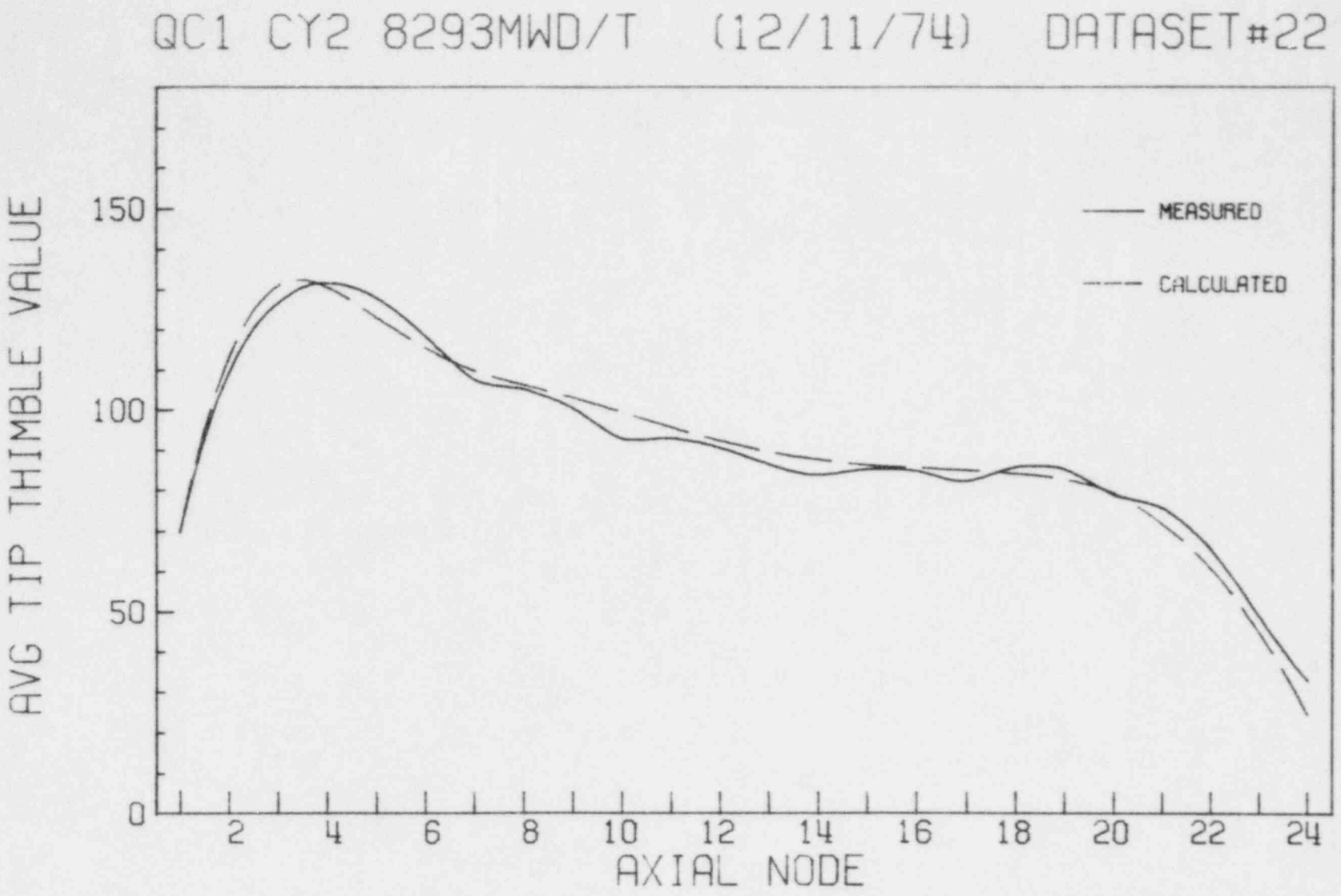
QC1 CY2 8293MWD/T (12/11/74) DATASET#22
AVG TIP THIMBLE VALUE
150
100
50
0
2
4
6
8
10
12
14
16
18
20
22
24
AXIAL NODE
MEASURED
CALCULATED

Figure 4.1-21

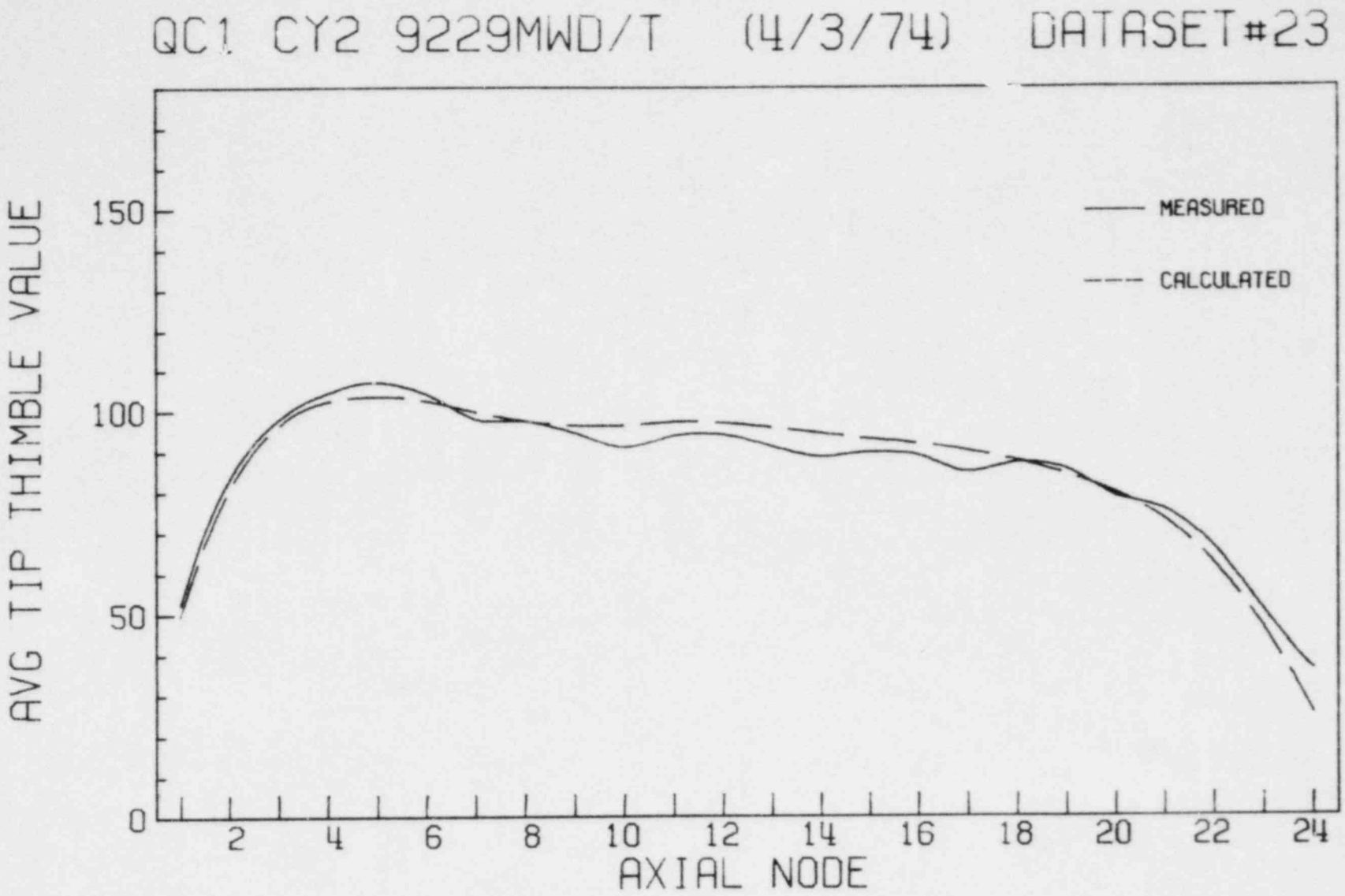
QC1 CY2 9229MWD/T (4/3/74) DATASET#23
AVG TIP THIMBLE VALUE
150
100
50
0
2
4
6
8
10
12
14
16
18
20
22
24
AXIAL NODE
MEASURED
CALCULATED

Figure 4.1-22

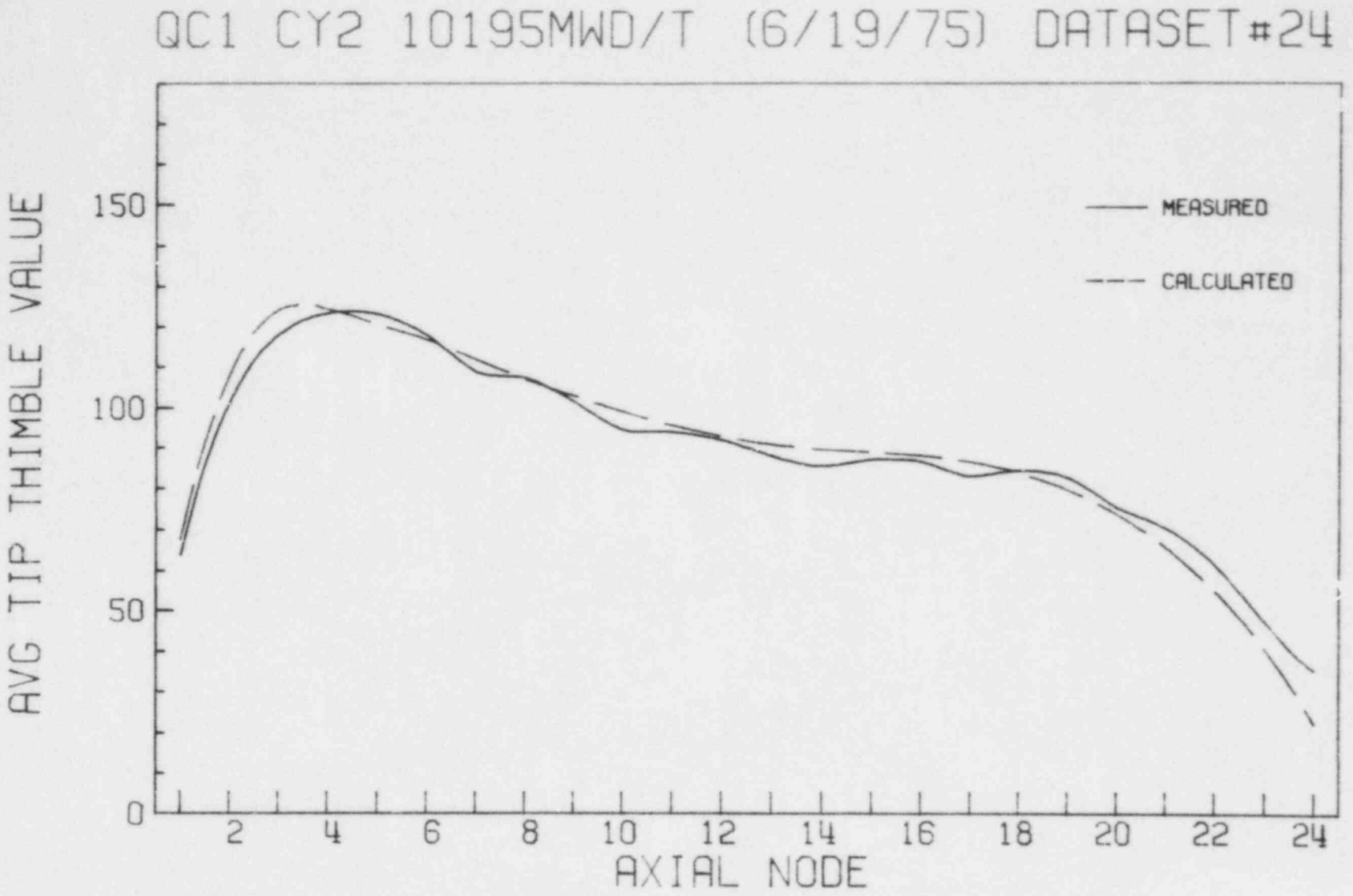
QC1 CY2 10195MWD/T (6/19/75) DATASET#24
AVG TIP THIMBLE VALUE
150
100
50
0
2
4
6
8
10
12
14
16
18
20
22
24
AXIAL NODE
MEASURED
CALCULATED

Figure 4.1-23

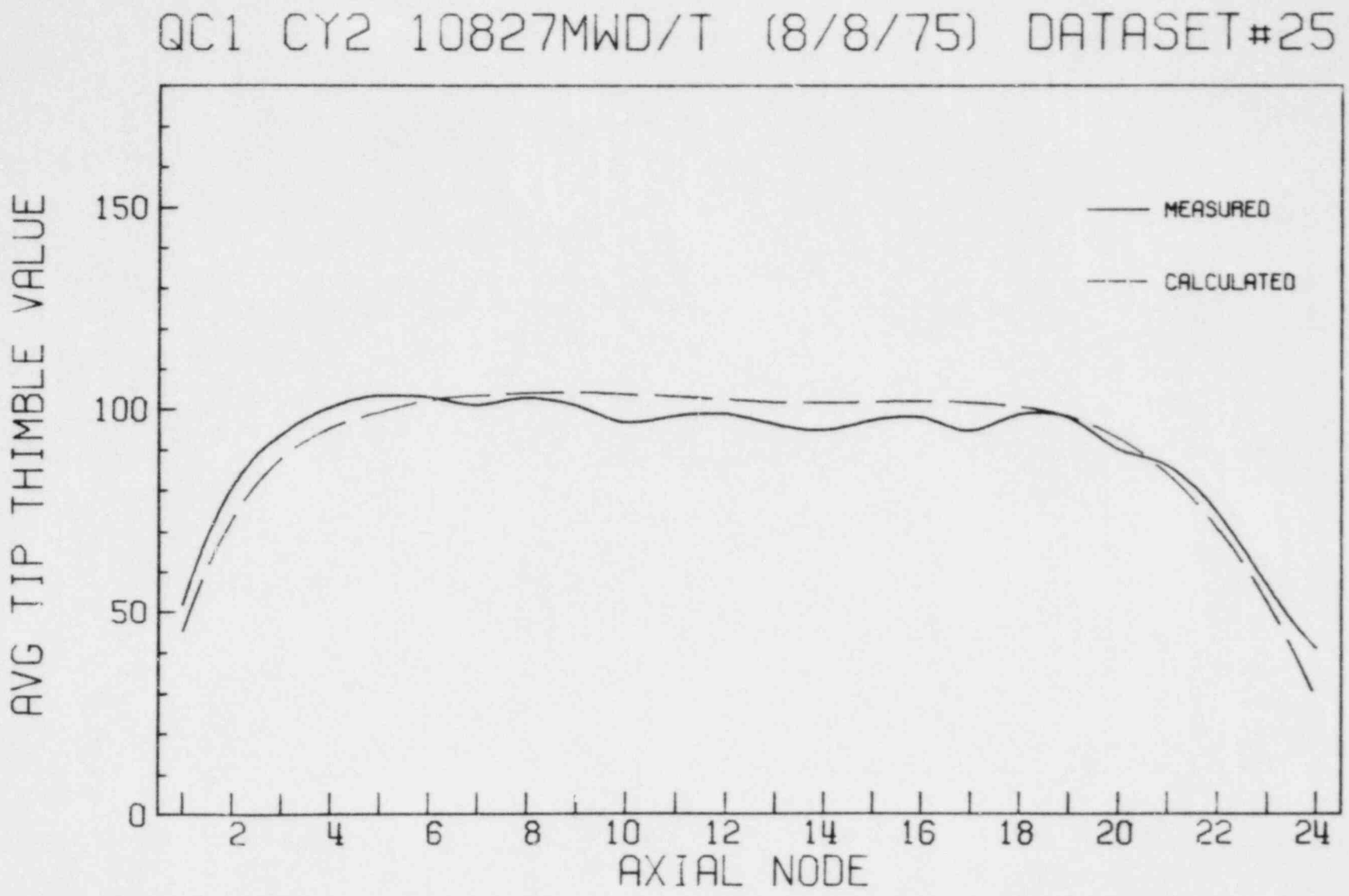
QC1 CY2 10827MWD/T (8/8/75) DATASET#25
AVG TIP THIMBLE VALUE
150
100
50
0
2
4
6
8
10
12
14
16
18
20
22
24
AXIAL NODE
MEASURED
CALCULATED

Figure 4.1-24

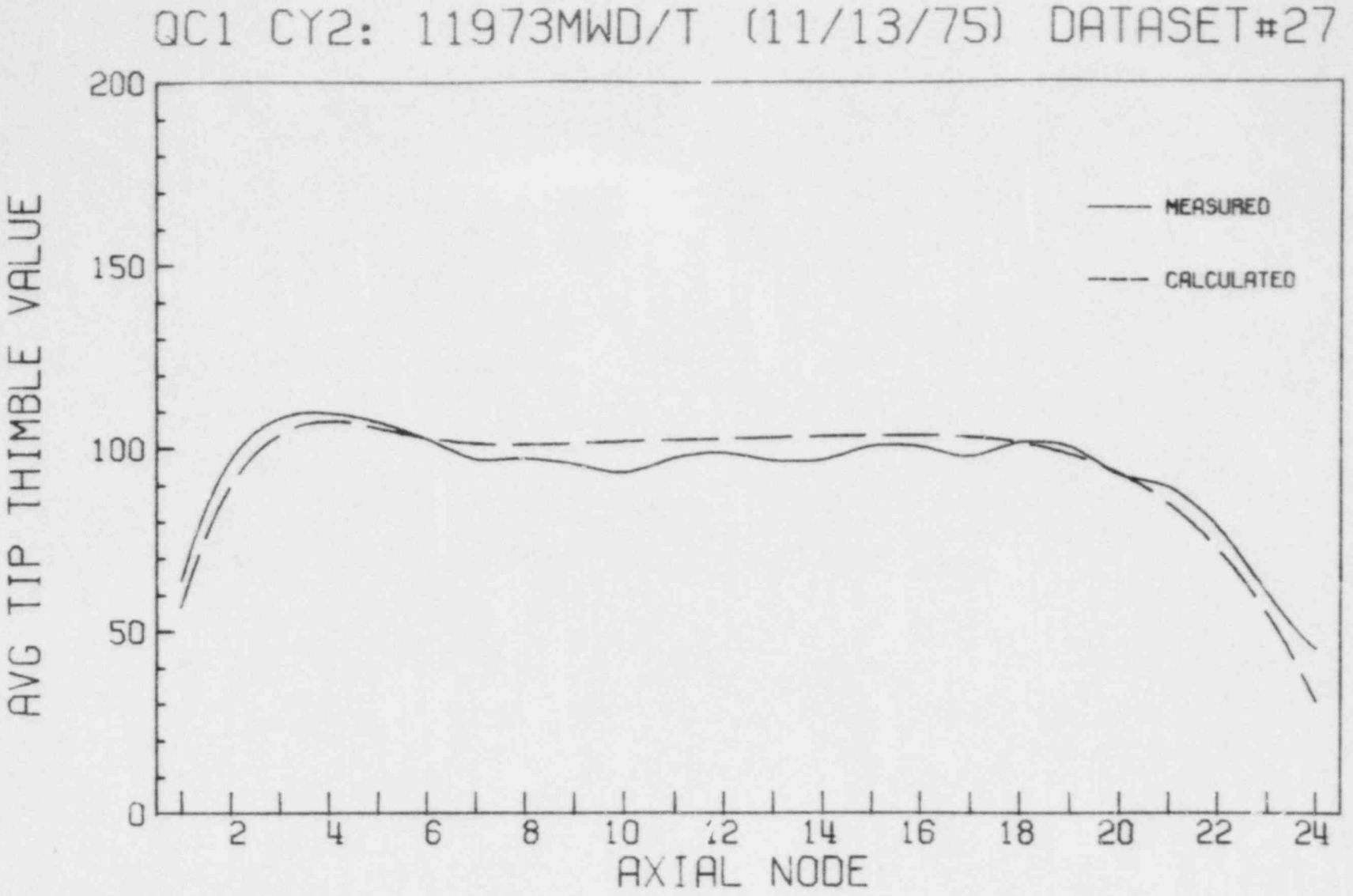
QC1 CY2: 11973MWD/T (11/13/75) DATASET#27
AVG TIP THIMBLE VALUE
200
150
100
50
0
2
4
6
8
10
12
14
16
18
20
22
24
AXIAL NODE
MEASURED
CALCULATED

Figure 4.1-25

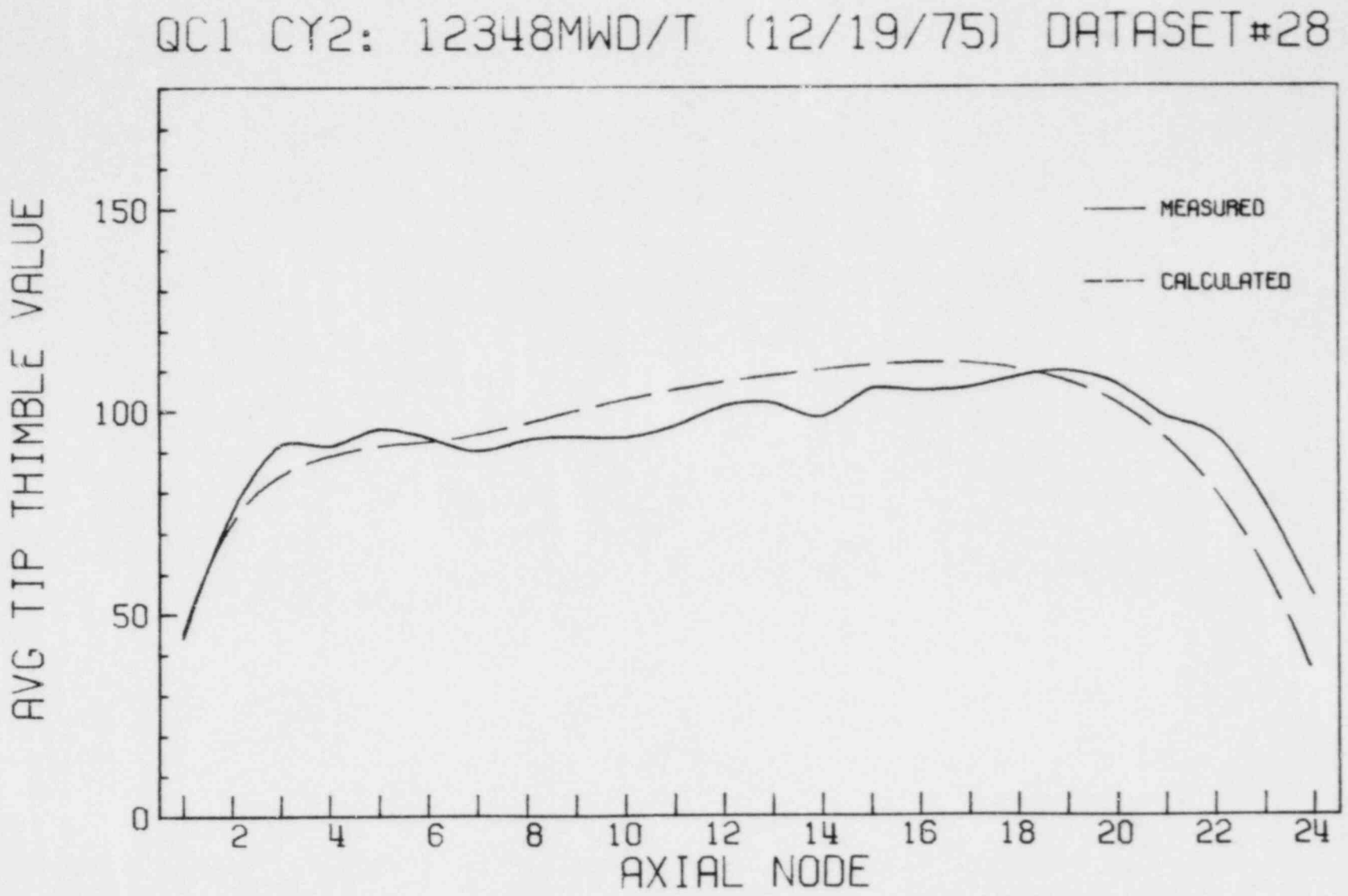
QC1 CY2: 12348MWD/T (12/19/75) DATASET#28
AVG TIP THIMBLE VALUE
150
100
50
0
2
4
6
8
10
12
14
16
18
20
22
24
AXIAL NODE
MEASURED
CALCULATED

Figure 4.i-26

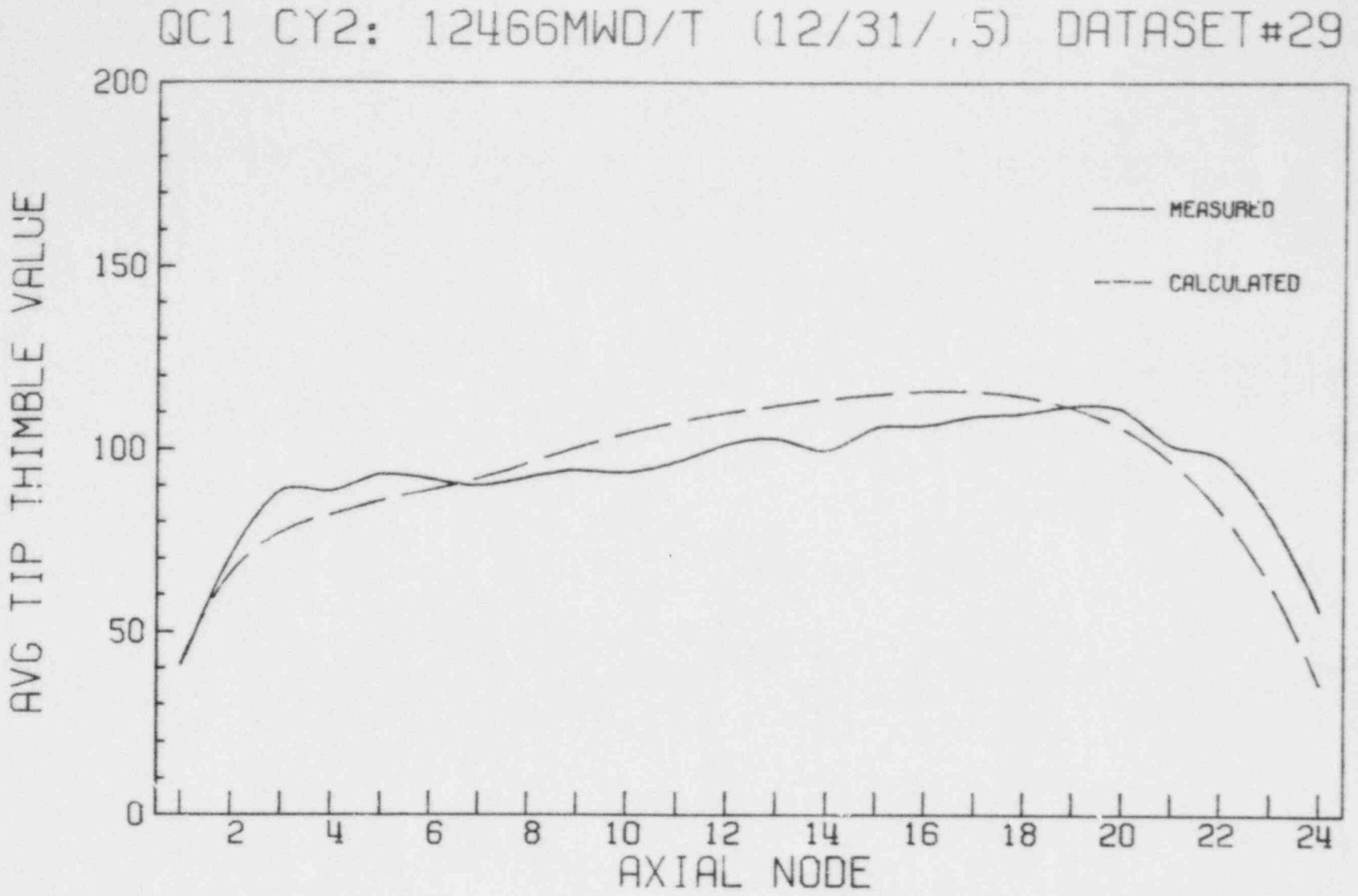
QC1 CY2: 12466MWD/T (12/31/.5) DATASET#29
AVG TIP THIMBLE VALUE
200
150
100
50
0
2
4
6
8
10
12
14
16
18
20
22
24
AXIAL NODE
MEASURED
CALCULATED

Figure 4.1-27

4.1.4 End-of-Cycle Gamma Scan Comparisons

The most precise information available for verification of power distributions predicted by CORE results from fuel assembly gamma scans. The gamma scan measures the relative La-140 activity distribution. La-140 is produced by decay of the fission product Ba-140 which has a half-life of approximately 13 days. Thus the La-140 distribution is proportional to the power distribution during the 40 to 60 days of operation prior to the scan. Since the power distribution may change during this time period, the CORE code maintains a calculated Ba-140 distribution by solving the differential equation for Ba-140 production and decay for each node in the core.

The gamma scan measurement data from Reference 4-4 for Quad Cities unit 1 at end-of-cycle 1 was utilized to verify CORE's capability to predict axial peaking factors and axial power shapes. Table 4.1-5 compares the calculated and measured axial peaking factors in each of 31 scanned bundles. For all 31 bundles CORE predicted an axial peaking factor which averaged 4.72 percent higher than the measured values; the standard deviation of the differences was 2.64 percent. Fourteen of the scanned bundles were adjacent to partially inserted control rods while the remainder were uncontrolled. CORE overpredicted the uncontrolled bundle peaking factors by an average of 3.68 percent compared to 5.98 percent overprediction for partially controlled bundles. The standard deviation of the error between calculation and measurement was essentially the same for controlled and uncontrolled bundles.

TABLE 4.1-5

MEASURED VS COMPUTED ASSEMBLY AXIAL La-140 ACTIVITY
PEAK-TO-AVERAGE VALUES FROM QUAD CITIES 1 - 1974 GAMMA SCAN

Rod Notch	Location XX - YY	Gamma Scan	CORE Code	Percent Difference
48	39 - 58	1.2712	1.3210	-3.84
48	41 - 58	1.2125	1.3035	-7.23
48	41 - 56	1.2236	1.2594	-2.89
48	17 - 48	1.2870	1.3288	-3.20
48	55 - 42	1.1854	1.2579	-5.93
48	57 - 42	1.1913	1.2992	-8.67
48	57 - 40	1.2452	1.3154	-5.49
48	07 - 34	1.1763	1.2096	-2.79
48	09 - 32	1.1476	1.1944	-4.00
48	07 - 26	1.1696	1.1958	-2.21
48	09 - 24	1.1859	1.2338	-3.96
48	31 - 26	1.3543	1.3765	-1.63
48	47 - 18	1.2498	1.3135	-4.97
48	23 - 10	1.1784	1.2013	-1.93
48	25 - 08	1.2390	1.2286	0.84
48	31 - 10	1.1718	1.1935	-1.83
48	33 - 08	1.2212	1.2553	-2.75
38	39 - 56	1.2815	1.3353	-4.11
14	17 - 50	1.6087	1.7427	-7.99
38	15 - 48	1.2800	1.3285	-3.72
38	55 - 40	1.2688	1.3316	-4.83
08	09 - 34	1.4180	1.5151	-6.62
28	07 - 32	1.3225	1.4142	-6.70
08	09 - 26	1.3660	1.5130	-10.21
38	07 - 24	1.2313	1.2803	-3.91
14	49 - 18	1.6017	1.7366	-8.08
38	47 - 16	1.2829	1.3161	-2.55
08	25 - 10	1.3579	1.4936	-9.52
38	23 - 08	1.2512	1.2814	-2.38
08	33 - 10	1.3851	1.5044	-8.26
28	31 - 08	1.3693	1.4366	-4.80

FOR ALL 31 BUNDLES:	Average Difference	= -4.72
	Standard Deviation	= 2.64
17 UNCONTROLLED BUNDLES:	Average Difference	= -3.68
	Standard Deviation	= 2.28
14 CONTROLLED BUNDLES:	Average Difference	= -5.98
	Standard Deviation	= 2.56

The quoted reproducability of the gamma scan measurements was 2 percent (Reference 4-4).

Figure 4.1-28 displays the measured and calculated 31 bundle averaged axial La-140 distributions from the Quad Cities unit 1 1974 gamma scan. The gross axial power shapes are in excellent agreement with the CORE code overestimating the axial peaking factor by 3.6 percent. Since many of the bundles were adjacent to partially inserted control rods during operation prior to the gamma scan, the measured axial distributions varied from bundle to bundle depending upon the nearest control rod position. Figures 4.1-29 and 4.1-30 show typical uncontrolled and partially controlled bundle axial La-140 distributions respectively, taken from Reference 4-4. The overall agreement between measurement and calculation is good for both bundles; however, there is a slight overprediction of the nodal powers immediately above the partially inserted control rod.

Following cycle 2 operation of Quad Cities unit 1, a large body of gamma scan data was collected. The 1976 Quad Cities gamma scan collected detailed data on the gross power distribution in one octant of the core and in additional bundles to test the degree of asymmetry. The 1976 Quad Cities gamma scan data presented in Reference 4-5 was utilized to verify several aspects of CORE's power distribution predictions. In Reference 4-5, the accuracy of the gamma scan data was given as approximately 3 percent considering measurement uncertainty and biases.

Table 4.1-6 presents the comparison of measured and calculated

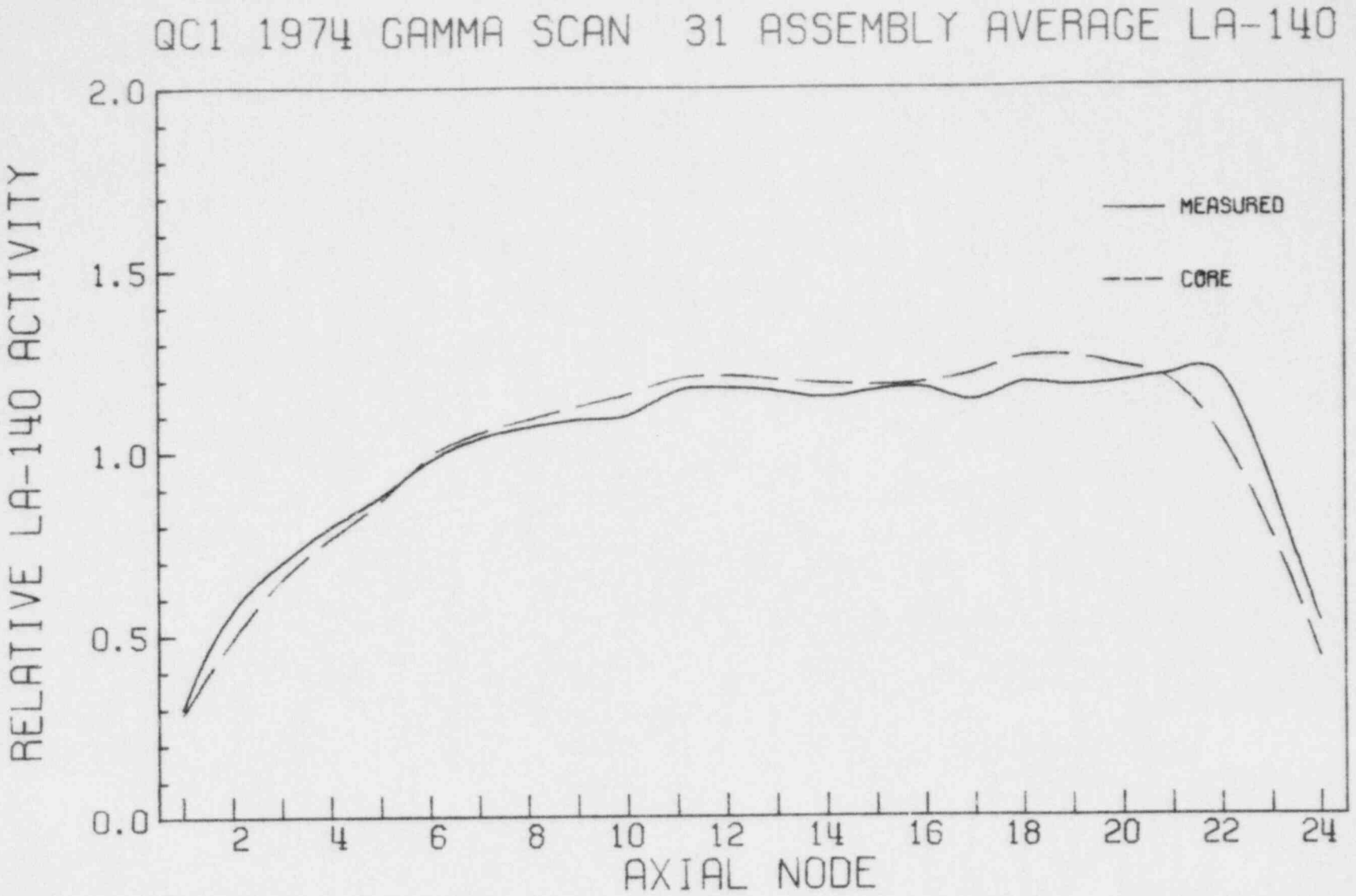
QC1 1974 GAMMA SCAN 31 ASSEMBLY AVERAGE LA-140
RELATIVE LA-140 ACTIVITY
2.0
1.5
1.0
0.5
0.0
2
4
6
8
10
12
14
16
18
20
22
24
AXIAL NODE
MEASURED
CORE

Figure 4.1-28

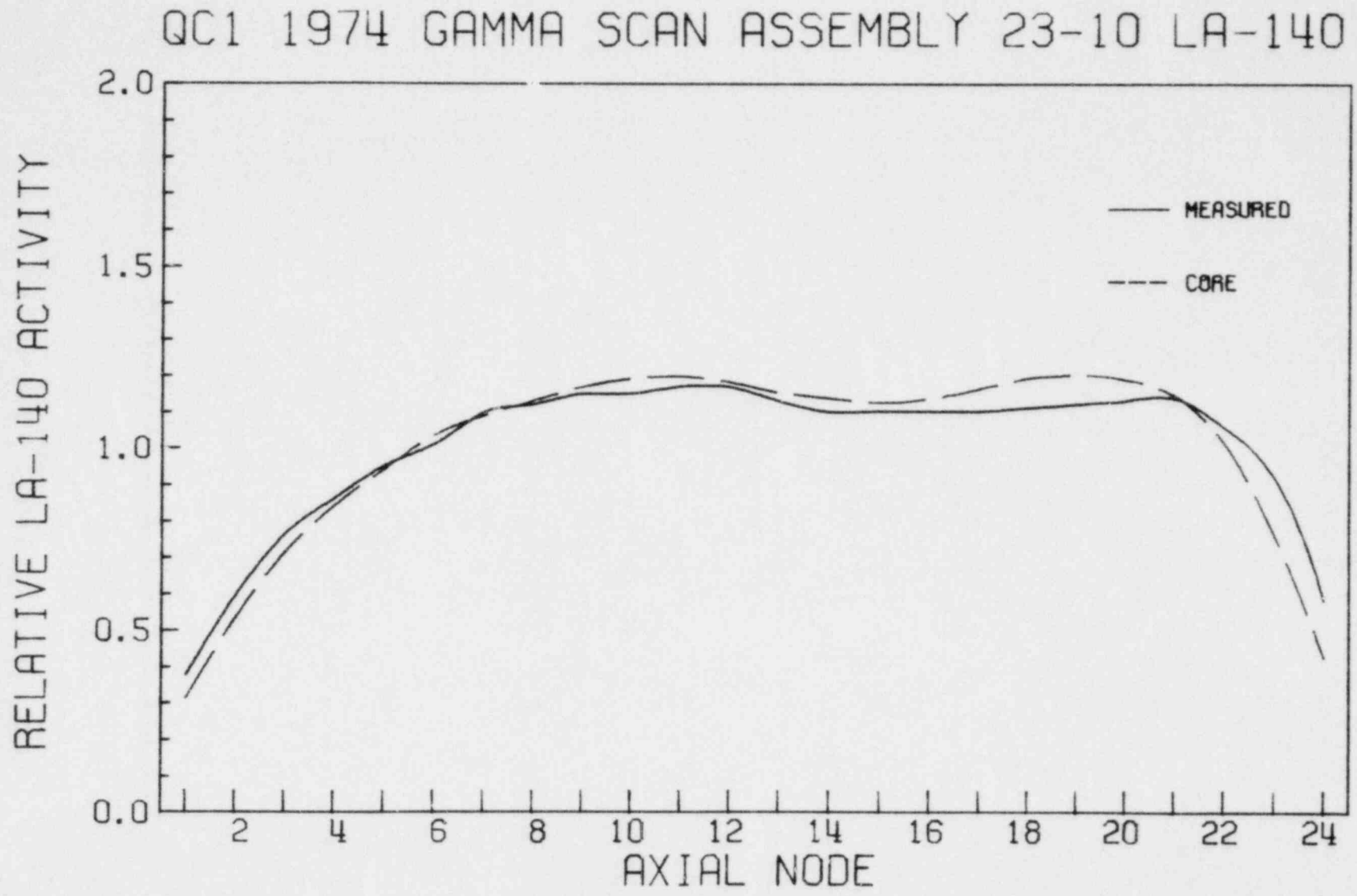

Figure 4.1-29: Typical Uncontrolled Assembly

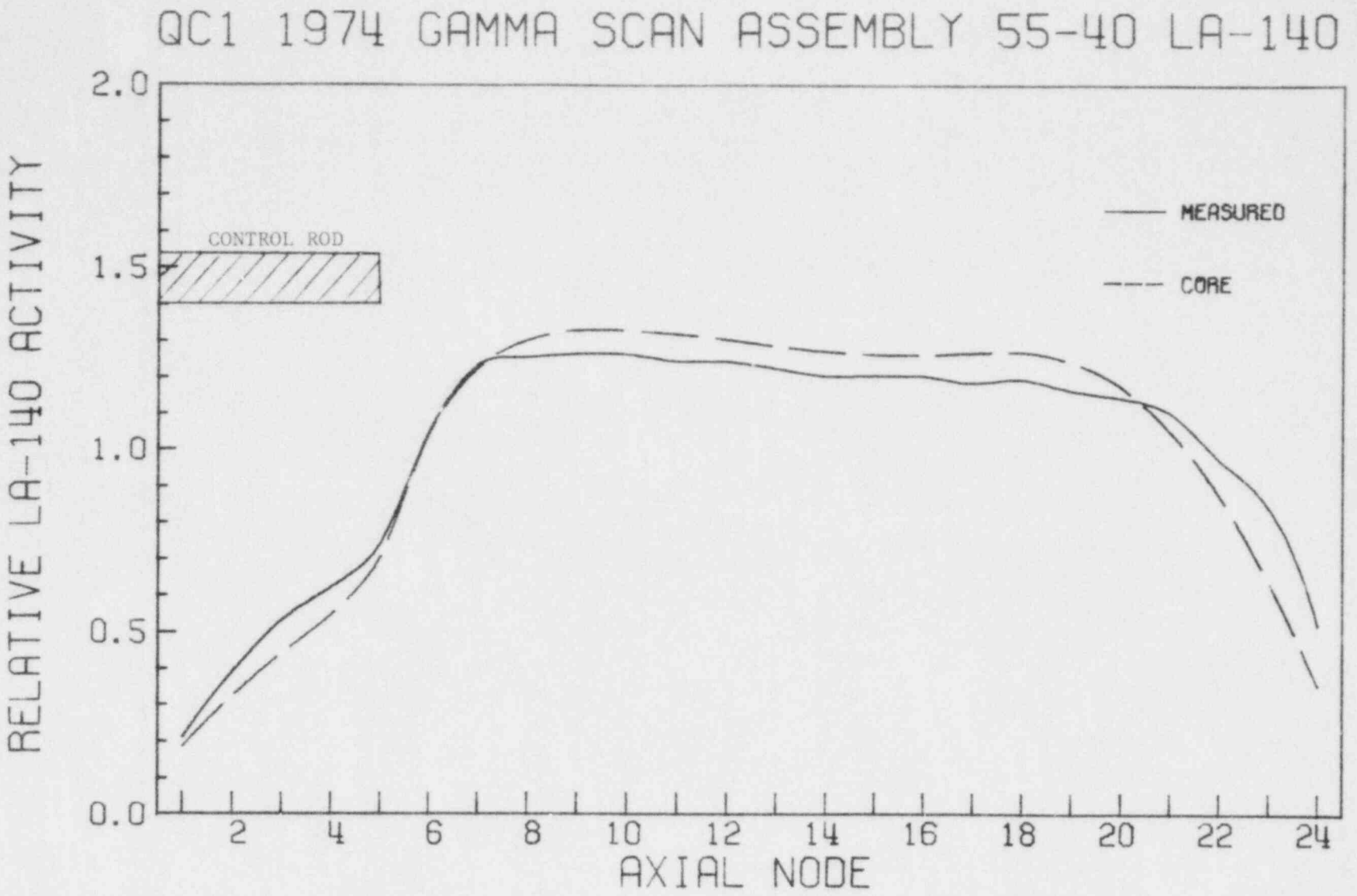

Figure 4.1-30: Typical Partially Controlled Assembly

TABLE 4.1-6

MEASURED VS COMPUTED ASSEMBLY AXIAL La-140 ACTIVITY
PEAK-TO-AVERAGE VALUES FROM QUAD CITIES 1 - 1976 GAMMA SCAN

Location XX - YY	Gamma Scan	CORE Code	Percent Diff.	Location XX - YY	Gamma Scan	CORE Code	Percent Diff.
33 - 44	1.1923	1.2181	-2.14	23 - 14	1.1946	1.2183	-1.97
31 - 32	1.1379	1.1642	-2.29	37 - 48	1.1852	1.2208	-2.96
31 - 30	1.1353	1.1639	-2.48	47 - 38	.1473	1.2126	-5.54
29 - 32	1.1335	1.1636	-2.62	09 - 48	1.3266	1.3401	-1.01
29 - 30	1.1302	1.1628	-2.84	05 - 36	1.2975	1.3176	-2.31
05 - 48	1.3518	1.3265	1.89	07 - 34	1.2445	1.2803	-2.83
31 - 34	1.1937	1.2049	-0.93	09 - 34	1.2285	1.2612	-2.63
33 - 32	1.1842	1.2096	-2.12	09 - 32	1.2341	1.2734	-3.13
07 - 48	1.3490	1.3748	-1.90	11 - 50	1.2933	1.3289	-2.71
05 - 46	1.3495	1.3167	2.46	13 - 32	1.2233	1.2487	-2.05
07 - 46	1.3333	1.3532	-1.48	27 - 34	1.1866	1.2090	-1.87
01 - 32	1.3311	1.3253	0.44	03 - 36	1.3468	1.3680	-1.56
03 - 32	1.3116	1.3580	-3.48	13 - 40	1.2187	1.2105	0.67
11 - 32	1.2263	1.2648	-3.09	23 - 38	1.1982	1.2244	-2.16
05 - 32	1.2785	1.3087	-2.33	03 - 40	1.3924	1.3893	0.22
47 - 06	1.3119	1.3031	0.68	15 - 46	1.1872	1.2276	-3.34
27 - 32	1.1802	1.2033	-1.94	21 - 32	1.1864	1.1933	-0.57
07 - 32	1.2420	1.2803	-3.03	09 - 46	1.3086	1.3149	-0.49
15 - 32	1.1990	1.2174	-1.52	15 - 38	1.2181	1.2175	0.05
19 - 32	1.1563	1.1846	-2.42	19 - 36	1.2103	1.2052	0.42
49 - 10	1.2911	1.3554	-4.86	05 - 38	1.3263	1.3308	-0.34
01 - 40	1.4128	1.3510	4.47	19 - 42	1.2039	1.2417	-3.09
13 - 36	1.1651	1.1948	-2.52	25 - 32	1.1932	1.2137	-1.70
23 - 34	1.1871	1.2067	-1.64	11 - 44	1.2169	1.2411	-1.97
17 - 42	1.2089	1.2282	-1.59	15 - 34	1.2006	1.2193	-1.54
09 - 40	1.2008	1.2141	-1.10	19 - 38	1.2237	1.2344	-0.87
07 - 42	1.3108	1.3087	0.16	13 - 46	1.2225	1.2416	-1.55
09 - 42	1.2586	1.2552	0.27	17 - 34	1.1857	1.1997	-1.18
07 - 40	1.2714	1.2692	0.18	09 - 36	1.1944	1.2176	-1.92
23 - 32	1.1975	1.2093	-0.98	17 - 36	1.1589	1.1895	-2.61
13 - 48	1.2107	1.2237	-1.07	13 - 44	1.1660	1.1977	-2.69
17 - 44	1.1664	1.2097	-3.65	21 - 36	1.1844	1.2038	-1.63
21 - 40	1.1861	1.2163	-2.51	17 - 32	1.1777	1.1915	-1.16
09 - 50	1.3328	1.3669	-2.52	09 - 38	1.2548	1.2318	1.85
41 - 18	1.2010	1.2293	-2.33	11 - 40	1.2054	1.2148	-0.78
17 - 40	1.2028	1.2321	-2.41	09 - 18	1.2007	1.2816	-6.52
15 - 42	1.1894	1.2063	-1.41	17 - 10	1.2137	1.2554	-3.38
15 - 40	1.2173	1.2303	-1.05	03 - 42	1.3827	1.3340	3.59
11 - 36	1.2028	1.2302	-2.25	01 - 34	1.3357	1.3295	0.47
15 - 36	1.1984	1.2134	-1.25	13 - 38	1.2103	1.2106	-0.02
13 - 34	1.2144	1.2364	-1.80	37 - 14	1.1634	1.2163	-4.45
25 - 36	1.1673	1.1863	-1.61	23 - 48	1.1941	1.2152	-1.75
25 - 34	1.1892	1.2059	-1.40	47 - 24	1.2168	1.2113	0.45
09 - 52	1.3590	1.3225	2.72	13 - 24	1.1558	1.2110	-4.67
05 - 44	1.3582	1.3061	3.92				

FOR ALL 89 ASSEMBLIES: Average Difference = -1.47
Standard Deviation = 1.89

peak-to-average La-140 activity in each of the 89 scanned bundles. The agreement between measurement and calculation is excellent with the calculated peaking factor averaging 1.5 percent higher than measured with a standard deviation of 1.9 percent. A measure of the agreement on maximum nodal power was obtained by comparing the relative La-140 activity for the 25 highest measured and calculated values as shown in Table 4.1-7. For the 25 highest powered nodes, the CORE value averaged 1.4 percent higher than the gamma scan, with a standard deviation of 1.3 percent.

The 1976 Quad Cities unit 1 gamma scan provided sufficient data to allow an excellent comparison of the calculated and measured radial distribution of bundle powers. Figure 4.1-31 shows the comparison of the relative radial La-140 activities obtained by averaging the nodal values in each assembly for the measured elevations. The standard deviation of the differences between measured and calculated radial powers was 3.82 percent. The CORE code slightly underestimated (5.7 percent) the power in the peripheral fuel bundles, but no gross distortion in the radial power shape is evident. The maximum measured radial activity of 1.352 (at coordinate 29-30) occurred in a mixed-oxide bundle and was underestimated by 3.46 percent by CORE. CORE overestimated the maximum radial value, regardless of location, by 1.25 percent. Table 4.1-8 presents the standard deviation of the differences between the 89 calculated and measured nodal values for each of the 12 axial planes with any axial bias removed. The average of the planar standard deviations is 4.85 percent and the maximum is 7.96 percent. A slight tendency for larger radial error exists

TABLE 4.1-7

COMPARISON OF 25 HIGHEST NODAL La-140 ACTIVITIES*
QUAD CITIES 1 - 1976 GAMMA SCAN

Gamma Scan	CORE Code	Percent Difference
1.584	1.655	-4.423
1.567	1.643	-4.729
1.558	1.632	-4.654
1.558	1.582	-1.519
1.547	1.564	-1.106
1.546	1.561	-0.995
1.531	1.560	-1.866
1.528	1.559	-1.994
1.528	1.555	-1.775
1.524	1.536	-0.794
1.523	1.529	-0.346
1.523	1.526	-0.187
1.519	1.522	-0.198
1.519	1.521	-0.157
1.511	1.518	-0.448
1.511	1.518	-0.462
1.511	1.518	-0.438
1.510	1.517	-0.426
1.505	1.517	-0.811
1.501	1.515	-0.897
1.501	1.514	-0.911
1.495	1.513	-1.237
1.485	1.513	-1.879
1.484	1.508	-1.569
1.484	1.507	-1.589
	Average Difference	-1.416
	Standard Deviation	1.331

*The 1,068 nodal activities (12 planes where all 89 assemblies were measured) were normalized to an average of 1.0

(NOTE: SEE CONTINUATION FOR ADDITIONAL VALUES)

FOR ALL 89 MEASURED ASSEMBLIES:
STANDARD DEVIATION OF DIFFERENCE = 3.82%

Y	X→ 01	03	05	07	09	11	13	15	17	19	21	23	25	27	29	31	33
52					0.479 0.437 9.27												
50					0.634 0.685 -7.83	0.789 0.825 -4.56											
48			0.450 0.389 14.45	0.603 0.658 -8.78	0.768 0.818 -6.35		1.223 1.191 2.68										
46			0.491 0.489 0.44	0.702 0.754 -7.02	0.851 0.898 -5.40		1.057 1.098 -3.87	1.101 1.128 -2.43									
44			0.584 0.563 3.62			1.041 1.068 -2.52	1.344 1.30? ?.14		1.326 1.369 -3.18	← GAMMA SCAN ← CORE CODE ← % DIFFERENCE							
42		0.484 0.437 10.19		0.863 0.885 -2.49	0.988 1.019 -3.08			1.137 1.151 -1.21	1.166 1.169 -0.23	1.138 1.140 -0.19							
40	0.389 0.364 6.72	0.596 0.637 -6.57		0.926 0.938 -1.29	1.265 1.199 5.37	1.115 1.094 1.87	1.102 1.106 -0.32	1.106 1.129 -1.98	1.189 1.218 -2.42		1.285 1.286 -0.11						
38			0.840 0.854 -1.56		1.078 1.075 0.30		1.092 1.109 -1.51	1.108 1.100 0.76		1.103 1.094 0.80		1.068 1.066 0.26					
36		0.708 0.741 -4.54	0.874 0.889 -1.68		1.326 1.238 6.93	1.117 1.116 0.07	1.337 1.278 4.57	1.124 1.113 0.99	1.321 1.292 2.27	1.104 1.098 0.56	1.085 1.077 0.74		1.273 1.246 2.13				
34	0.500 0.493 1.53			0.981 0.991 -1.00	1.057 1.059 -0.21		1.094 1.088 0.59	1.110 1.082 2.57	1.098 1.090 0.74			1.071 1.054 1.56	1.078 1.068 0.96	1.082 1.072 0.84		1.094 1.091 0.25	1.081 1.071 0.95
32	0.510 0.501 1.75	0.732 0.765 -4.29	0.865 0.886 -2.39	0.942 0.971 -3.05	1.013 1.025 -1.12	1.051 1.047 0.43	1.057 1.058 -0.09	1.083 1.074 0.84	1.088 1.060 2.58	1.068 1.050 1.70	1.047 1.033 1.38	1.046 1.031 1.42	1.071 1.054 1.65	1.110 1.094 1.46	1.349 1.306 3.24	1.339 1.306 2.54	1.080 1.092 -1.17
30															1.352 1.306 3.42	1.331 1.306 1.89	

FIGURE 4.1-31: ASSEMBLY AVERAGE RADIAL LA-140 ACTIVITY DISTRIBUTION COMPARISON FROM QUAD CITIES 1 1976 GAMMA SCAN

BUNDLE LABEL	LOCATION XX - YY	GAMMA SCAN	CORE CODE	PERCENT DIFFERENCE
CX 622	47 - 06	0.404	0.391	3.44
CX 711	49 - 10	0.619	0.685	-10.17
CX 445	41 - 18	1.145	1.171	-2.24
CX 359	37 - 14	1.087	1.131	-3.96
CX 398	23 - 48	1.076	1.128	-4.72
CX 401	47 - 24	1.103	1.113	-0.92
CX 318	13 - 24	1.123	1.108	1.33
CX 384	23 - 14	1.116	1.129	-1.17
CX 412	37 - 48	1.125	1.130	-0.42
CX 414	47 - 38	1.135	1.112	2.03
CX 096	09 - 18	0.974	0.967	0.73
CX 124	17 - 10	0.963	0.988	-2.54

FIGURE 4.1-31: Assembly Average Radial La-140 Activity Distribution Comparison from Quad Cities 1 - 1976 Gamma Scan (continued)

TABLE 4.1-8

NODAL STANDARD DEVIATIONS FOR THE 12 AXIAL PLANES
FROM QUAD CITIES 1 - 1976 GAMMA SCAN

Plane (Bottom)	% Planar Standard Deviation*
1	5.61
3	4.04
5	3.41
7	3.79
9	4.09
11	4.19
13	4.15
15	4.51
17	4.60
19	5.30
21	6.59
23 (Top)	7.96

*For each axial plane the 89 measured (M) and calculated (C) nodal values were normalized to an average of 1.0 and the difference at each node calculated by:

$$D_i = 200 * (M_i - C_i)/(M_i + C_i)$$

The standard deviation of the differences was calculated using the standard method:

$$\sigma = \sqrt{\frac{\sum_{i=1}^{n} (D_i - \bar{D})^2}{n-1}}$$

where $\bar{D}$ is the average of the D_i values and n is equal to 89

near the top and bottom boundaries, but overall the planar results are consistent with the 3.82 percent standard deviation for bundle radial powers.

Figure 4.1-32 shows the comparison of the 89 bundle average axial La-140 activity for the Quad Cities 1976 gamma scan. The CORE code underpredicts the power at the ends of the core and overpredicts the power in the center. The overall agreement is fair and is consistent with the axial TIP comparisons near end-of-cycle 2 presented in Section 4.1.3. The Quad Cities core was operated with all control rods withdrawn for a significant time prior to the 1976 gamma scan; therefore, the individual assembly axial comparisons are similar to the 89 assembly average, as shown in Figures 4.1-33 through 4.1-36 for typical bundles.

4.2 BROWNS FERRY UNITS 1 AND 2 COMPARISONS

The Browns Ferry units 1 and 2 initial cores each consisted of 168 fuel bundles with an average enrichment of 1.10 weight percent and 596 bundles with an average enrichment of 2.50 weight percent. All of the bundles were of standard 7 x 7 design. The higher enrichment bundles contained gadolinia in some of the fuel rods for power shaping and supplemental reactivity control. Both units were refueled with 8 x 8 design fuel with an average enrichment of 2.74 weight percent (168 reload bundles for unit 1 and 132 for unit 2). Details of the core designs are given in References 4-6, 4-7, and 4-8.

The measured data used for comparisons to CORE was obtained from data collected by plant personnel for records and contractual

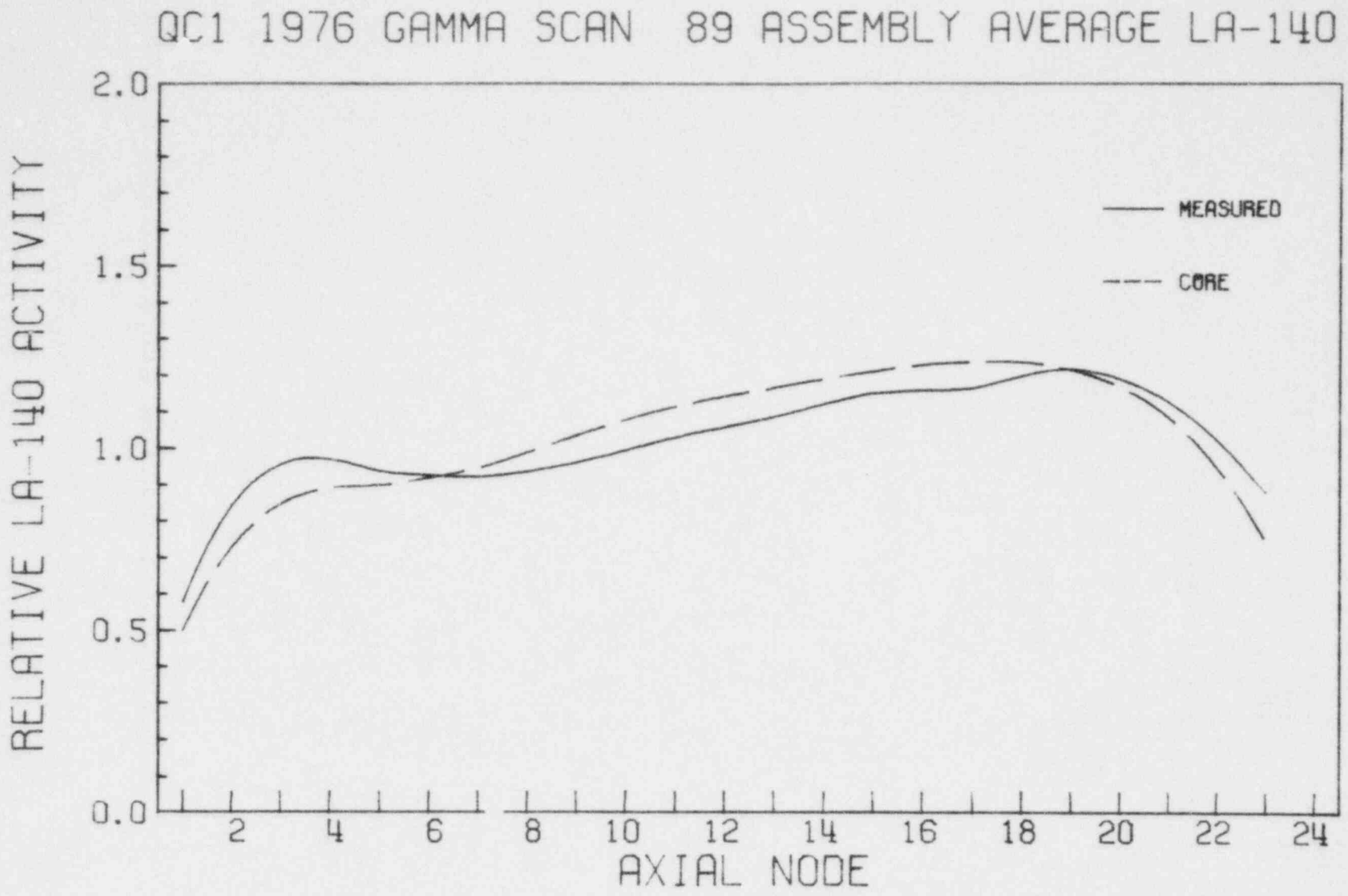
QC1 1976 GAMMA SCAN 89 ASSEMBLY AVERAGE LA-140
RELATIVE LA-140 ACTIVITY
2.0
1.5
1.0
0.5
0.0
2
4
6
8
10
12
14
16
18
20
22
24
AXIAL NODE
MEASURED
CORE

Figure 4.1-32

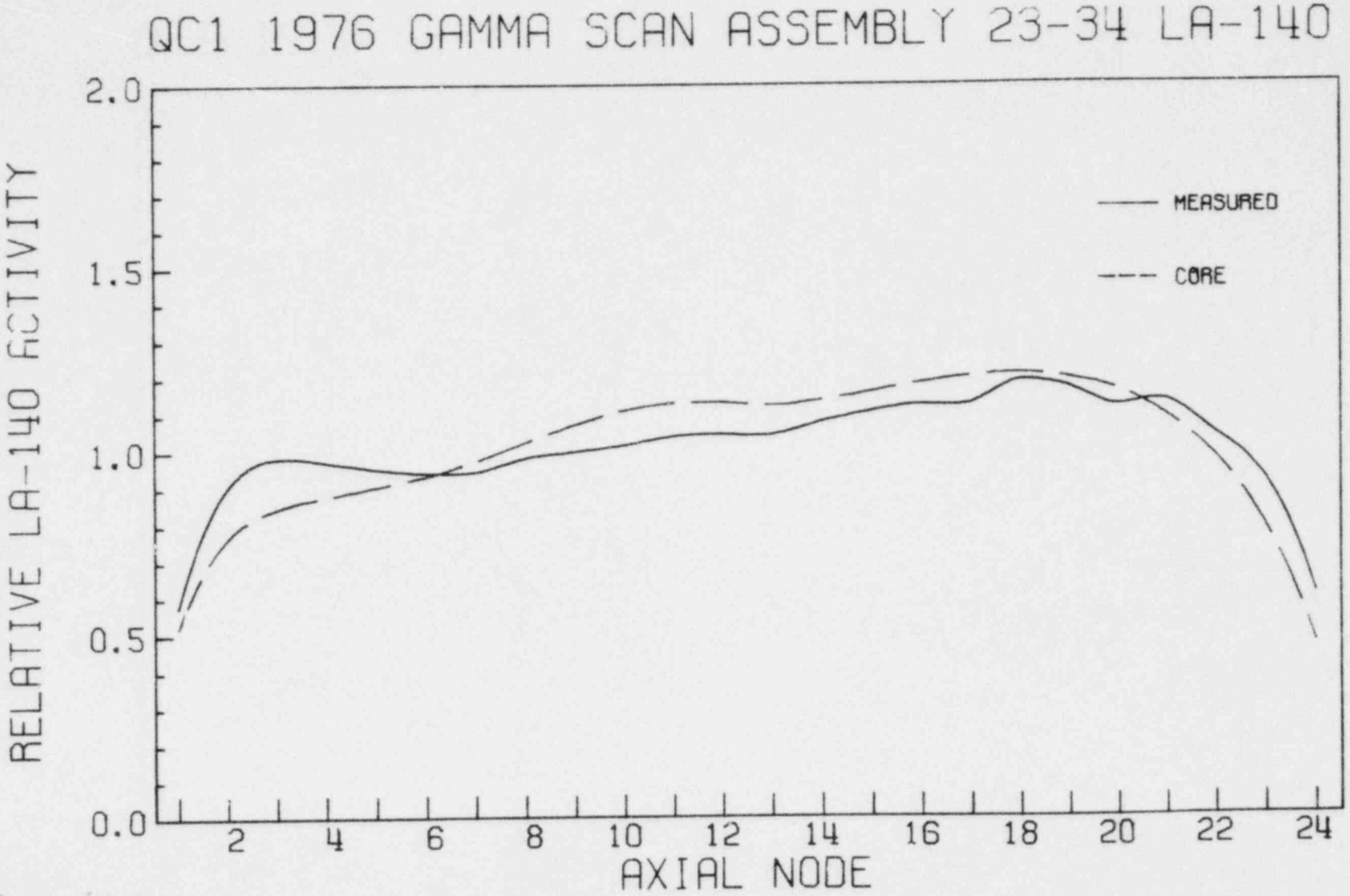

Figure 4.1-33: Initial Core 7 x 7 UO_2 Central Assembly

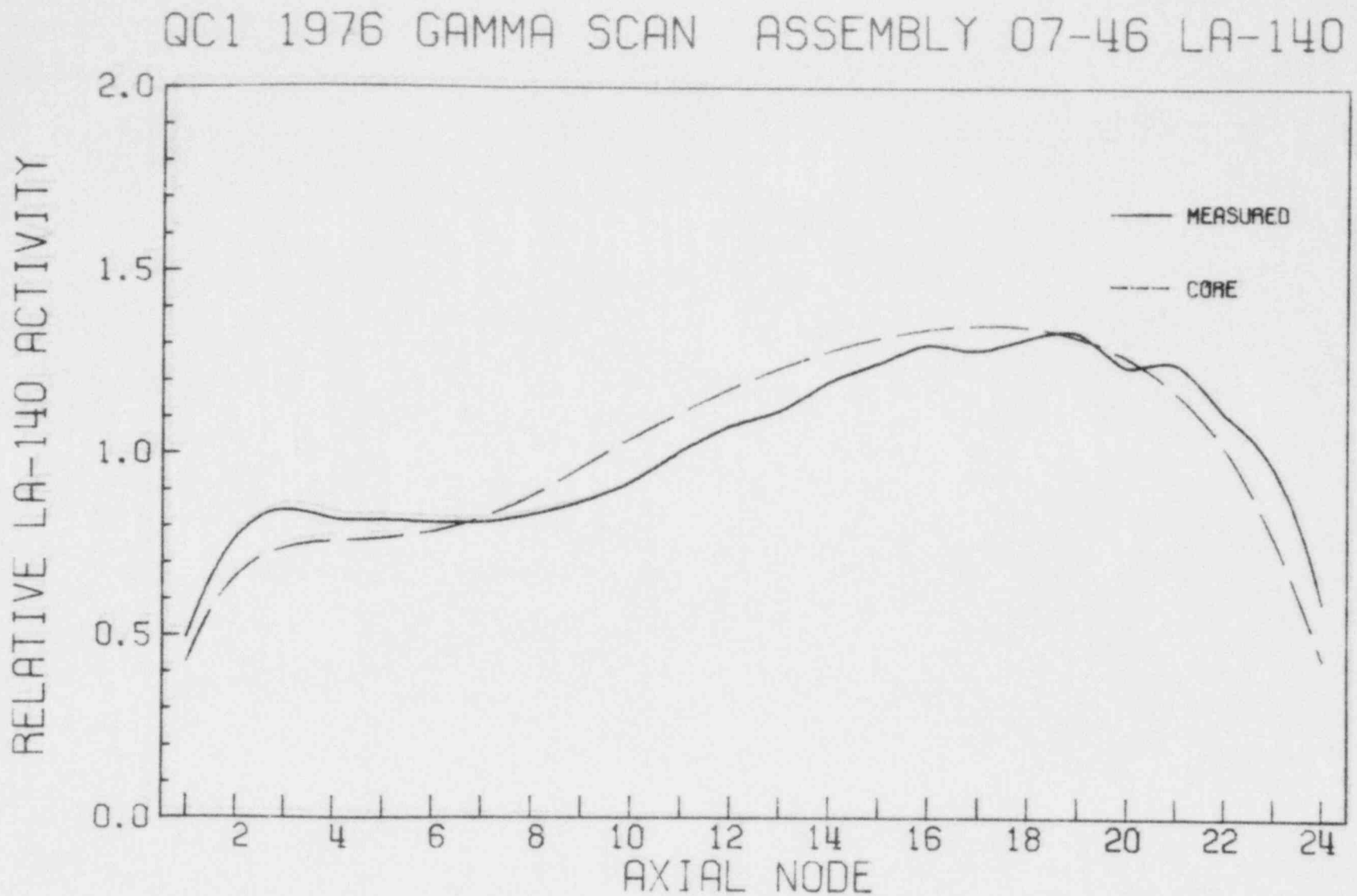

Figure 4.1-34 Initial Core 7 x 7 UO_2 Peripheral Assembly

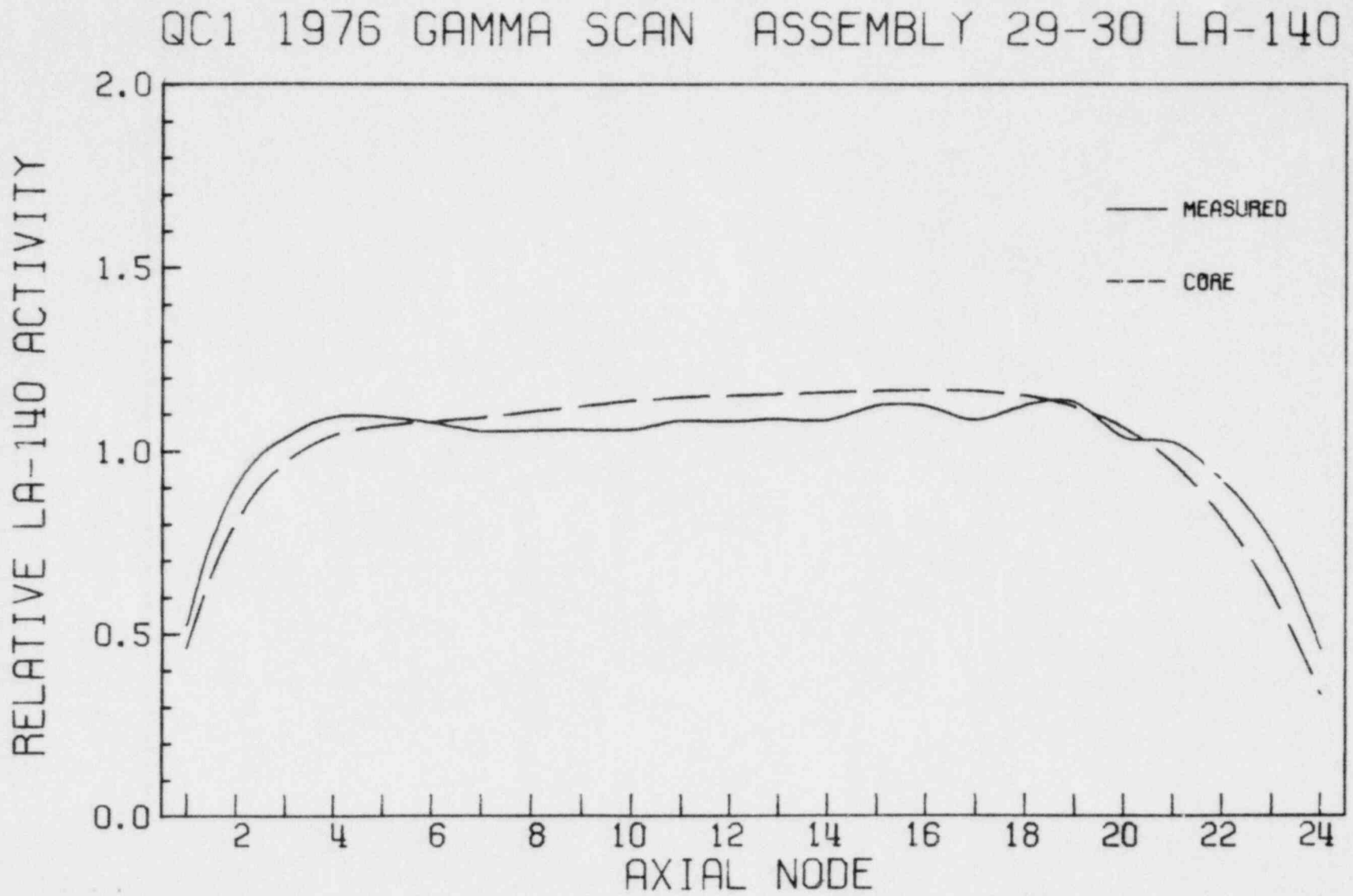

Figure 4.1-35: Reload 7 x 7 MO_2 Assembly

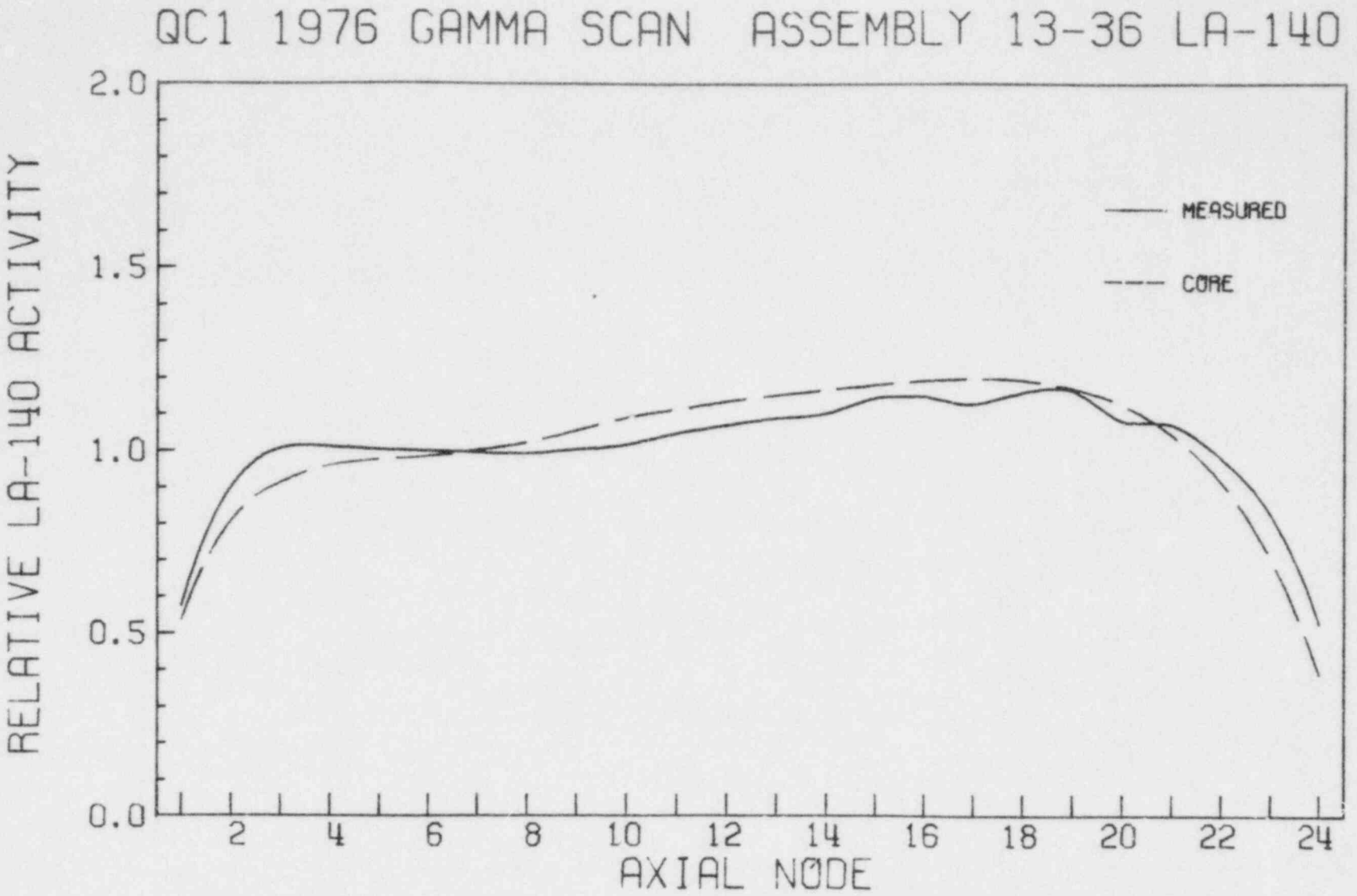

Figure 4.1-36: Reload 8 x 8 UO_2 Assembly

purposes. The data consisted of observed critical configurations (rod pattern, core thermal power level, total core flow rate, reactor pressure, core inlet temperature, and core average exposure) and power distribution information. The power distribution information was obtained from the plant process computer. The CORE code calculations for these comparisons were generated as part of normal core follow work performed by TVA. The lattice physics data used by CORE was generated with the LATTICE program (Reference 4-3). A full core model consisting of 30 x 30 x 24 nodes (24 equal length axial segments in each fuel bundle) was employed in the core follow calculations. The core average exposure accumulation between operating configurations was determined from the process computer data and the average increase allocated to individual nodes according to the power distribution computed by CORE at the beginning of the interval. In a similiar manner, the water density and control histories were updated for the interval. Generally, the core average exposure increment between operating states was between 250 and 500 MWD/MTU.

4.2.1 Zero Power, Xenon-Free Criticals

As a normal part of plant operations, the critical configuration of the reactor core is recorded fo each startup. The critical configurations occurring after sufficiently long shutdowns to allow the xenon-135 concentration to reach negligible levels are shown in Table 4.2-1 for cycles 1 and 2 of Browns Ferry units 1 and 2. These criticals cover the range of core average exposures from zero to approximately 14,200 MWD/MTU and coolant temperatures ranging from 101°F to 400°F. The rod patterns employed include

TABLE 4.2-1

ZERO POWER XENON-FREE CRITICALS FOR BROWNS FERRY UNITS 1 AND 2

Unit No.	Cycle No.	Date	Core Average GWD/MTU	Rod Pattern Information Seq.	Rods Out	Rod Moving Co-or	Notch	Coolant Temp. (°F)	Reactor Period (Sec)	Corrected* k-eff
1	1	9/25/73	0.0	Test	11	38-39	08	101	125	0.9973
1	1	9/25/73	0.0	A	52	46-35	20	112	140	0.9965
1	1	9/26/73	0.0	A	56	22-11	22	140	141	0.9962
1	1	3/08/74	0.963	A	72	38-19	14	330	78	0.9907
1	1	4/12/74	1.313	A	66	30-03	42	182	105	0.9953
1	1	5/22/74	1.617	A	56	38-11	18	170	89	0.9947
1	1	6/29/74	1.906	A	49	14-35	22	140	142	0.9943
1	1	10/04/74	3.519	A	44	30-35	20	200	147	0.9911
1	1	11/24/74	4.354	Test	5	30-23	10	132	76	0.9999
1	1	11/24/74	4.354	A	44	30-35	14	132	137	0.9996
1	1	2/09/75	5.759	A	32	10-23	30	215	76	0.9976
1	1	3/01/75	6.042	A	29	42-23	10	195	180	0.9979
1	1	9/14/76	6.345	A	29	42-23	12	185	112	0.9984
1	1	1/09/77	7.601	B	27	38-15	08	210	152	0.9942
1	2	1/13/78	9.730	B	24	42-31	12	150	79	0.9972
1	2	9/20/78	14.198	A	44	30-35	04	242	80	0.9954
2	1	7/20/74	0.0	Test	10	22-39	16	90	138	0.9977
2	1	8/03/74	0.0	A	54	46-19	16	124	125	0.9960
2	1	7/21/74	0.0	A	52	46-35	10	110	350	0.9968
2	1	8/27/76	2.486	A	48	34-19	24	146	200	0.9958
2	1	4/21/77	5.937	A	45	26-27	16	410	85	0.9924
2	2	6/26/78	9.176	A	24	30-31	10	160	123	0.9971
									Average	0.9960
									Standard Deviation	0.0024

*The corrected k-eff has the reactivity equivalent of the observed period subtracted from the calculated k-eff.

both normal (distributed) withdrawal sequences (A and B) as well as a special test withdrawal sequence which successively removes rods in the center of the core in a checkerboard pattern. The test sequence was used for shutdown margin determination during startup testing.

The effective multiplication factor obtained by CORE for each critical is also shown in Table 4.2-1. The CORE k-effective has been corrected by subtracting the reactivity equivalent of the observed reactor period from the code output values. No other corrections, normalizations or biases were employed. The average k-effective obtained by CORE for the 22 critical configurations was 0.9960 with a standard deviation of 0.0024. There are no apparent systematic trends in predicted k-effective versus exposure or control rod pattern. In particular, there is not a significant difference in the calculated k-effective for in-sequence and the more localized test sequence criticals at the same core average exposure.

4.2.2 Hot Operating Reactivity

Table 4.2-2 lists the critical configurations with equilibrium xenon and high reactor power for which comparisons were made for Browns Ferry unit 1 during cycles 1 and 2. The average k-effective calculated by CORE for the 20 configurations in Table 4.2-2 was 1.0041 with a standard deviation of 0.0040. However, there is a definite trend in the predicted k-effective versus exposure. The observed trend is similar to that observed in Reference 4-4 for first cycle gadolinia bearing cores. The tendency to predict

TABLE 4.2-2

BROWNS FERRY 1, CYCLES 1 AND 2, HOT OPERATING k-eff

Date	Cycle	Core Average GWD/MTU	Fraction of Rated Power	Calculated k-eff
2/02/74	1	0.639	0.639	0.9966
6/21/74	1	1.852	0.982	1.0024
7/18/74	1	2.359	0.989	1.0010
10/29/74	1	3.942	0.972	0.9987
11/02/74	1	4.026	0.976	1.0006
1/15/75	1	5.389	0.931	0.9981
2/18/75	1	5.908	0.943	0.9987
3/22/75	1	6.346	0.985	1.0010
1/19/77	1	7.698	0.981	1.0068
2/22/77	1	8.296	0.957	1.0064
4/21/77	1	9.416	0.947	1.0083
6/13/77	1	10.370	0.942	1.0085
7/20/77	1	11.021	0.893	1.0091
8/09/77	1	11.378	0.819	1.0086
9/13/77	1	11.994	0.598	1.0084
4/14/78	2	11.281	0.967	1.0050
4/26/78	2	11.521	0.978	1.0055
5/26/78	2	12.203	0.947	1.0059
6/29/78	2	12.798	0.966	1.0059
8/08/78	2	13.591	0.894	1.0056
			Average	1.0041
			Standard Deviation	0.0040

higher k-effectives near the end of the first cycle may have been accentuated in the Browns Ferry unit 1 comparisons due to the presence of boiling in the bypass region. All of the cycle 1 data in Table 4.2-2 for core average exposures greater than 7500 MWD/MTU was collected after plugging of the bypass flow holes in the core plate to eliminate instrument tube vibrations. Alternate flow paths were drilled into the fuel bundle lower tie plates after cycle 1 and significant bypass boiling did not occur in cycle 2. For core average exposures less than 7500 MWD/MTU, the average calculated k-effective was 0.9996 with a standard deviation of 0.0019. For core average exposures greater than 7500 MWD/MTU, the calculated values were 1.0070 and 0.0015 respectively.

4.2.3 Process Computer Comparisons

Table 4.2-3 contains a comparison of axial and total peaking factors from the Browns Ferry unit 1 process computer during cycles 1 and 2 to the peaking factors calculated by the CORE code. For the 16 cases in Table 4.2-3, the core average axial peak-to-average power was overpredicted by CORE by 0.5 percent with a standard deviation of 4.3 percent. The total peaking factor (radial x axial x local) was overpredicted by 1.0 percent with a 5.6 percent standard deviation.

Table 4.2-4 summarizes the results obtained by comparing the relative power in individual nodes and fuel assemblies predicted by CORE to their values from the process computer. For the seven configurations considered, the root-mean-square (RMS) difference in process computer and CORE calculated relative powers was 7.0 percent for assemblies and 11.4 percent for nodes.

TABLE 4.2-3

BROWNS FERRY 1, CYCLES 1 AND 2, COMPARISON OF CORE CODE AND PROCESS COMPUTER PEAKING FACTORS

Date	Core Average GWD/MTU	Core Average Axial Peak-to-Average Power P.C.	CORE	% Diff	Total Peaking Factor P.C.	CORE	% Diff
2/02/74	0.639	1.27	1.27	0.0	2.39	2.44	-2.07
6/21/74	1.852	1.30	1.24	4.72	2.47	2.29	7.56
7/18/74	2.359	1.34	1.29	3.80	2.44	2.25	8.10
10/29/74	3.942	1.37	1.34	2.22	2.61	2.53	3.11
11/02/74	4.026	1.36	1.31	3.75	2.58	2.43	5.99
1/15/75	5.389	1.40	1.48	-5.56	2.71	2.78	-2.55
2/18/75	5.908	1.32	1.43	-8.0	2.55	2.67	-4.60
3/22/75	6.346	1.27	1.35	-6.11	2.39	2.52	-5.30
2/22/77	8.296	1.27	1.28	-0.78	2.57	2.49	3.16
4/21/77	9.416	1.34	1.38	-2.94	2.52	2.70	-6.90
7/20/77	11.021	1.29	1.28	0.78	2.17	2.13	1.86
8/09/77	11.378	1.32	1.29	2.30	-	-	-
4/14/78	11.281	1.29	1.43	-10.30	2.29	2.52	-9.56
5/26/78	12.203	1.24	1.29	-3.95	2.15	2.29	-6.31
6/29/78	12.798	1.15	1.22	-5.91	2.02	2.11	-4.36
8/08/78	13.591	1.15	1.23	-6.72	2.05	2.12	-3.36
			Average	-0.49		Average	-1.02
			Standard Deviation	4.27		Standard Deviation	5.53

The percent difference is calculated as:

% Diff = 200*(P.C. - CORE)/(P.C. + CORE)

TABLE 4.2-4

BROWNS FERRY 1, CYCLES 1 AND 2, COMPARISON OF CORE CODE AND PROCESS COMPUTER POWER DISTRIBUTIONS

Date	Cycle	Core Average GWD/MTU		RMS Difference in Relative Powers Assembly	Nodal
7/18/74	1	2.359		8.43	11.50
11/02/74	1	4.026		6.52	11.54
1/19/77	1	7.698		5.75	8.37
6/13/77	1	10.370		5.45	9.87
8/09/77	1	11.378		6.45	10.42
4/26/78	2	11.521		7.37	13.73
6/29/78	2	12.705		8.17	13.50
			Combined	6.96	11.42

The RMS difference between the process computer (PC) and core code (CORE) relative power distributions was calculated as:

$$D_i = 100*(PC_i - CORE_i) \qquad \text{(percent)}$$

$$RMS = \sqrt{\frac{1}{n}\left(\sum_{i=1}^{n} D_i^2\right)}$$

where n is 764 for assembly comparisons and 18,336 for nodal comparisons.

A comparison of the radial peaking factors (maximum bundle relative powers) as determined by CORE and the Browns Ferry unit 1 process computer is shown in Table 4.2-5. The radial peaking factors predicted by CORE during cycles 1 and 2 averaged 2.8 percent higher than the process computer values; the standard deviation of the differences was 3.2 percent. There is a slight tendency for CORE to underpredict the radial peaking factor early in the cycles and overpredict the values near the end of cycles relative to the process computer.

Figures 4.2-1 through 4.2-7 present comparisons of the core average relative power versus axial node for CORE and the process computer for several points in cycles 1 and 2 of Browns Ferry unit 1. The overall agreement between the axial distributions is good but CORE slightly underestimated the power in the bottom half of the core early in cycle 1. Near the end of cycle 1, CORE slightly overestimated the power in the bottom half of the core and this overestimation remained into cycle 2.

4.3 BROWNS FERRY UNIT 3 COMPARISONS

The Browns Ferry unit 3 initial core consisted of 764 fuel bundles of 8 x 8 design (one water rod and 146 inch active fuel length) with a bundle average enrichment of 2.19 weight percent. Two bundle types with different gadolinia content were employed. Details of the initial core design are given in Reference 4-6. The reload bundles were of 8 x 8 design (2 water rods and 150 inch active fuel length) with a bundle average enrichment of 2.65 weight percent. The cycle 2 core design is described in Reference 4-9.

TABLE 4.2-5

BROWNS FERRY 1, CYCLES 1 AND 2, COMPARISONS OF
CORE CODE AND PROCESS COMPUTER RADIAL PEAKING FACTORS

Date	Cycle	Core Average GWD/MTU	Maximum Bundle Power CORE	P.C.	Percent Difference
7/18/74	1	2.359	1.295	1.346	3.86
11/02/74	1	4.026	1.322	1.367	3.35
1/19/77	1	7.698	1.336	1.333	-0.22
6/13/77	1	10.370	1.349	1.310	-2.93
8/09/77	1	11.378	1.296	1.273	-1.79
4/26/78	2	11.521	1.349	1.356	0.52
6/29/78	2	12.798	1.397	1.332	-4.76
				Average	-2.81
				Standard Deviation	3.17

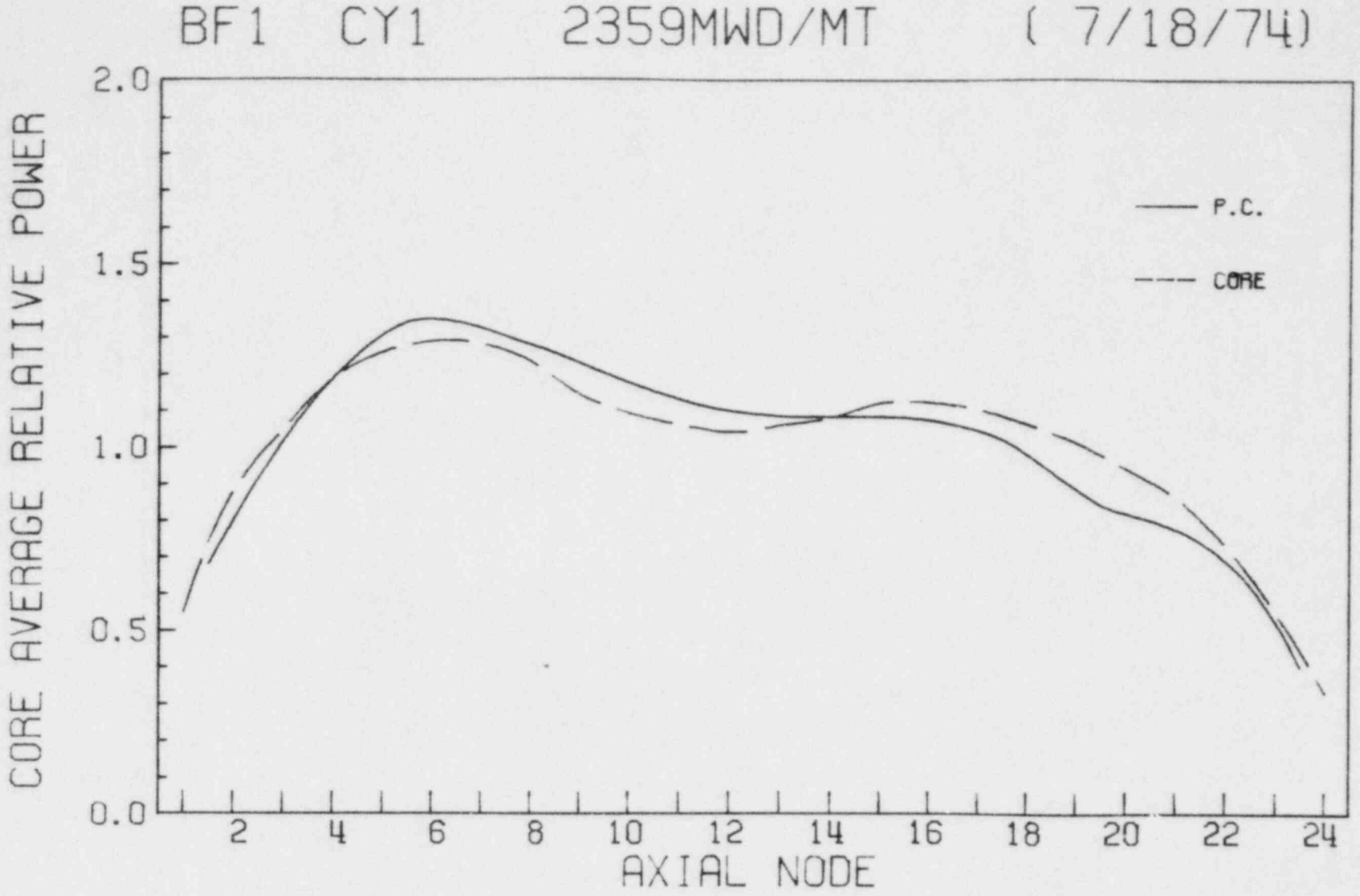
BF1 CY1 2359MWD/MT (7/18/74)
CORE AVERAGE RELATIVE POWER
2.0
1.5
1.0
0.5
0.0
P.C.
CORE
2
4
6
8
10
12
14
16
18
20
22
24
AXIAL NODE

Figure 4.2-1

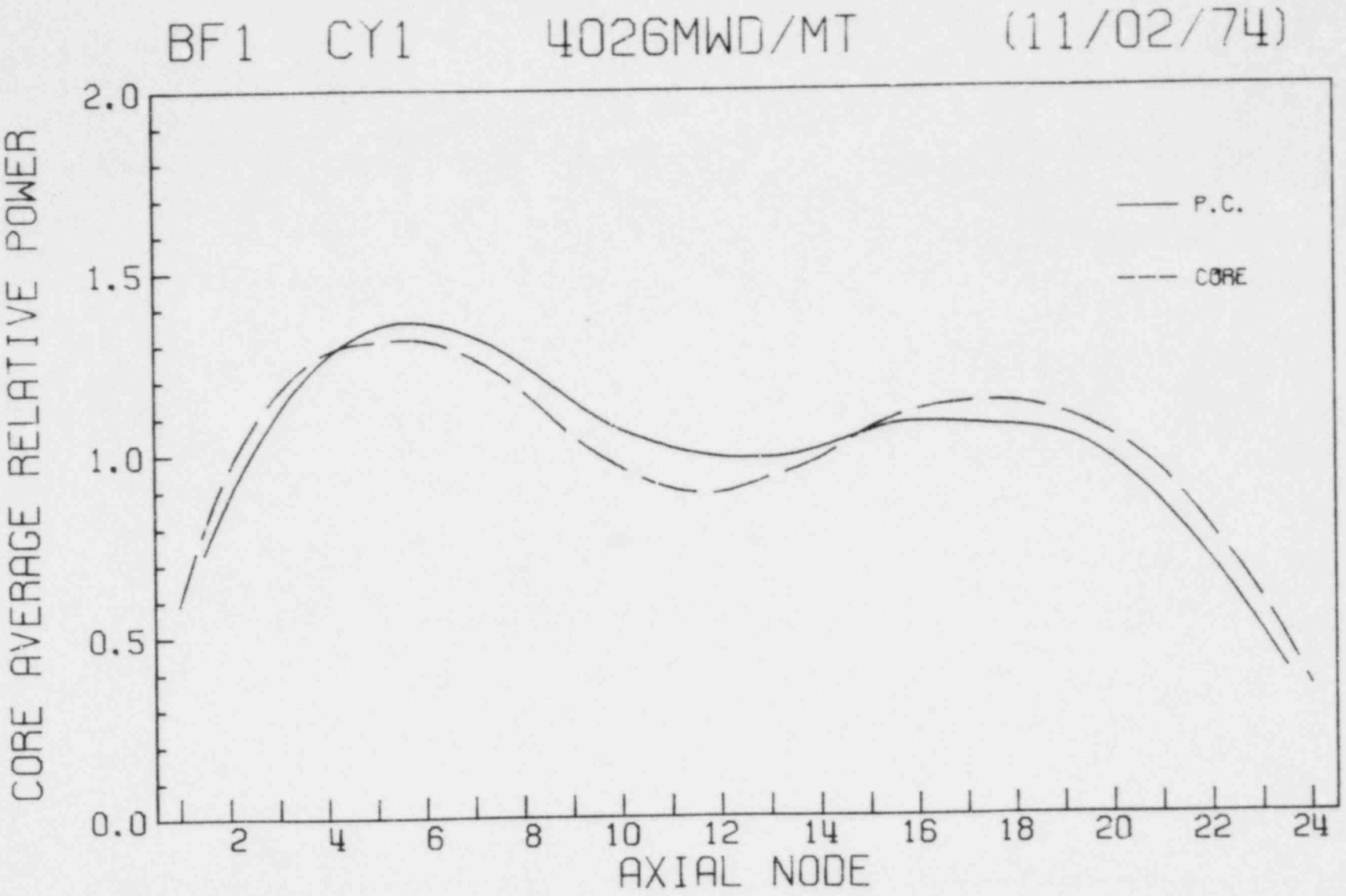
BF1 CY1 4026MWD/MT (11/02/74)
CORE AVERAGE RELATIVE POWER
2.0
1.5
1.0
0.5
0.0
2
4
6
8
10
12
14
16
18
20
22
24
AXIAL NODE
P.C.
CORE

Figure 4.2-2

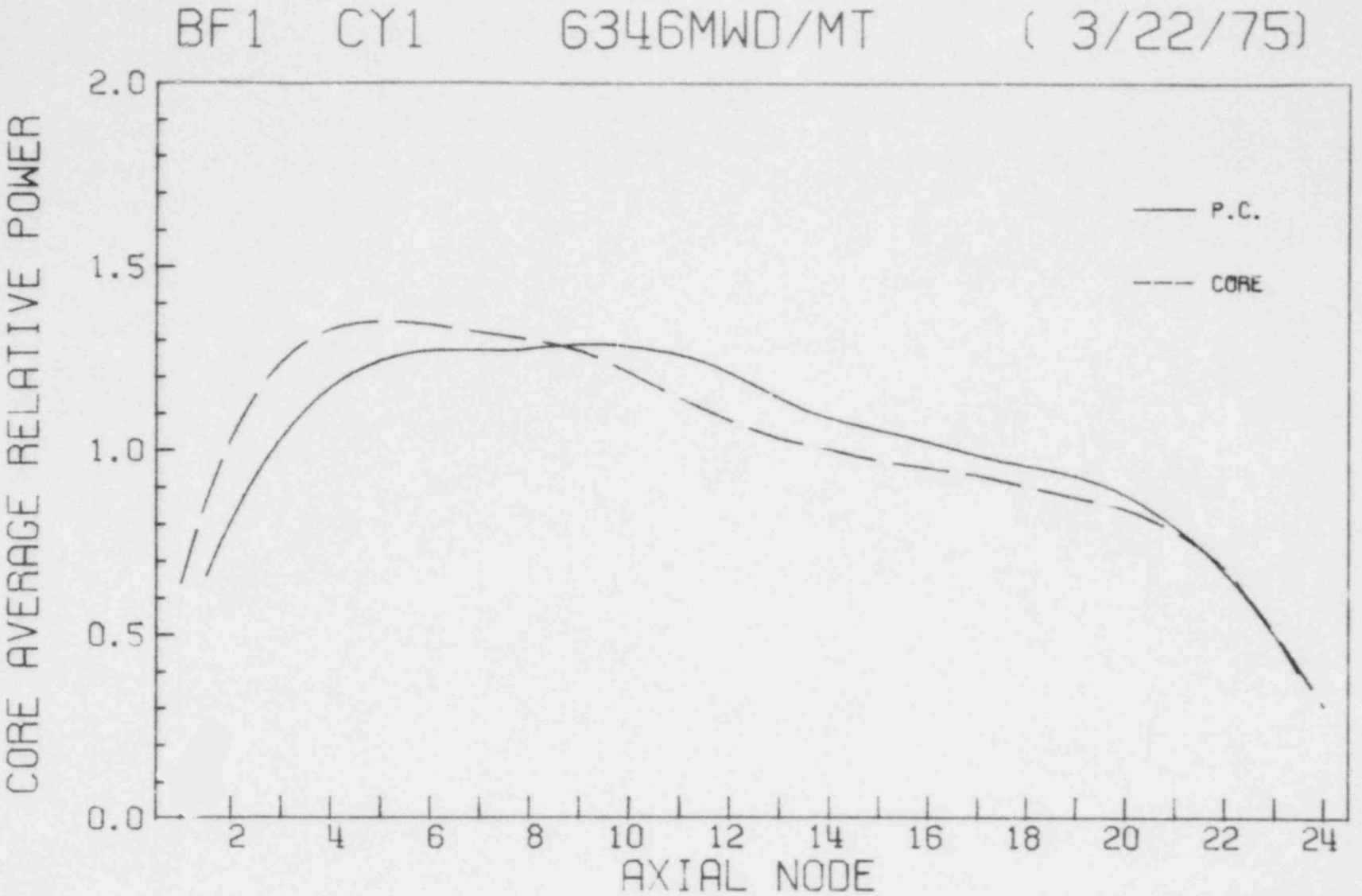
BF1 CY1 6346MWD/MT (3/22/75)
CORE AVERAGE RELATIVE POWER
2.0
1.5
1.0
0.5
0.0
P.C.
CORE
2
4
6
8
10
12
14
16
18
20
22
24
AXIAL NODE

Figure 4.2-3

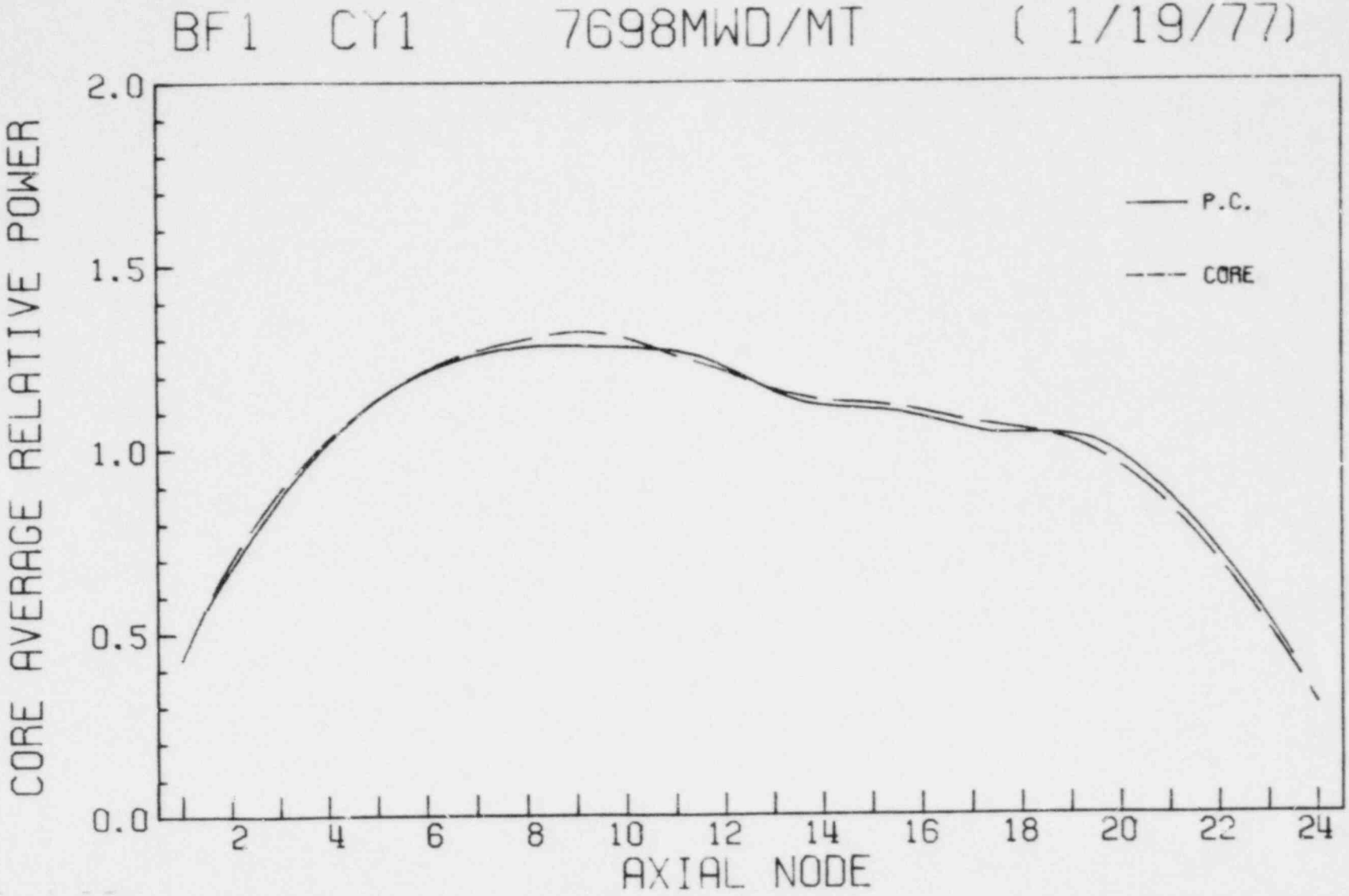
BF1 CY1 7698MWD/MT (1/19/77)
CORE AVERAGE RELATIVE POWER
2.0
1.5
1.0
0.5
0.0
P.C.
CORE
2
4
6
8
10
12
14
16
18
20
22
24
AXIAL NODE

Figure 4.2-4

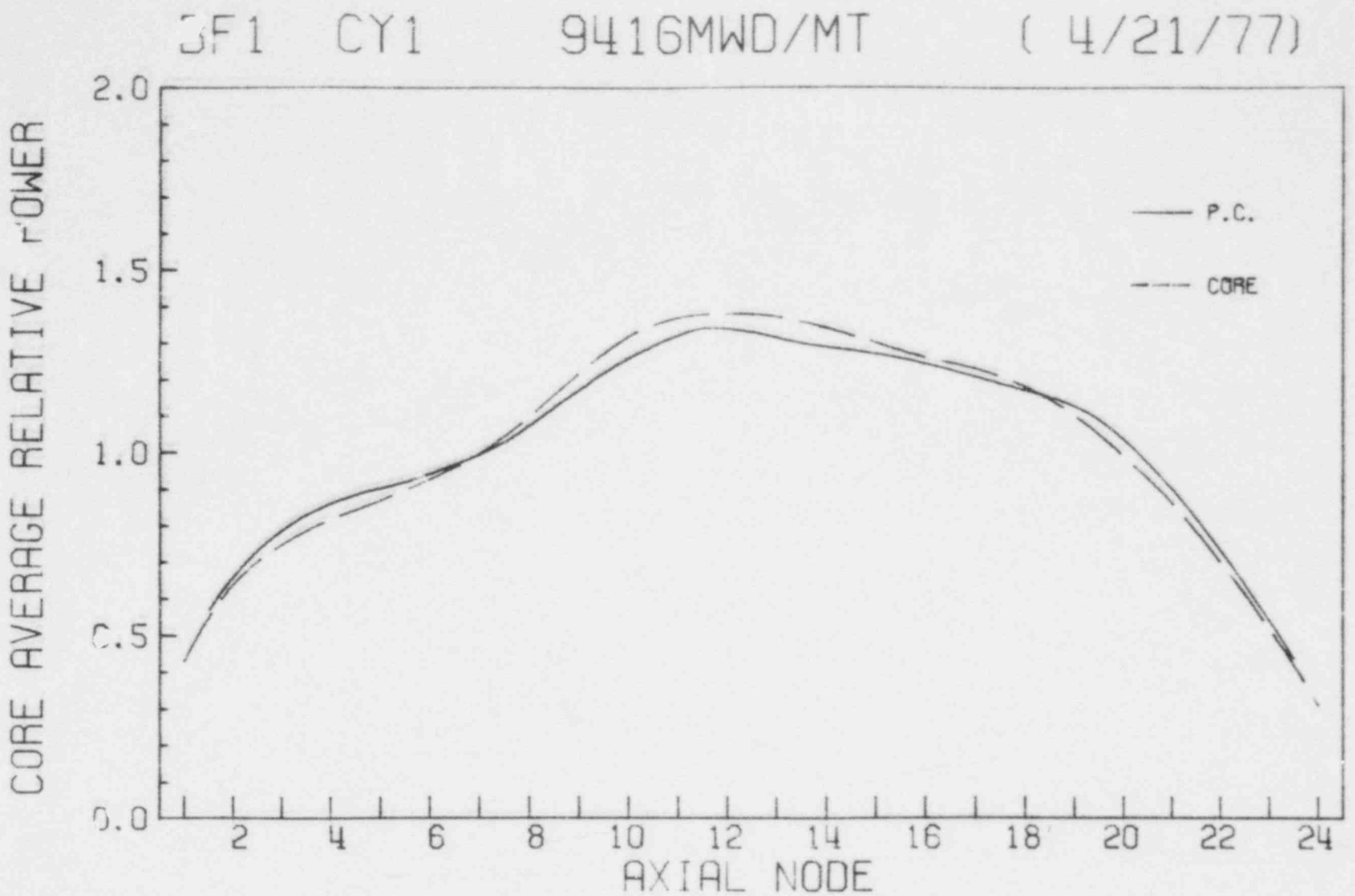
3F1 CY1 9416MWD/MT (4/21/77)
CORE AVERAGE RELATIVE POWER
2.0
1.5
1.0
0.5
0.0
P.C.
CORE
2
4
6
8
10
12
14
16
18
20
22
24
AXIAL NODE

Figure 4.2-5

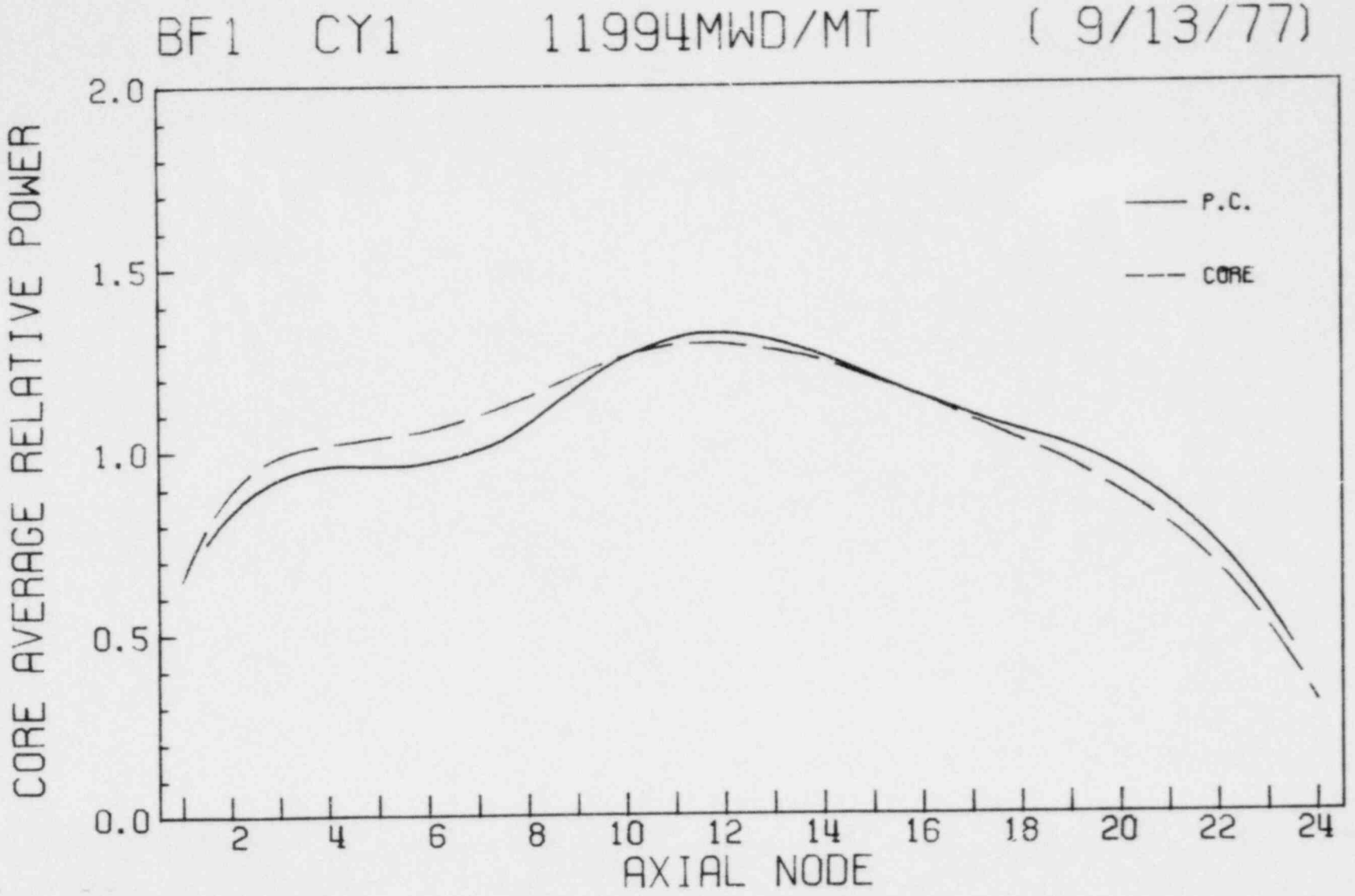
BF1 CY1 11994MWD/MT (9/13/77)
CORE AVERAGE RELATIVE POWER
2.0
1.5
1.0
0.5
0.0
2
4
6
8
10
12
14
16
18
20
22
24
AXIAL NODE
P.C.
CORE

Figure 4.2-6

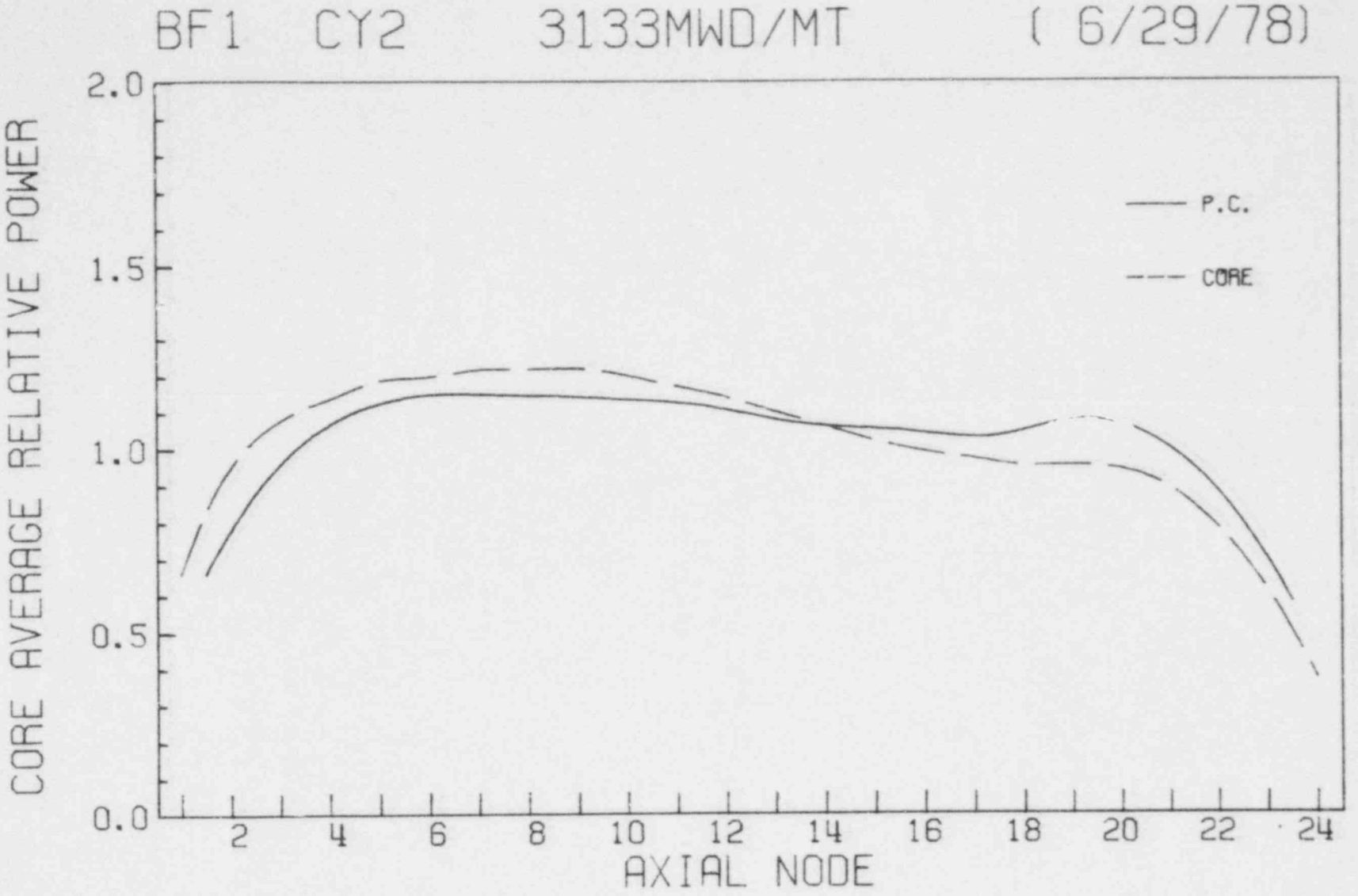
BF1 CY2 3133MWD/MT (6/29/78)
CORE AVERAGE RELATIVE POWER
2.0
1.5
1.0
0.5
0.0
P.C.
CORE
2
4
6
8
10
12
14
16
18
20
22
24
AXIAL NODE

Figure 4.2-7

The measured data utilized for comparisons to CORE was obtained as described for units 1 and 2. The CORE code input data and the exposure accumulation procedure were also as described for Browns Ferry units 1 and 2.

4.3.1 Zero Power Criticals

Table 4.3-1 presents the zero power criticals calculated for Browns Ferry unit 3 comparisons. The xenon concentration is not negligible for three of these criticals due to the short length of time the plant was shutdown (less than 60 hours). However, for the criticals for which xenon is not negligible, the reactor was operating at a condition of equilibrium xenon prior to the shutdown and shutdown occurred rapidly. Thus the xenon concentration after shutdown was readily calculated utilizing the transient xenon capability in CORE. The corrected k-effective values are the direct code output with the reactivity equivalent of the observed reactor period subtracted from them. The average k-effective obtained for the Browns Ferry unit 3 zero power criticals was 0.9991 with a standard deviation of 0.0036.

4.3.2 Hot Operating Reactivity

The principal high power critical configurations occurring during cycle 1 operation of Browns Ferry unit 3 are described in Table 4.3-2 along with the eigenvalue obtained from CORE. A beginning of cycle 2 high power configuration is also presented. The average k-effective for the 20 cases is 1.0015 with a standard deviation of 0.0033. The tendency to calculate higher k-effective values near the end of first cycles of gadolinia bearing cores is

TABLE 4.3-1

ZERO POWER CRITICALS FOR BROWNS FERRY UNIT 3

Date	Core Average GWD/MTU	Rod Pattern Information Rods Seq	Rods Out	Rod Moving Co-or	Notch	Coolant Temperature (°F)	Reactor Period (Sec)	Corrected*** k-eff
8/08/76	0.0	B	28	38-15	18	92	132	1.0023
4/30/77	3.599	B	45	26-27	12	212	162	1.0003
6/19/77	4.492	A	44	30-35	22	335	49	0.9980
7/10/77	4.755	A	45	38-27	14	455	140	0.9941
9/05/77*	5.695	A	44	30-35	06	170	69	1.0027
10/17/77	6.502	B	47	42-27	04	518	90	0.9972
11/26/77	7.262	A	45	38-27	24	514	45	0.9937
1/29/78*	8.480	B	51	18-35	20	230	84	1.0021
3/20/78	9.425	A	45	38-27	14	300	65	0.9927
4/2[illegible]/78	9.895	A	46	30-19	14	270	69	1.0020
7/14/78*	11.574	B	73	[illegible]-35	10	230	59	1.0021
8/21/78	12.201	B	74	[illegible]27	04	250	107	1.0010
11/22/78**	8.651	B	45	26-[illegible]7	12	150	45	0.9997
							Average	0.9991
							Standard Deviation	0.0036

*Calculated using the transient Xe option.

**Critical at beginning of cycle 2.

***The corrected k_{eff} has the reactivity equivalent of the observed period subtracted from the calculated k_{eff}.

TABLE 4.3-2

HOT OPERATING CASES FOR BROWNS FERRY UNIT 3

Date	Core Average GWD/MTU	Fraction of Rated Power	Flow	Calculated k-eff
11/08/76	0.454	0.847	0.981	0.9976
12/08/76	0.933	0.980	0.980	1.0000
1/11/77	1.544	0.997	0.951	1.0006
2/17/77	2.255	0.994	0.961	0.9989
4/05/77	3.197	0.937	0.912	0.9985
6/09/77	4.320	0.965	0.884	0.9980
8/10/77	5.196	0.967	0.998	0.9989
9/21/77	6.035	0.970	0.990	0.9994
10/26/77	6.675	0.963	1.022	0.9987
11/11/77	7.013	1.000	1.028	0.9992
1/04/78	7.993	0.952	0.984	0.9992
1/24/78	8.411	0.910	1.001	1.0006
3/31/78	9.628	0.969	0.996	1.0037
4/28/78	10.024	0.945	1.001	1.0040
5/24/78	10.569	0.962	0.984	1.0054
6/22/78	11.180	0.963	1.001	1.0072
7/31/78	11.866	0.939	1.003	1.0089
9/01/78	12.348	0.767	0.683	1.0019
9/08/78	12.460	0.770	0.804	1.0035
12/20/78*	8.984	0.992	0.959	1.0048
			Average	1.0015
			Standard Deviation	0.0033

*This case is near the beginning of cycle 2.

also present in the Browns Ferry unit 3 data. The average k-effective for exposures less than 8,000 MWD/MTU is 0.9990 with a standard deviation of 0.0008. The corresponding values for exposures greater than 8,000 MWD/MTU are 1.0044 and 0.0027 respectively.

4.3.3 Process Computer Comparisons

Table 4.3-3 presents a comparison of process computer and CORE code values of axial peak-to-average power for high power configurations in Browns Ferry unit 3. On the average, CORE overpredicted the axial peaking factor by 1.73 percent with a standard deviation of 6.50 percent. The core average axial power shapes near beginning-of-cycle, middle-of-cycle and end-of-cycle are shown in Figures 4.3-1, 4.3-2, and 4.3-3 respectively. The beginning-of-cycle power shapes are in good agreement, but CORE underpredicted the power in the bottom section of the core which had the highest gadolinia content. By the middle-of-cycle, the effect of the high gadolinia section had burned out and the power distributions from CORE and the process computer are in excellent agreement. During the latter part of the cycle the trend was reversed and CORE overpredicted the power in the bottom section of the reactor compared to the process computer as shown in Figure 4.3-3. Figure 4.3-4 gives a comparison of core average relative exposure versus axial position for CORE and the process computer near the end of the first cycle. The excellent agreement of the end-of-cycle relative exposure shapes indicates that the underprediction of power in the bottom of the CORE early in the cycle was effectively cancelled by the overprediction in the last half of the cycle.

TABLE 4.3-3

CORE AVERAGE AXIAL PEAK-TO-AVERAGE POWER RATIOS
FOR BROWNS FERRY UNIT 3

Date	Core Average GWD/MTU	CORE Code	Process Computer	Percent Difference
11/08/75	0.454	1.276	1.239	-2.94
12/08/76	0.933	1.340	1.355	1.11
1/11/77	1.544	1.500	1.471	-1.95
2/17/77	2.255	1.387	1.430	3.05
4/05/77	3.197	1.255	1.313	4.52
6/09/77	4.320	1.419	1.450	2.16
8/10/77	5.196	1.317	1.255	-4.82
9/21/77	6.035	1.285	1.262	-1.81
10/26/77	6.675	1.236	1.293	4.51
11/11/77	7.013	1.147	1.244	8.11
1/04/78	7.993	1.239	1.267	2.23
1/24/78	8.411	1.193	1.316	9.80
3/31/78	9.628	1.302	1.157	-11.79
4/28/78	10.024	1.226	1.150	-6.40
5/24/78	10.569	1.294	1.135	-13.09
6/22/78	11.188	1.234	1.180	-4.47
7/31/78	11.866	1.309	1.211	-7.78
9/01/78	12.348	1.194	1.229	2.89
9/08/78	12.460	1.267	1.158	-8.99
12/20/78*	8.984	1.301	1.190	-8.91
			Average	-1.73
			Standard Deviation	6.50

*This case is near the beginning of cycle 2

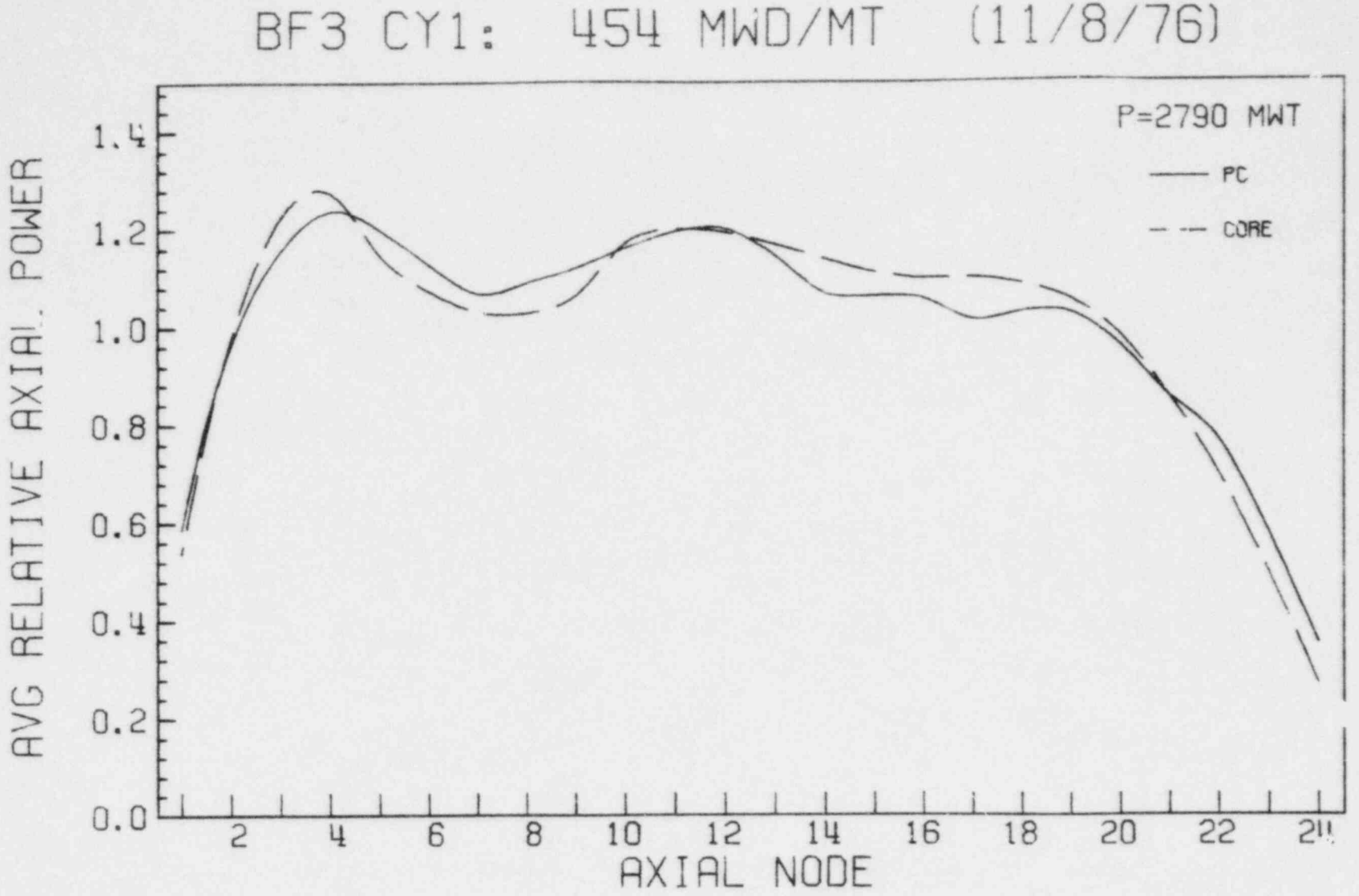

Figure 4.3-1: Near Beginning-of-cycle 1

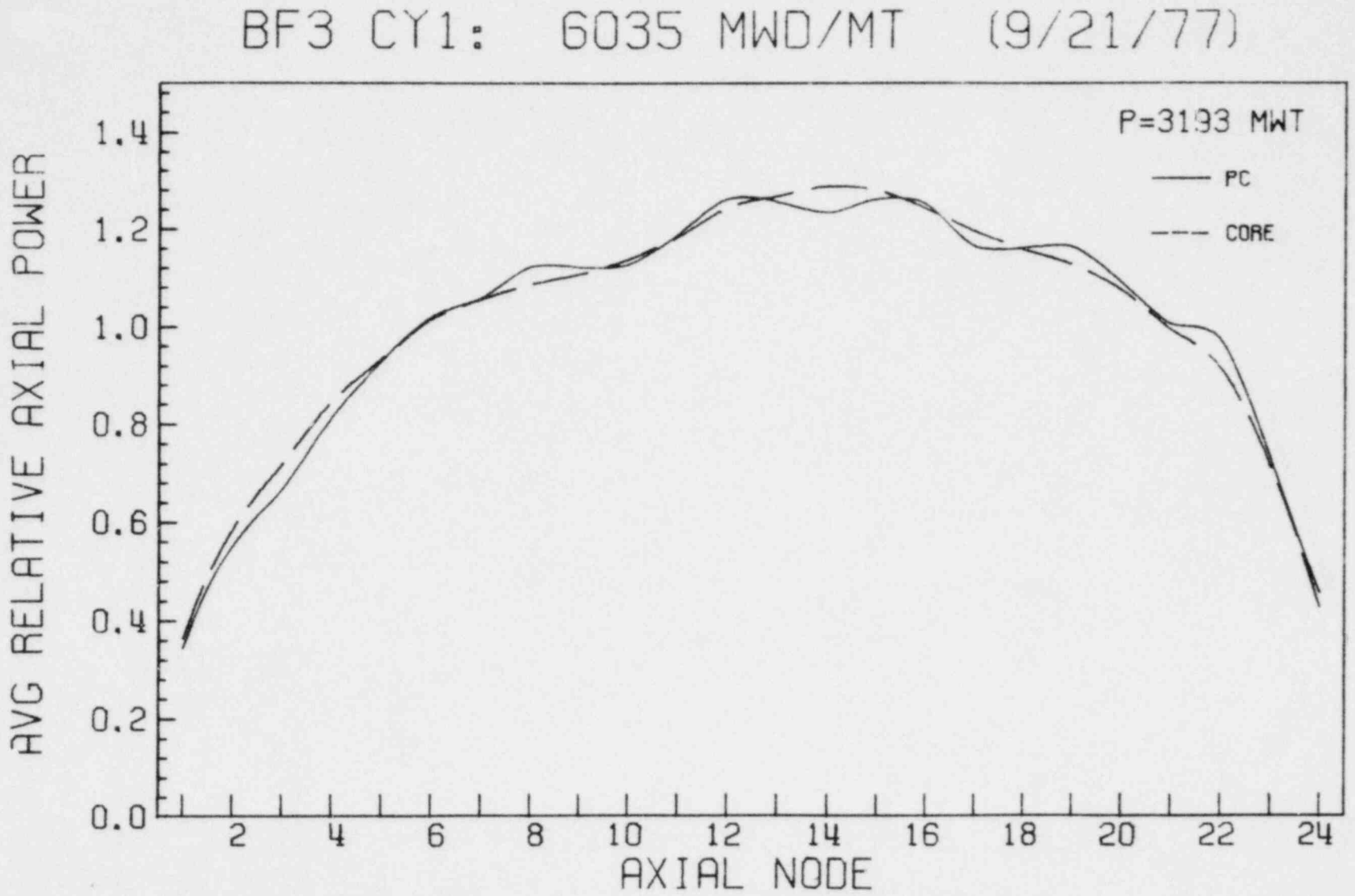

Figure 4.3-2: Near Middle-of-cycle 1

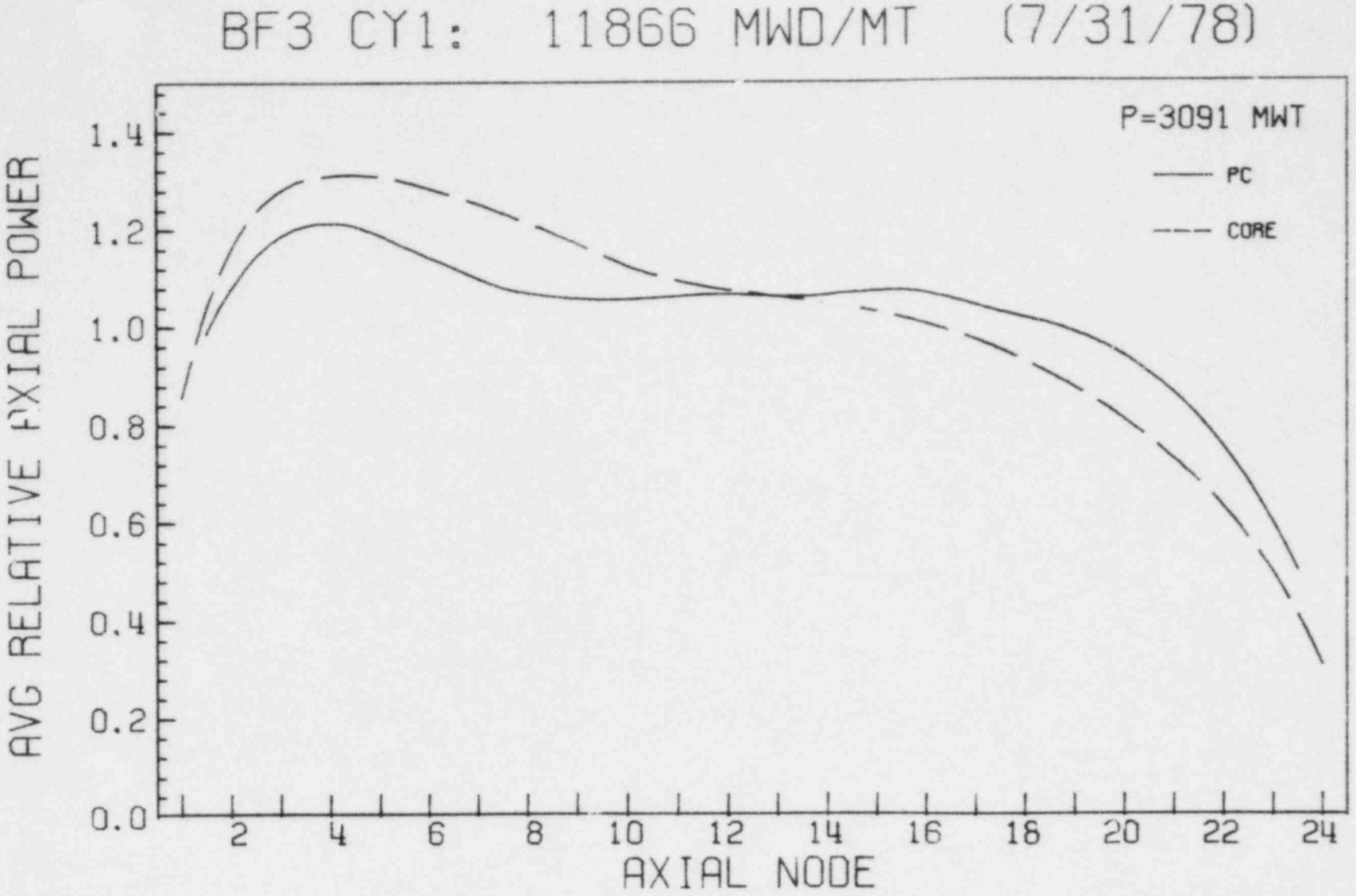

Figure 4.3-3: Near End-of-cycle 1

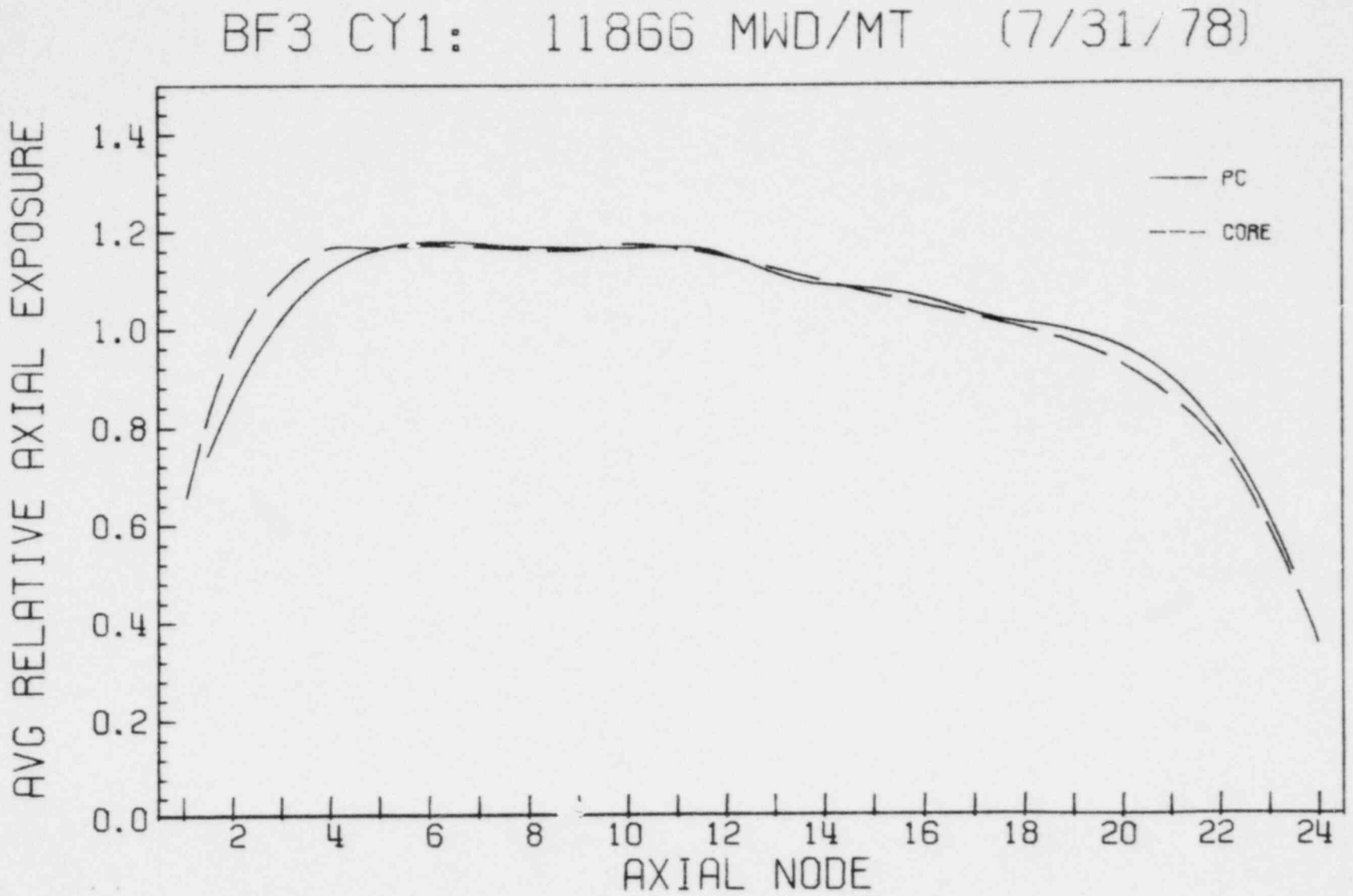

Figure 4.3-4: Near End-of-cycle 1

Table 4.3-4 shows the comparison of radial peaking factors (maximum relative bundle power) and individual bundle RMS power differences for CORE and the process computer. On the average, CORE underpredicted the maximum bundle relative power by 3.7 percent with a standard deviation of 1.76 percent compared to the process computer values. Comparison of individual bundle relative power differences results in an average RMS difference of 4.46 percent between the process computer and CORE. Comparison of individual process computer bundle relative powers in symmetric locations but based on different TIP thimbles resulted in a RMS difference of 3.5 percent.

Table 4.3-5 presents a comparison of CORE and process computer total peaking factors (maximum nodal times local value) and the RMS difference between individual nodal powers. Since the local peaking factors for CORE and the process computer are approximately identical, the total peaking factor comparison primarily reflects differences in the maximum nodal powers. On the average, CORE underpredicted the total peaking factor with respect to the process computer value by only 0.66 percent with a 5.04 percent standard deviation. However, this was obtained by underpredicting the total peaking factor by 4.1 percent during the first part of cycle 1 and overpredicting the peak by 1.74 percent for the remainder of the cases. The average RMS difference in individual nodal relative power for CORE and the process computer was 12.49 percent for the 9 cases where detailed data was available. The RMS nodal difference for symmetric process computer locations was found to be approximately 4.5 percent.

TABLE 4.3-4

RADIAL POWER DISTRIBUTION FOR BROWNS FERRY UNIT 3, CYCLE 1

Date	Core Average GWD/MTU	Radial Peaking Factor CORE Code	Process Computer	Percent Difference	Percent RMS Bundle Power Difference
11/08/76	0.454	1.311	1.355	3.30	4.436
12/08/76	0.933	1.286	1.348	4.71	4.019
1/11/77	1.544	1.263	1.340	5.92	-
2/17/77	2.255	1.267	1.330	4.85	-
4/05/77	3.197	1.286	1.360	5.59	-
6/09/77	4.320	1.260	1.323	4.88	4.652
8/10/77	5.196	1.319	1.370	3.79	-
9/21/77	6.035	1.300	1.329	2.21	4.274
10/26/77	6.675	1.361	1.419	4.17	4.498
11/11/77	7.013	1.367	1.420	3.80	-
1/04/78	7.993	1.378	1.435	4.05	4.543
1/24/78	8.411	1.351	1.410	4.27	-
3/31/78	9.628	1.382	1.398	1.15	4.18
4/28/78	10.024	1.351	1.350	-0.07	-
5/24/78	10.569	1.225	1.310	6.71	-
6/22/78	11.180	1.249	1.257	0.64	4.301
7/31/78	11.866	1.197	1.230	2.72	-
9/01/78	12.348	1.265	1.315	3.88	5.240
9/08/78	12.460	1.183	230	3.90	-
			Average	3.70	4.461
			Standard Deviation	1.76	

TABLE 4.3-5

NODAL POWER DISTRIBUTION FOR BROWNS FERRY UNIT 3

Date	Core Average GWD/MTU	Total Peaking Factor CORE Code	Total Peaking Factor Process Computer	Total Peaking Factor Percent Difference	Percent RMS Nodal Power Difference
11/08/76	0.454	2.241	2.173	-3.08	8.104
12/08/76	0.933	2.230	2.261	1.38	8.964
1/11/77	1.544	2.450	2.440	-0.41	-
2/17/77	2.255	2.176	2.332	6.92	-
4/05/77	3.197	2.079	2.311	10.57	-
6/09/77	4.320	2.281	2.482	8.44	11.306
8/10/77	5.196	2.449	-	-	-
9/21/77	6.035	2.050	2.151	4.81	6.991
10/26/77	6.675	2.272	2.228	-1.96	11.361
11/11/77	7.013	2.162	2.222	2.74	-
1/04/78	7.993	2.382	2.271	-4.77	19.838
1/24/78	8.411	2.207	2.321	5.04	-
3/31/78	9.628	-	1.995	-	16.083
4/28/78	10.024	2.055	1.998	-2.81	-
5/24/78	10.509	1.907	1.820	-4.67	-
6/22/78	11.180	1.898	1.839	-3.16	13.681
7/31/78	11.866	1.836	1.727	-6.12	-
9/01/78	12.348	1.870	-	-	16.108
9/08/78	12.460	1.743	1.690	-3.09	-
12/20/78*	8.984	2.323	2.356	1.41	-
			Average	0.66	12.493
			Standard Deviation	5.04	

*This case is near the beginning of cycle 2

CHAPTER 4 REFERENCES

1. S. L. Forkner, G. H. Meriwether, and T. D. Beu, "Three-Dimensional LWR Core Simulation Methods," TVA-TR78-03, 1978.

2. N. H. Larsen, G. R. Parkos, and O. Raza, "Core Design and Operating Data for Cycles 1 and 2 of Quad Cities 1," EPRI NP-240, 1976.

3. B. L. Darnell, T. D. Beu, and G. W. Perry, "Methods for the Lattice Physics Analysis of LWR's," TVA-TR78-02, 1978.

4. G. R. Parkos, "BWR Simulator Methods Verification," General Electric Company, NEDO-20946A, 1977.

5. M. B. Cutrone and G. F. Valby, "Gamma Scan Measurements at Quad Cities Nuclear Power Station Unit 1 Following Cycle 2," EPRI NP-214, 1976.

6. Browns Ferry Nuclear Plant Final Safety Analysis Report.

7. NEDO-24020, "General Electric Boiling Water Reactor Reload 1 Licensing Amendment for Browns Ferry Nuclear Plant Unit 1," May 1977.

8. NEDO-24095, "Supplemental Reload Licensing Submittal for Browns Ferry Nuclear Plant Unit 2 Reload 1," December 1977.

9. NEDO-24128, "Supplemental Reload Licensing Submittal for Browns Ferry Nuclear Plant Unit 3 Reload 1," June 1978.

5. SUMMARY

5.1 LATTICE PHYSICS METHODS

Although a more meaningful indication of the adequacy of the physics methods used in the LATTICE code lies in the results obtained from the CORE simulator that were presented in Chapter 4, data was included in Chapters 2 and 3 to demonstrate the overall suitability of the models used. Comparisons were presented to measurements and to calculated results from other codes with more detailed models.

In Section 2.1, values of k-effective for 25 critical experiments were presented; the average was 0.9954 with a standard deviation of 0.0107. It was shown that by grouping similar experiments, considerably smaller standard deviations resulted. In Section 2.2, reaction rate distributions in space and energy calculated by LATTICE and ESP, a general Monte Carlo reactor analysis code, were compared for 15 of the experiments analyzed in Section 2.1. The largest bias and standard deviation was for the absorption of fast neutrons in the fuel. Agreement was good for k_∞ and thermal reaction rates; the bias and standard deviation were 0.00228 and 0.0108 for k_∞. Section 2.3 presented comparisons to measured data for the calculation of isotopic concentrations of uranium and plutonium as a function of burnup. Excellent agreement was obtained for all isotopic ratios except for the ratio of Pu-242 to Pu-241, which was underpredicted by approximately 35 percent at an exposure of 12,000 MWD/MTM. This discrepancy does not affect the ability of LATTICE to fulfill its intended function.

The comparisons given in Chapter 2 demonstrate that the basic models used in LATTICE accurately represent the neutronic phenomena important to light water reactor analyses.

Chapter 3 contains information which confirms the adequacy of the LATTICE calculation of important bundle physics parameters. Comparisons to measured data were presented for the local power distribution of exposed bundles. For unexposed bundles, comparisons were made to reactivity and local power distributions calculated by more exact codes. The ESP Monte Carlo code and the CPM collision probability code were used for these comparisons.

Table 3.1-1 exhibited k_∞ values calculated for unexposed fuel for a variety of fuel types and water densities. For the 23 cases, the bias of LATTICE relative to ESP was 0.0074 with a standard deviation of 0.0079. Good agreement for the calculated worth of the burnable poison in a particular bundle design was also discussed.

Comparisons of local power distributions were given in Section 3.2. Beginning-of-life comparisons to ESP and/or CPM were presented in Figures 3.2-2 through 3.2-12. RMS differences ranged from 3.1 to 6.5 percent relative to ESP, and from 2.4 to 3.7 percent relative to CPM. The RMS differences were statistically combined with a result of 4.0 percent. LATTICE predicted bundle peaking factors well compared to ESP, obtaining a bias of 0.1 percent and a standard deviation of 2.2 percent; relative to CPM there was a bias of -1.8 percent with a standard deviation of 1.8 percent. Thus LATTICE adequately predicts local power distributions and peaking factors compared to two other codes using more exact theory.

Local power distributions for exposed fuel were compared in Figures 3.2-13 to 3.2-19 to gamma scan measurements taken at the end-of-cycle 2 of Quad Cities unit 1. RMS differences ranged from 1.6 to 4.9 percent. The statistical combination of the RMS differences for UO_2 bundles was 2.4 percent. The power of the burnable poison pins was in good agreement. For peaking factors of exposed fuel, the resulting bias and standard deviation were -1.2 and 1.5 percent. Chapters 2 and 3 confirm the conclusion, reached by examining results from the CORE simulator, that LATTICE well predicts parameters of interest in commercially available BWR fuel bundles.

5.2 CORE SIMULATION

The capability of TVA methods to accurately simulate the steady-state physics of boiling water reactor cores was verified by comparisons to measured data from Quad Cities unit 1 and all three Browns Ferry units. For zero power criticals, a total of 53 critical configurations was calculated. Figure 5.2-1 presents all of the k-effective values from CORE for the zero power criticals as a function of core average exposure. The average k-effective for all 53 points is 0.9977 with a standard deviation of 0.0025. There is no apparent trend in the predicted k-effective for cold criticals versus core average exposure. Additionally, there was not a significant bias between the calculated k-effective values for localized and in-sequence control rod patterns.

Calculated k-effective values were presented for a total of 69 high-power critical configurations. Figure 5.2-2 presents the calculated hot operating k-effectives versus core average exposure.

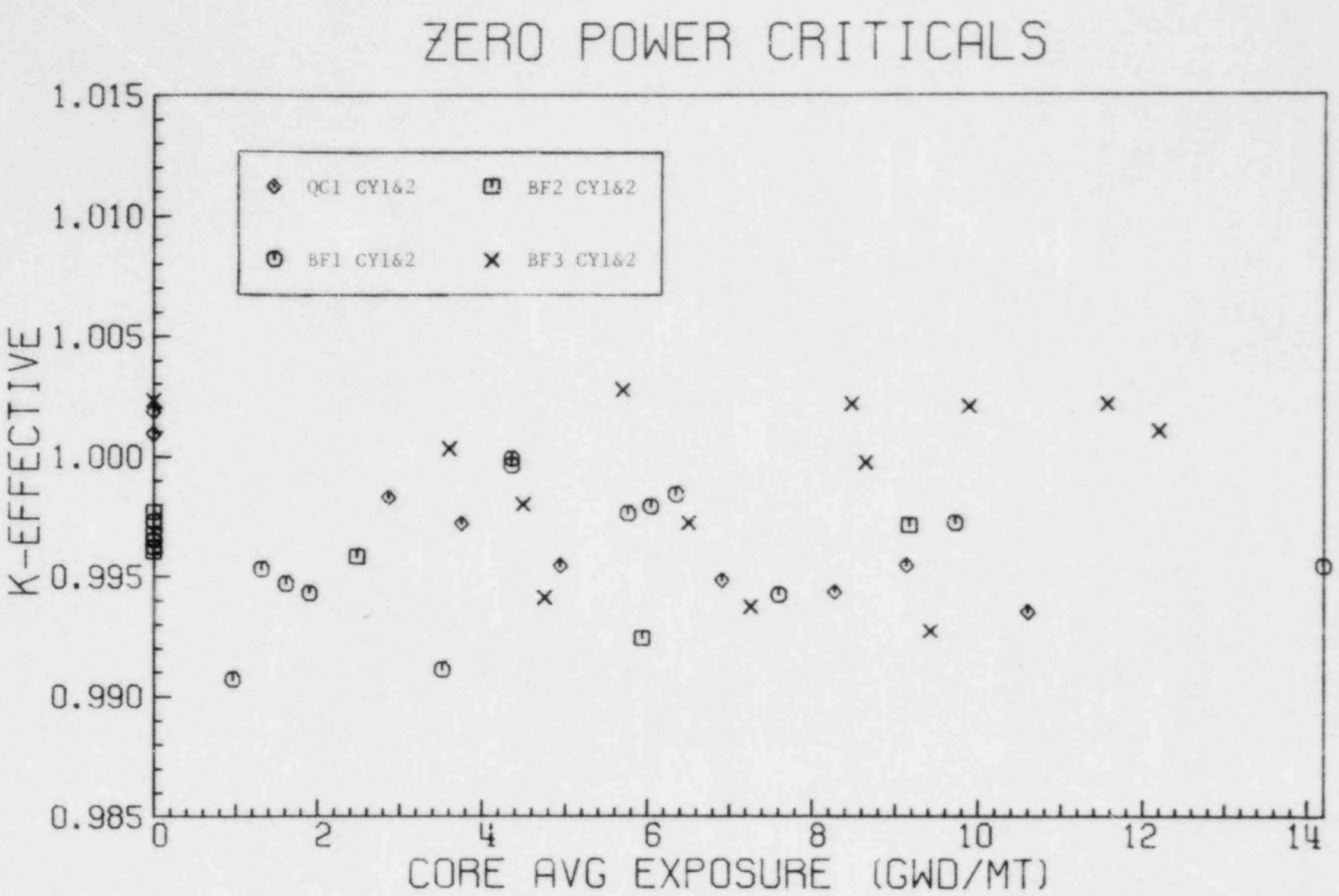
ZERO POWER CRITICALS
QC1 CY1&2
BF2 CY1&2
BF1 CY1&2
BF3 CY1&2
K-EFFECTIVE
1.015
1.010
1.005
1.000
0.995
0.990
0.985
0
2
4
6
8
10
12
14
CORE AVG EXPOSURE (GWD/MT)

Figure 5.2-1

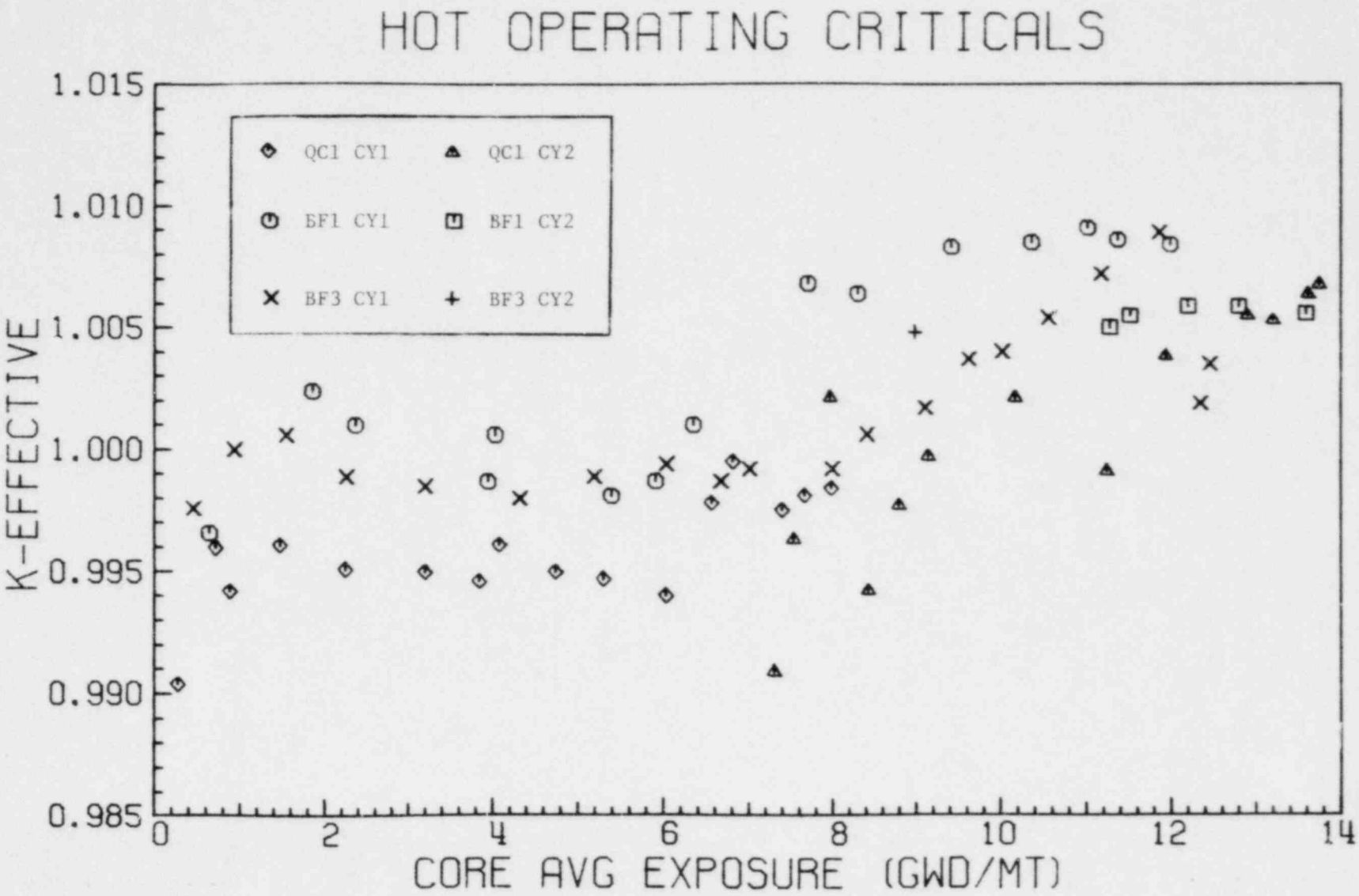
HOT OPERATING CRITICALS
QC1 CY1
QC1 CY2
BF1 CY1
BF1 CY2
BF3 CY1
BF3 CY2
K-EFFECTIVE
1.015
1.010
1.005
1.000
0.995
0.990
0.985
0
2
4
6
8
10
12
14
CORE AVG EXPOSURE (GWD/MT)

Figure 5.2-2

The average k-effective for all 69 points is 1.0008 with a standard deviation of 0.0039. However, a trend toward higher predicted k-effective values for increasing core average exposures is evident. For core average exposures typical of reload cores (greater than 10,000 MWD/MTU), the average k-effective value for 22 points is 1.0056 with a standard deviation of 0.0025.

Comparisons of simulated (by CORE) and measured TIP readings were performed for 27 operating points in Quad Cities unit 1 cycles 1 and 2. The standard deviation of differences between calculated and measured readings for 6-inch segments and integrated thimble values is approximately the same as the standard deviation of differences between symmetric measurements. The bundle axial peak-to-average values of La-140 activity from CORE were compared to gamma scan measurements for Quad Cities performed at the end of cycles 1 and 2. For the end-of-cycle 1 gamma scan, CORE overestimated the axial peaking factor by 4.72 percent with a standard deviation of 2.64 percent. The end-of-cycle 2 values were overpredicted by 1.47 percent with a standard deviation of 1.89 percent. The average and individual bundle axial La-140 distributions were in good agreement with the measured data.

For the end-of-cycle 2 Quad Cities gamma scan measurements, CORE overpredicted the 25 highest nodal La-140 activities by 1.4 percent with a standard deviation of 1.3 percent. The radial power distribution (as indicated by bundle average La-140 activities) predicted by CORE was in good agreement with the measured data. The standard deviation of differences for individual bundles was 3.82 percent.

Comparisons to process computer power distributions for the Browns Ferry units confirm that CORE reliably predicts the the reactor power distribution throughout the operating cycle.